Some Boundary-Value Problems for Water Waves

Vishal Vasan

A dissertation submitted in partial fulfillment
of the requirements for the degree of

Doctor of Philosophy

University of Washington

2012

Bernard Deconinck, Chair

Anne Greenbaum

Robert E. O'Malley, Jr.

Program Authorized to Offer Degree:
Department of Applied Mathematics

University of Washington

Abstract

Some Boundary-Value Problems for Water Waves

Vishal Vasan

Chair of the Supervisory Committee:
Professor Bernard Deconinck
Department of Applied Mathematics

Euler's equations describe the evolution of waves on the surface of an ideal incompressible fluid. In this dissertation, I discuss some boundary-value problems associated with Euler's equations. My approach is motivated by the ideas generated by Fokas and collaborators, particularly the notion of a global relation for boundary-value problems for partial differential equations. I introduce a new method to compute the evolution of the free surface of a water wave based on a reinterpretation of the relevant global relation. Next I consider the bathymetry reconstruction problem *i.e.,* the reconstruction of the bottom boundary of a fluid from measurements of the free-surface elevation alone. By analyzing the global relation for the water-wave problem, I derive an exact, fully nonlinear equation which is solved for the bottom boundary. Finally, I present a method of reconstructing the free surface of a water wave using measurements of the pressure at the bottom boundary. Using this reconstruction, I obtain several new asymptotic approximations of the surface elevation in terms of the pressure at the bottom. Comparisons with numerical and experimental data show excellent agreement with my predicted reconstructions.

TABLE OF CONTENTS

Page

LIST OF FIGURES

LIST OF TABLES

ACKNOWLEDGMENTS

I would like to thank my advisor Bernard Deconinck for his guidance and encouragement. Without his direction I could not have completed this journey. I would also like to thank my committee members Anne Greenbaum, Robert E. O'Malley and Ka-Kit Tung for their assistance and helpful comments. I acknowledge my Graduate School Representative John Sylvester for several fruitful conversations. In many ways, he has been a full committee member and I truly appreciate his support. The past few years have been some of my happiest and I thank my fellow students and friends for the great times and memories. Lastly, I would like to thank my family for their love, patience and understanding. They helped me through the toughest of times and without them none of this would have been possible.

This work was supported by the National Science Foundation and a Boeing Research Fellowship.

DEDICATION

to those I galled most:
my parents, my brother, Kritika
and Saba the Sargunaraj.

Chapter 1

INTRODUCTION

Mathematics has always benefited from an honest-to-goodness hard problem. Throughout history, mathematicians' struggles with difficult problems have led to some of the most crucial advances in the subject. Even the most cursory attempt at compiling a list of significant developments, instantly brings to mind examples such as Calculus, Fourier Analysis and Linear Algebra amongst others, all of which were created to solve the most relevant and challenging problems of the day. The mathematical investigation of fluid motion has been a particularly difficult quest and consequently one of the most productive endeavors. Luminaries from every generation of mathematicians including Newton, Euler, Stokes, Kolmogorov and Leray have made their mark on this most regarded of subjects. Yet, as unimaginable as it may seem, there still are many unanswered questions and much progress is still being made today. Indeed this is the hallmark of a good problem: to provide an endless source of inspiration for the creation of new mathematical tools and ideas.

Surface water waves, the topic of this thesis, have provided a veritable playground for ideas. From perturbation methods to bifurcation theory; from complex analysis to Hamiltonian dynamics, almost every conceivable branch of modern mathematics has played some role in their investigation. Occasionally, these ideas were developed for the exclusive purpose of being applied to the theory of water waves [14]. Other times, water waves are the prototypical example, as in the case of free-boundary value problems.

The theory of integrable systems and in particular integrable partial-differential equations (PDEs) owes a great deal to the study of water waves. Many of the classical equations from the theory of solitons, such as the Korteweg-deVries (KdV) and Boussinesq equations, arose originally within the context of water waves, typically as reductions of the full system of equations describing water-wave motion. The usual domain for such integrable PDEs is either the periodic interval or the whole real line. The investigation of such equations on

these domains revealed their remarkable and unique status among differential equations. These equations are the closest nonlinear relatives of linear PDEs and can in fact be solved by techniques which are an appropriate nonlinearization of Fourier transform methods [4, 8].

Over the last few decades, substantial progress has been made by researchers with regards to the relation between linear PDEs and their integrable nonlinear cousins. Building upon the pioneering work of Fokas [38], significant progress has been achieved regarding *boundary-value problems* for linear and integrable PDEs. Of particular relevance for this thesis, is the idea of a **global relation** and its symmetries. The global relations for a PDE are conditions that the values of the solution to the PDE (and its derivatives) must satisfy on the boundary of the domain in question. In the context of Laplace's equation, the global relation has sometimes been known as the adjoint relation. By analyzing the global relations one can characterize the unknown boundary conditions using those that are given. In the case of linear PDEs, it is also possible to explicitly solve the PDE *i.e.*, to obtain an expression with explicit dependence on the independent variables. In a sense, the purpose of this thesis is to feed back the ideas of integrable systems to their source: the original water-wave problem. Our aim is to pose and answer several boundary-value problems for water waves. Some of these problems are as old as the water-wave equations themselves. Others are motivated by more modern but nonetheless pertinent applications.

1.1 The water-wave equations

Without further delay, let us acquaint ourselves with the equations governing surface water waves, also known as Euler's Equations:

$$\phi_{xx} + \phi_{yy} + \phi_{zz} = 0, \qquad -\zeta < z < \eta, \tag{1a}$$

$$\phi_z - \phi_x\eta_x - \phi_y\eta_y = \eta_t, \qquad z = \eta(x, y, t), \tag{1b}$$

$$\phi_t + \frac{1}{2}\left(\phi_x^2 + \phi_y^2 + \phi_z^2\right) + g\eta = 0, \qquad z = \eta(x, y, t), \tag{1c}$$

$$\phi_z + \phi_x\zeta_x + \phi_y\zeta_y = 0 \qquad z = -\zeta(x, y). \tag{1d}$$

These equations were derived first by Leonard Euler in the 17^{th} century [26]. They govern the behavior of an inviscid, irrotational, incompressible fluid with zero surface tension [15].

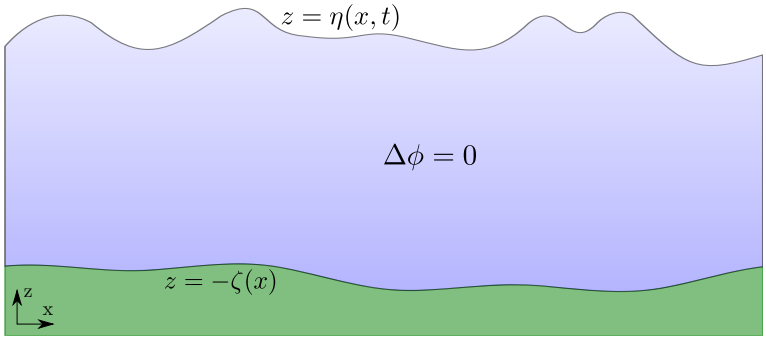

Figure 1.1: Fluid domain for the water-wave problem.

Here ϕ is the velocity potential of the fluid *i.e.*, the fluid velocity at a point is given by the gradient of ϕ. Hereafter, subscripts indicate partial derivatives with respect to the independent variables. The free surface of the fluid is described by the function $\eta(x, y, t)$ whereas the solid boundary on which the fluid rests is given by the equation $z = -\zeta(x, y)$. Thus the fluid domain extends between $-\zeta$ and η in the z-direction (which we shall take to be the vertical direction). The boundary $z = -\zeta$ is also known as the bottom surface or the bathymetry. Figure 1.1 is a cartoon of a two-dimensional fluid.

The fluid surface moves under the influence of two forces: the pressure gradient across the free surface and gravity. The acceleration due to gravity is given by g in equation (1c). According to equation (1a), the velocity potential is a harmonic function while the other equations describe boundary conditions at the free and bottom surfaces. In the horizontal directions (*i.e*, along x and y), one may impose a variety of boundary conditions including but not limited to decay at infinity and periodicity (of period L, say). The reader may notice that two boundary conditions have been imposed at the same boundary, namely at $z = \eta(x, y, t)$. However, the problem is not overdetermined as the surface η itself is one of the unknowns in the water-wave problem. Indeed, one might be inclined to say that the free surface itself is the object of our investigation and the velocity potential is merely a mathematical device that allows us to model the surface. This, however, would be a

controversial statement.

The standard problem in the theory of water waves is that of the evolution in time of the fluid. The above set of equations are supplemented with initial conditions for the velocity potential ϕ and surface η at some $t = t_0$. The goal is to describe the temporal evolution of the surface. I shall refer to this boundary-value problem as the Forward Problem. The water-wave equations are a unique mixture of linear and nonlinear PDEs. Indeed one of the unknowns, ϕ, satisfies a linear PDE in the bulk of the fluid whereas the free surface satisfies nonlinear evolution equations at the boundary. At every instant of time, with a given boundary η and potential ϕ at $z = \eta(x, y, t)$, we solve Laplace's equation which in turn governs the evolution of the surface and the potential through equations (1b) and (1c). It may not come as a surprise that general explicit solutions in closed form to this nonlinear, free-boundary value problem do not exist. However, equations (1a-1d) are known to possess unique solutions depending continuously on initial data [49, 69].

For the particular case of a two-dimensional fluid (no y dependence), considerable progress is made using the theory of functions of a complex variable, specifically with techniques involving conformal maps. This thesis will not discuss such techniques as they cannot be extended to the full three-dimensional problem. Although this thesis will not present details for the general three-dimensional water-wave problem, the methods discussed here are based only on Laplace's equation and hence extend to three dimensions in a straightforward manner.

In a sense, all the "action" is at the free surface *i.e.*, the temporal evolution is stated in terms of quantities defined on the boundary. This intuition is fully rewarded, for the system of equations (1a-1d) may be rewritten as a Hamiltonian system of differential equations in variables defined at the free surface: $\eta(x, y, t)$ and $q(x, y, t) = \phi(x, y, \eta, t)$ [71]. The Hamiltonian for this system is

$$H = \frac{1}{2}\int_R \int_{-\zeta}^{\eta} \left(\phi_x^2 + \phi_y^2 + \phi_z^2\right)\, dzdydx + \frac{1}{2}\int_R g\eta^2\, dydx.$$

Here R represents the horizontal extent of the fluid domain. Thus for the problem with periodic boundary conditions in x and y, R represents a period lattice in $\mathbb{R}^2$ and for the problem on the infinite plane $R = \mathbb{R}^2$. Thus Euler's equations for water waves have the

following compact representation:

$$\frac{\partial \eta}{\partial t} = \frac{\delta H}{\delta q}, \tag{2a}$$

$$\frac{\partial q}{\partial t} = -\frac{\delta H}{\delta \eta}, \tag{2b}$$

where the right-hand sides are variational derivatives of the functional H. Evidently, the surface variables $\eta(x, y, t)$ and $q(x, y, t)$ are the canonical variables for the Hamiltonian system. The Hamiltonian nature of the water-wave problem will not be of central importance to the discussion in this dissertation. However, any numerical simulation should maintain this integral of motion. Indeed the water-wave problem has several constants of motion [56]. Craig & Sulem [25] presented one of the first numerical solutions of the water-wave problem to directly employ the Hamiltonian equations. An application of Green's Identity allows one to express the Hamiltonian in terms of canonical variables alone:

$$H = \frac{1}{2} \int_R \left[g\eta^2 + q\, G(\eta, \zeta) q \right] dy dx,$$

where $G(\eta, \zeta)$ is the Dirichlet→Neumann operator. It was this form of the Hamiltonian that Craig & Sulem [25] employed.

The Dirichlet→Neumann operator is defined as follows. Consider a function $\psi(x, y, z)$, harmonic in $R \times [-\zeta, \eta]$ with

$$\psi(x, y, \eta) = q(x, y),$$

$$\psi_z(x, y, -\zeta) + \zeta_x \psi_x(x, y, -\zeta) + \zeta_y \psi_y(x, y, -\zeta) = 0.$$

For definiteness, assume $R = [0, L_1] \times [0, L_2]$ with L_1, L_2 representing periods in the horizontal directions. Hence ϕ is a periodic function of the horizontal variables. This boundary-value problem is well posed with a unique solution. The operator G is given in terms of the solution to the boundary-value problem by

$$G(\eta, \zeta) q = \psi_z(x, y, \eta) - \eta_x \psi_x(x, y, \eta) - \eta_y \psi_y(x, y, \eta).$$

Thus G maps the Dirichlet data of a harmonic function along a surface to the associated normal derivative at that location.

With the Dirichlet→Neumann operator defined, the water-wave equations take the following form suggested by Craig & Sulem [25]

$$\frac{\partial \eta}{\partial t} = G(\eta, \zeta) q, \tag{3a}$$

$$\frac{\partial q}{\partial t} = -g\eta - \frac{1}{2}|\nabla q|^2 + \frac{(\nabla q \cdot \nabla \eta + G(\eta, \zeta) q)^2}{2(1 + |\nabla \eta|^2)}. \tag{3b}$$

The first equation above may be derived from the Hamiltonian itself or more simply by noting that the left-hand side of equation (1b) is just the definition of the Dirichlet→Neumann operator. The equation for the evolution of q may be obtained from (1c) and the relations

$$q_x = \phi_x + \eta_x \phi_z, \quad q_y = \phi_y + \eta_y \phi_z,$$

which are consequences of the definition of q and the chain rule. But for the rather abstract definition of the Dirichlet→Neumann operator, (3a-3b) would seem to be a simple set of equations for the evolution of the surface quantities. However, it is known that the Dirichlet→Neumann operator is analytic in η [16, 54, 45]. Indeed Craig & Sulem [25] (in their original work on the numerical simulation of water waves) present an alternate characterization of G, as a Taylor series expansion in powers of η. Thus truncating the Taylor series of the Dirichlet→Neumann operator in powers of η, one obtains an approximation to the overall operator which can be efficiently computed using fast Fourier transforms for problems posed on periodic domains [25, 53, 44].

It is worth noting that the equations of motion for water waves are unusual in at least one respect: the order of the nonlinearity is essentially infinite. Indeed, almost all the complexity of these equations (computationally and otherwise) arises from the Dirichlet→Neumann operator. Though the operator is analytic in η with exponentially decaying terms, the explicit form of these terms in the Taylor series of the operator is known to be poorly conditioned for higher-order Taylor approximations. At higher orders, these expressions possess high-frequency oscillations resulting in errors in the Neumann value [53, 44, 70].

Our final reformulation of the water-wave problem, perhaps the one most relevant to the material presented in this dissertation, is that of Ablowitz, Fokas & Musslimani (AFM) [2]. The AFM reformulation is essentially an alternate characterization of the Dirichlet→Neumann operator. This characterization is based on the global relations for

Laplace's equation. Here the global relation connects the various boundary values of Laplace's equation in the context of the water-wave problem. For the case $\zeta = h$ (a fluid bounded by a flat bottom surface), the AFM formulation is

$$\int_R e^{-ik_x x - ik_y y} \left\{ \eta_t \cosh(k(\eta + h)) + \frac{i \sinh(k(\eta + h))}{k} (k_x q_x + k_y q_y) \right\} dxdy = 0, \tag{4a}$$

$$q_t = -g\eta - \frac{1}{2}\left(q_x^2 + q_y^2\right) + \frac{(q_x \eta_x + q_y \eta_y + \eta_t)^2}{2(1 + \eta_x^2 + \eta_y^2)}, \tag{4b}$$

where $k = \sqrt{k_x^2 + k_y^2}$ and k_x, k_y are real numbers for the problem with decay at infinity, and are discrete wave numbers based on the period lattice for problems with periodic boundary conditions. Equation (4a) is the global relation for Laplace's equation. It relates the Dirichlet value q to the Neumann value η_t and is an implicit representation of the Dirichlet→Neumann operator. This form of the water-wave equations is wholly equivalent to the other formulations. Indeed one may also obtain the Taylor series representation of the Dirichlet→Neumann operator from equation (4a) as shown in [3]. The AFM formulation may also be extended to generic ζ, see below for details. Finally, it is noted that equations (3b) and (4b) are effectively the same.

1.2 Overview of the dissertation

This thesis presents the solution of certain boundary-value problems for Laplace'e equation in non-convex domains, particularly in the context of the water-wave problem. As the water-wave problem is a free-boundary problem, it is important that no *a priori* assumptions about the free surface, such as convexity, are made. The solutions to these boundary-value problems are obtained by analyzing the global relation. The global relation for Laplace's equation is derived below. It should be noted that this is not the only global relation for the PDE [59, 60], however other such relations do not extend to three-dimensions unlike the version presented here. The discussion of the global relation presented below is adapted from [2].

Let ϕ satisfy the Laplace equation in the domain $-\zeta < z < \eta$. In the horizontal directions, assume the gradient of ϕ vanishes for large $x^2 + y^2$. Define

$$E^{\pm} = e^{-ik_x x - ik_y y \pm kz},$$

where $k = \sqrt{k_x^2 + k_y^2}$ and k_x, k_y are real numbers. Clearly, $E^{\pm}$ satisfies Laplace's equation and hence

$$\phi_z \left(E^{\pm}_{xx} + E^{\pm}_{yy} + E^{\pm}_{zz}\right) + E^{\pm}_z \left(\phi_{xx} + \phi_{yy} + \phi_{zz}\right) = 0, \quad k \neq 0.$$

This equation can be rewritten in the form

$$\left(E^{\pm}\left(-ik_x\phi_z \pm k\phi_x\right)\right)_x + \left(E^{\pm}\left(-ik_y\phi_y \pm k\phi_x\right)\right)_y + \left(E^{\pm}\left(\pm k\phi_z + ik_x\phi_x + ik_y\phi_y\right)\right)_z = 0.$$

Integrating this equation over the domain $-\zeta < z < \eta$ and applying the Divergence Theorem we obtain, after some rearrangement,

$$\begin{aligned}
&\int_{-\infty}^{\infty}\int_{-\infty}^{\infty} e^{-ik_x x - ik_y y \mp k\zeta}\left\{-ik_x(\phi_x + \zeta_x\phi_z) - ik_y(\phi_y + \zeta_y\phi_z) \pm k(\zeta_x\phi_x + \zeta_y\phi_y + \phi_z)\right\} dxdy \\
&= \int_{-\infty}^{\infty}\int_{-\infty}^{\infty} e^{-ik_x x - ik_y y \pm k\eta}\left\{-ik_x(\phi_x + \eta_x\phi_z) - ik_y(\phi_y + \eta_y\phi_z) \pm k(\eta_x\phi_x + \eta_y\phi_y + \phi_z)\right\} dxdy.
\end{aligned}$$

Let $\Phi = \phi(x, y, -\zeta)$ and $q = \phi(x, y, \eta)$. Using (1b) and (1d), we obtain

$$\begin{aligned}
&\int_{-\infty}^{\infty}\int_{-\infty}^{\infty} ie^{-ik_x x - ik_y y - k\zeta}(k_x\Phi_x + k_y\Phi_y)dxdy \\
&\qquad = \int_{-\infty}^{\infty}\int_{-\infty}^{\infty} e^{-ik_x x - ik_y y + k\eta}\{i(k_x q_x + k_y q_y) + k\eta_t\}dxdy,
\end{aligned} \tag{5}$$

and

$$\begin{aligned}
&\int_{-\infty}^{\infty}\int_{-\infty}^{\infty} ie^{-ik_x x - ik_y y + k\zeta}(k_x\Phi_x + k_y\Phi_y)dxdy \\
&\qquad = \int_{-\infty}^{\infty}\int_{-\infty}^{\infty} e^{-ik_x x - ik_y y - k\eta}\{i(k_x q_x + k_y q_y) - k\eta_t\}dxdy.
\end{aligned} \tag{6}$$

The above two equations may be used to characterize the boundary data if, say for instance, q is known. Thus given q, we may use the above equations to obtain a representation for the Dirichlet→Neumann operator. For generic ζ, we see that we must solve for Φ as well. However, for the simpler case when $\zeta = h$ we may eliminate Φ algebraically. In this case, we multiply the first equation by e^{kh} and the second equation by e^{-kh}. Subtracting one equation from the other we obtain (4a). The global relations for the problem on the periodic interval can be similarly obtained when k_x, k_y are limited to a discrete set of wave-numbers obtained from the period lattice [28].

The bulk of this thesis is concerned with the application of the global relation to different boundary-value problems. These boundary-value problems differ only in the data that is

assumed given. I hope to convince the reader that global relations are a useful technique to approach boundary-value problems, particularly with respect to the water-wave problem. Of course, global relations exist for many PDEs and are equally helpful in problems other than the water-wave problem. For more details about global relations for linear constant coefficient PDEs and how they may be used to solve such equations see Chapter 2. The main goal there is to obtain expressions for solutions to linear diffusive and dispersive PDEs that depend explicitly on the independent variables. This chapter introduces the notion of global relations as well as their derivation. Although some of the techniques in this chapter will not translate to the water-wave problem, the ideas involved will form the basis of our intuition in later chapters. Specifically, we develop the notion that the global relations define maps from given boundary data to the unknown boundary data.

One of the primary advantages of Fokas' method is the ability to algorithmically deduce which boundary-value problems are well posed. A novel extension of Fokas' method to PDEs with mixed partial derivatives is provided in Appendix A, where we discuss the well-posedness of the linear Benjamin-Bona-Mahony equation. Using the global relations, we see that PDEs with mixed partial derivatives display a peculiar behavior for special boundary conditions. For these special boundary conditions, the initial and boundary data must satisfy a constraint and hence they are not independent of one another.

It is a common feature of global relations that they connect transforms of boundary data. For instance, equation (4a) is a relation between a transform of the Dirichlet and Neumann values on the boundary. Thus to explicitly obtain the Dirichlet→Neumann operator the transforms present in the global relation need to be inverted. One possibility is to linearize the equation in η and apply Fourier transforms. This leads to the recursion relation of Craig & Sulem [25]. Using ideas from [3], in Chapter 3 I reinterpret the global relation in a distributional sense which leads to an alternate representation of the Dirichlet→Neumann operator that is not perturbative. We shall see how this alternate representation is used to numerically solve the water-wave equations for the time-dependent motion of the surface.

In Chapter 4 I discuss a particular inverse problem associated with the water-wave equations, namely, the reconstruction of the shape of the solid bottom boundary of the fluid ζ from measurements of the free surface η alone. The overall idea consists of two steps:

1. Translate the inverse problem to a suitable boundary-value problem.

2. Employ the global relation to derive a nonlinear function whose zero is the bottom surface.

Using the data obtained from the forward simulation of the time-dependent motion of the surface, the bottom surface is reconstructed for several test cases. The bottom surface is accurately reconstructed using measurements of the surface elevation at several instances. Next, I examine various numerical issues pertaining to accurate reconstruction such as the effect of deep water, near zero surface deviations, *etc.* The method is readily extended to two-dimensional surfaces and is most accurate for shallow water.

The next inverse problem (Chapter 5) is concerned with how one can reconstruct the shape of the free surface η given the pressure at the bottom boundary $z = -h$. Upon limiting ourselves to traveling water waves, I employ the Bernoulli condition (1c) to relate the surface η and the pressure at the bottom, to boundary data for the velocity potential ϕ at the free and bottom surfaces respectively. Once again, I use the global relation to relate these boundary values leading to a single nonlinear expression involving the pressure and surface. Next, I derive several approximations to the nonlinear equation by suitably expanding and truncating the expression at various orders. I evaluate these approximations and the exact nonlinear expression for accuracy in reconstructing the free surface using numerically generated data as well as data from physical experiments.

1.3 A note on the physics of water waves

Water waves in nature exhibit a tremendous variety of length and time scales. At one end of the spectrum are capillary waves not larger than a centimeter, while at the other extreme we have tsunamis and rogue waves capable of wrecking coastlines and large oil tankers. Waves in the oceans quite often possess non-negligible vorticity which has a significant impact on the wave dynamics. Of course, real water waves suffer from viscous effects, breaking and overturning, and most dreaded of all, turbulence. It may be impossible to treat water waves in all their generality and so I limit myself to inviscid, irrotational water waves with no overturning. Further, the water-wave problems addressed in this thesis do not consider

the effect of currents. This is a mathematical idealization and the reader may well assume I refer to such a mathematical object when I use the term "water wave". For the most part, this thesis discusses the mathematical idealization and how one may solve associated problems. Indeed the analysis presented here is largely a statement of Laplace's equation. Also, this thesis does not contain a derivation of the water wave equations from first principles. Reference [15] discusses the physics and derivation of the water wave equations from fundamental laws of nature.

The extent to which the results presented here, transfer to real water waves depend on the assumptions used in deriving the water-wave equations. In Chapter 5 I provide some evidence in favor of the present model. There I compare theoretical predictions with experimental data and observe good agreement. This agreement upholds the applicability of the equations (1a-1d) to real flows.

Chapter 2

THE METHOD OF FOKAS AND GLOBAL RELATIONS

In this chapter, I introduce a method for solving boundary-value problems for linear constant coefficient partial differential equations. The method is relatively new. It was discovered by A. S. Fokas in his quest to generalize the method of inverse scattering, which solves the IVP for $x \in \mathbb{R}$ for so-called soliton equations (*e.g.* Korteweg-deVries, Nonlinear Schrödinger, *etc.*), to BVPs posed either on the half line $x \geq 0$ or on the finite interval $x \in [0, L]$ [35, 36, 38]. It was observed immediately [37, 40] that the method produces interesting results for linear equations as well. Just like the classical method of separation of variables, the method of Fokas produces an explicit solution for the dependent variable $u(x, t)$. Although the method of Fokas is more general, in this chapter I restrict the discussion to scalar problems with one spatial independent variable x and one temporal independent variable t. An initial- or boundary-value problem (IVP or BVP) is considered solved if an expression for $u(x, t)$ is constructed as a function of the independent variables (x, t) and of the given initial and boundary conditions. Such an expression should have explicit dependence on x and t. The solution formula obtained through the method of Fokas is in terms of one or more integrals along paths in the complex plane of an auxiliary variable k. The goal here is to give the reader some understanding of Fokas's method and of global relations. For a short introduction with several examples see [29]. See [38] for a more detailed discussion and connections to boundary-value problems for nonlinear integrable PDEs. The new method has several advantages over the standard tools for solving constant coefficient problems.

- The method of Fokas encompasses the standard methods. For those cases where a standard method produces an explicit solution, the method of Fokas does so as well. In fact, as shown in several examples below, the resulting solution formulas are equivalent, as one would expect.

- It is more general than the standard methods: one can obtain solution formulas for many problems where the classical methods are not applicable. This is particularly clear for problems containing higher than second-order derivatives.

- Where the standard methods are a collection of situation-specific approaches, tailored to specific equations and boundary conditions, the method of Fokas produces a solution using the same ideas for all these different problems, with the differences appearing only in the calculational details.

- In addition to producing an explicit formula for the solution, the method allows one to determine in a straight-forward way how many and which boundary conditions result in a well-posed problem. Especially for BVPs for equations with more than second-order derivatives, this is a nontrivial issue.

- The background required for the method is limited to the knowledge of the Fourier and inverse Fourier transform pair, the Residue Theorem and Jordan's Lemma, see [1] or [6], for instance.

We start by revisiting the IVP on the whole line in the framework of the new method, see Section 2.1. This merely results in the construction of the familiar Fourier transform expression for the solution, but it does allow us to generalize the approach to the half-line and finite interval problems more naturally. Section 2.2 discusses the problem on the half-line. For details on the finite-interval problem see [29, 38] and for problems with periodic boundary conditions see [64]. Appendix A to this thesis presents a non-trivial extension of Fokas's method to PDEs with mixed partial derivatives considered on the half-line as well as the finite interval. In particular, certain boundary conditions for PDEs with mixed partial derivatives are ill-posed in the sense that initial and boundary conditions cannot be imposed independently of one another.

In the following discussion the reader will find examples of problems that can be solved using the standard methods, in which case I demonstrate the equivalence of the classical results with those obtained using Fokas's method. Other examples illustrate the use of

the method in situations where the standard methods fail or are unable to proceed. The emphasis is not on rigor and no comments are made about function spaces. I assume whatever conditions are necessary for the calculations to proceed: for instance, functions are at least as differentiable as dictated by the equation, and boundary and initial conditions are compatible at $(x,t) = (0,0)$. The aim is to generate formal expressions for the solution which may be verified or studied rigorously.

2.1 The initial-value problem on the whole line

In contrast to a traditional introduction to PDEs we begin by considering the IVP for linear constant coefficient equations on the entire real line. Fokas's method is the appropriate generalization of Fourier transform methods to boundary-value problems. As such, it will be informative to review the problem on the whole-line. Consider the IVP for the heat equation:

$$q_t = q_{xx}, \qquad x \in \mathbb{R},\ t \in (0,T], \tag{1a}$$

$$q(x,0) = q_0(x), \qquad x \in \mathbb{R}, \tag{1b}$$

where subscripts denote partial differentiation. Here T is a positive real number, and $q_0(x)$ is a function on $\mathbb{R}$, decaying sufficiently fast as $|x| \to \infty$. The solution to this problem is given by

$$q(x,t) = \frac{1}{2\pi}\int_{-\infty}^{\infty} \hat{q}_0(k) e^{ikx-\omega(k)t} dk, \tag{2}$$

where $\omega(k) = k^2$ is the dispersion relation[1] for the heat equation, and $\hat{q}_0(k)$ is the Fourier transform of the initial condition:

$$\hat{q}_0(k) = \int_{-\infty}^{\infty} q_0(x) e^{-ikx} dx. \tag{3}$$

Further, letting $T \to \infty$ does not affect the validity of the solution. In a traditional text, this result is obtained by taking the Fourier transform of the original PDE (1a). This results in a one-parameter family of ordinary differential equations (ODEs) with parameter

[1]For consistency with the literature on Fokas's method [38], I adopt the convention that the dispersion relation $\omega(k)$ is found by substitution of $\exp(ikx - \omega(k)t)$ in the PDE.

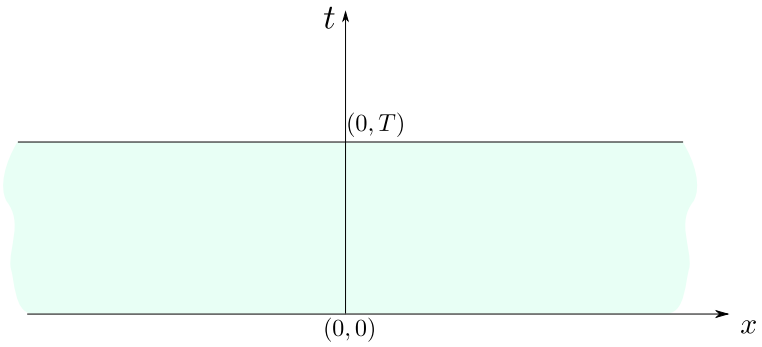

Figure 2.1: The region of integration in the (x, t) plane for problems posed on the whole-line.

k. Solving this ODE gives the Fourier transform of the solution at any time t. Using the inverse transform, the above result is obtained.

In the new approach, we start by rewriting the heat equation as a one-parameter family of PDEs in divergence form

$$\partial_t \rho(x,t,k) + \partial_x j(x,t,k) = 0, \tag{4}$$

where

$$\rho(x,t,k) = e^{-ikx+\omega(k)t} q,$$

with $k \in \mathbb{C}$. Equation (4) is known as the *local relation*. The explicit form of j is easily obtained using integration by parts:

$$\begin{aligned}
\left(e^{-ikx+\omega(k)t}q\right)_t &= \omega(k)e^{-ikx+\omega(k)t}q + e^{-ikx+\omega(k)t}q_t \\
&= \omega(k)e^{-ikx+\omega(k)t}q + e^{-ikx+\omega(k)t}q_{xx} \\
&= \omega(k)e^{-ikx+\omega(k)t}q + \left(e^{-ikx+\omega(k)t}q_x\right)_x + ike^{-ikx+\omega(k)t}q_x \\
&= \omega(k)e^{-ikx+\omega(k)t}q + \left(e^{-ikx+\omega(k)t}q_x\right)_x + \left(ike^{-ikx+\omega(k)t}q\right)_x - k^2 e^{-ikx+\omega(k)t}q \\
&= \left(e^{-ikx+\omega(k)t}(q_x + ikq)\right)_x,
\end{aligned} \tag{5}$$

so that $j = -e^{-ikx+\omega(k)t}(q_x + ikq)$. Note that this calculation also determines $\omega(k)$.

We are now in a position to apply Green's Theorem in the (x, t) plane. Consider (5) on an infinite horizontal strip $\mathcal{D}$ of height T (see Figure 2.1). Using the decay properties of the

solution where necessary, we have

$$\begin{aligned}
&\iint_{\mathcal{D}} \left(\left[e^{-ikx+\omega(k)s} q(x,s) \right]_s - \left[e^{-ikx+\omega(k)s} (q_x(x,s) + ikq(x,s)) \right]_x \right) dsdx = 0 \\
\Rightarrow \quad &\int_{\partial\mathcal{D}} \left(e^{-ikx+\omega(k)s} q(x,s)dx + e^{-ikx+\omega(k)s} (q_x(x,s) + ikq(x,s))ds \right) = 0 \\
\Rightarrow \quad &\int_{-\infty}^{\infty} e^{-ikx} q_0(x)dx - \int_{-\infty}^{\infty} e^{-ikx+\omega(k)T} q(x,T)dx = 0 \\
\Rightarrow \quad &\int_{-\infty}^{\infty} e^{-ikx} q(x,T)dx = e^{-\omega(k)T} \int_{-\infty}^{\infty} e^{-ikx} q_0(x)dx. \qquad (6)
\end{aligned}$$

Under the assumption that the solution decays uniformly in t for large $|x|$, the contribution of the second integrand on the second line vanishes. In the next section, we will observe how such terms lead to contributions from the boundary data. The last line relates the Fourier transform of the solution at time T to the Fourier transform of the initial value $q_0(x)$, as expected. Inverting the transform we obtain the solution (2).

Although it appears we have obtained the traditional result in a roundabout way, I claim progress has been made. The procedure used here is particularly suited for solving problems other than those posed on the whole line. By working with different domains (as those used below) for the application of Green's Theorem to the local relation we shall obtain the integral expressions for solutions to the corresponding BVP.

Remark 2.1.1 *The procedure above works equally well for equations other than the heat equation. In fact, the solution formula (2) stands as is, as long as the appropriate dispersion relation is filled in, see the Appendix of [4] for details. For problems on the half-line, more detail is found below.*

Remark 2.1.2 *The conversion of the PDE to the local relation (4) is always possible for linear constant coefficient PDEs [38]. The explicit form of $j(x,t,k)$ in terms of $\omega(k)$, avoiding integration by parts, is given in (42).*

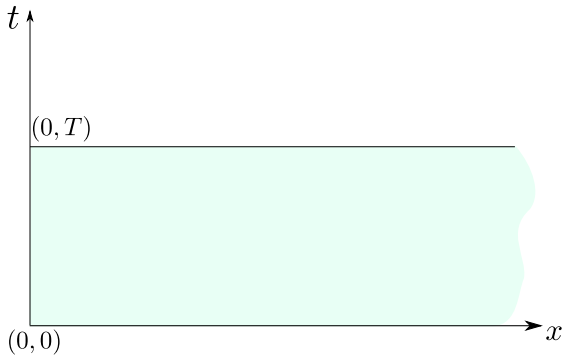

Figure 2.2: The region of integration in the (x, t) plane for boundary-value problems posed on the positive half-line.

2.2 The problem on the half line

2.2.1 The heat equation with Dirichlet boundary conditions

In section 2.1 the heat equation on the whole real line was solved. The success of this method was due to the properties of the Fourier transform which incorporates the "boundary condition" of decay at infinity. In this section we solve the heat equation on the half line with Dirichlet boundary data:

$$q_t = q_{xx}, \qquad x > 0,\ t \in (0, T], \tag{7a}$$

$$q(x, 0) = q_0(x), \qquad x \geq 0, \tag{7b}$$

$$q(0, t) = g_0(t), \qquad t \in [0, T]. \tag{7c}$$

Let us begin by considering the local relation of the heat equation (5), which holds independent of the solution domain and the boundary conditions, as it is a local statement. Applying Green's Theorem to this equation with the domain of integration $\mathcal{R} = \{x \geq 0,\ 0 < t \leq T\}$ (see Figure 2.2) we obtain

$$\int_{\partial\mathcal{R}} \left(e^{-ikx+\omega(k)s} q(x,s)dx + e^{-ikx+\omega(k)s}(q_x(x,s) + ikq(x,s))ds \right) = 0$$

$$\Rightarrow \quad \int_0^\infty e^{-ikx} q_0(x)dx - \int_0^\infty e^{-ikx+\omega(k)T} q(x,T)dx - \int_0^T e^{\omega(k)s}(q_x(0,s) + ikq(0,s))ds = 0$$

$$\Rightarrow \quad \int_0^\infty e^{-ikx} q_0(x)dx - \int_0^T e^{\omega(k)s}(q_x(0,s) + ikq(0,s))ds = e^{\omega(k)T} \int_0^\infty e^{-ikx} q(x,T)dx$$

$$\Rightarrow \quad \hat{q}_0(k) - [\tilde{g}_1(\omega(k),T) + ik\tilde{g}_0(\omega(k),T)] = e^{\omega(k)T}\hat{q}(k,T), \tag{8}$$

where $\partial\mathcal{R}$ denotes the boundary of the domain $\mathcal{R}$, oriented so that $\mathcal{R}$ is on the left when the boundary is traversed. Further, $\hat{q}_0, \hat{q}$ are the Fourier transforms of the initial condition and the solution at time T respectively. Similarly, $\tilde{g}_0$ and $\tilde{g}_1$ are defined in terms of the boundary data as

$$\tilde{g}_0(\omega,T) = \int_0^T e^{\omega s} q(0,s)ds, \quad \tilde{g}_1(\omega,T) = \int_0^T e^{\omega s} q_x(0,s)ds.$$

Equation (8) is the global relation for the heat equation on the half line. The time transforms $\tilde{g}_0, \tilde{g}_1$ arise because of the presence of the boundary at $x = 0$. For the problem under consideration, the Dirichlet data are given, so $\tilde{g}_0$ is determined, whereas $\tilde{g}_1$ is not.

The spectral parameter k associated with the Fourier transform is typically real. However, the terms in the global relation (8) are analytic for $\mathrm{Im}(k) < 0$. Indeed, the Fourier transforms may be analytically continued into the lower-half of the complex k plane, assuming sufficient decay of $q(x,t)$ for large x and all t. Further, the time transforms $(\tilde{g}_0, \tilde{g}_1)$ are entire functions (analytic and bounded for all finite k).

Remark 2.2.1 *The continuation of the global relation into the lower half plane, for the equation on the half line, should be contrasted with the "global relation" for the whole-line case (6) where such an extension to complex k is not possible.*

The global relation (8) is equally valid for any $t \in (0,T]$. Replacing T by t in the global relation (8) and inverting the Fourier transform we arrive at an integral expression

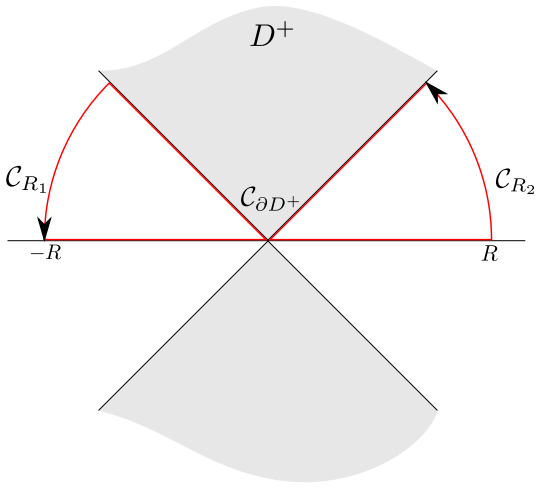

Figure 2.3: The domain D for the heat equation is indicated in gray. The contour $\mathcal{C}$, shown in red, is used to justify the deformation of the line-integral along the real line up to the boundary of D^+.

for $q(x,t)$:

$$\hat{q}_0(k) - [\tilde{g}_1(\omega(k),t) + ik\tilde{g}_0(\omega(k),t)] = e^{\omega(k)t}\hat{q}(k,t)$$

$$\Rightarrow \quad q(x,t) = \frac{1}{2\pi}\int_{-\infty}^{\infty} e^{ikx-\omega(k)t}\hat{q}_0(k)dk - \frac{1}{2\pi}\int_{-\infty}^{\infty} e^{ikx-\omega(k)t}[\tilde{g}_1(\omega(k),t) + ik\tilde{g}_0(\omega(k),t)]dk. \tag{9}$$

Let $D = \{k \in \mathbb{C} \,:\, \mathrm{Re}(\omega(k)) < 0\}$. Further, let $D^+ = D \cap \mathbb{C}^+$ where $\mathbb{C}^+ = \{k \in \mathbb{C} : \mathrm{Im}(k) > 0\}$. The integrand of the second integral in (9) is entire and decays as $k \to \infty$ for $k \in \mathbb{C}^+ \backslash D^+$. Consider a contour $\mathcal{C} = [-R, R] \cup \mathcal{C}_{R_2} \cup \mathcal{C}_{\partial D^+} \cup \mathcal{C}_{R_1}$ as shown in red in Figure 2.3. Let $\mathcal{C}_{\partial D^+}$ be the part of $\mathcal{C}$ on the boundary of D^+ and $\mathcal{C}_{R_1}$, $\mathcal{C}_{R_2}$ be circular arcs of radius R. Using the analyticity of the integrand

$$\int_{\mathcal{C}} e^{ikx-\omega(k)t}\tilde{g}(\omega(k),t)dk = \left(\int_{-R}^{R} + \int_{\mathcal{C}_{R_2}} + \int_{\mathcal{C}_{\partial D^+}} + \int_{\mathcal{C}_{R_1}}\right) e^{ikx-\omega(k)t}\tilde{g}(\omega(k),t)dk = 0, \tag{10}$$

where $\tilde{g}(\omega(k),t) = \tilde{g}_1(\omega(k),t) + ik\tilde{g}_0(\omega(k),t)$. Taking the limit $R \to \infty$ of the above expression, contour $\mathcal{C}_{\partial D^+}$ becomes the contour $-\partial D^+$. The negative sign arises from the convention that the positive orientation of a boundary is defined so that the region is to

the left as the boundary is traversed. Further, an application of Jordan's Lemma in the wedge-like regions shows that for large R, the contribution of the integrals along $\mathcal{C}_{R_1}$ and $\mathcal{C}_{R_2}$ vanishes. Thus the integral of $\exp(ikx - \omega(k)t)\tilde{g}(\omega(k), t)$ along the real line may be replaced by one along ∂D^+. Thus

$$q(x,t) = \frac{1}{2\pi}\int_{-\infty}^{\infty} e^{ikx-\omega(k)t}\hat{q}_0(k)dk - \frac{1}{2\pi}\int_{\partial D^+} e^{ikx-\omega(k)t}\left[\tilde{g}_1(\omega(k),t) + ik\tilde{g}_0(\omega(k),t)\right]dk. \tag{11}$$

Summarizing the argument, the contour $\mathcal{C}$ may be replaced by $\partial(\mathbb{C}^+\backslash D^+)$ as $R \to \infty$. The integral of $\exp(ikx - \omega(k)t)\tilde{g}(\omega(k), t)$ along $\partial(\mathbb{C}^+\backslash D^+)$ is zero due to the analyticity and decay properties of the integrand. Adding this integral to the right-hand side of (9) we obtain (11).

Although (11) is an expression for $q(x,t)$, it does not present a solution since it depends on boundary data we have not prescribed through $\tilde{g}_1$, the transform of the Neumann data. To resolve this problem, we could solve the global relation (8) for $\tilde{g}_1$. This results in an expression for $\tilde{g}_1$ valid in $\mathbb{C}^- = \{k : \mathrm{Im}(k) < 0\}$, whereas (11) requires an expression for $\tilde{g}_1$ valid along ∂D^+. To this end we seek a transform that maps the contour ∂D^+ to a contour in the lower-half plane $\mathbb{C}^-$ but leaves $\tilde{g}_1(\omega(k), t)$ invariant. Thus we turn to the discrete symmetries of $\omega(k) = k^2$. The dispersion relation $\omega(k)$ is invariant under the transform $k \to -k$. Applying this transformation to the global relation (8) (and replacing T by t) we have

$$\hat{q}(-k,t) = e^{-\omega(k)t}\hat{q}_0(-k) - e^{-\omega(k)t}[\tilde{g}_1(\omega(k),t) - ik\tilde{g}_0(\omega(k),t)], \quad \mathrm{Im}(k) \geq 0. \tag{12}$$

Solving this version of the global relation yields an expression for $\tilde{g}_1(\omega(k), t)$ which *is* valid along ∂D^+. The integral expression for $q(x,t)$ becomes

$$\begin{aligned} q(x,t) =& \frac{1}{2\pi}\int_{-\infty}^{\infty} e^{ikx-\omega(k)t}\hat{q}_0(k)dk - \frac{1}{2\pi}\int_{\partial D^+} e^{ikx-\omega(k)t}\left[2ik\tilde{g}_0(\omega(k),t) + \hat{q}_0(-k)\right]dk \\ &+ \frac{1}{2\pi}\int_{\partial D^+} e^{ikx}\hat{q}(-k,t)dk. \end{aligned} \tag{13}$$

The above expression does not depend on the unknown boundary data. However, the function we wish to solve for, $q(x,t)$, also appears in the third integral on the right-hand side. Using analyticity, this problem is resolved as follows. The function $\hat{q}(-k,t)$ is bounded

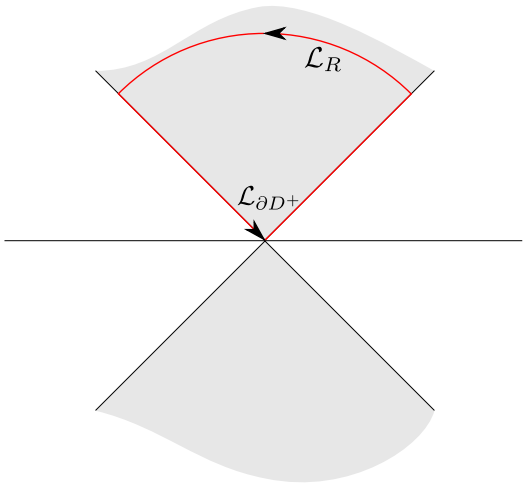

Figure 2.4: The contour $\mathcal{L}$ is shown in red. Application of Cauchy's Integral Theorem using this contour allows one to eliminate the contribution of $\hat{q}(-k,t)$ from the integral expression (13).

and analytic in $\mathbb{C}^+$ with $\hat{q}(-k,t) \to 0$ uniformly as $k \to \infty$. This implies that the integral of $\exp(ikx)q(-k,t)$ along a closed, bounded curve in $\mathbb{C}^+$ vanishes. In particular, consider the closed curve $\mathcal{L} = \mathcal{L}_{\partial D^+} \cup \mathcal{L}_R$ where $\mathcal{L}_{\partial D^+} = \partial D^+ \cap \{k : |k| < R\}$ and $\mathcal{L}_R = \{k \in D^+ : |k| = R\}$ (see Figure 2.4). We have

$$\int_{\mathcal{L}} e^{ikx}\hat{q}(-k,t)dk = \int_{\mathcal{L}_{\partial D^+}} e^{ikx}\hat{q}(-k,t)dk + \int_{\mathcal{L}_R} e^{ikx}\hat{q}(-k,t)dk = 0. \tag{14}$$

If it can be shown that the integral along $\mathcal{L}_R$ vanishes for large R, then the third integral on the right-hand side of (13) must also vanish since the contour $\mathcal{L}_{\partial D^+}$ becomes ∂D^+ as $R \to \infty$. From Jordan's Lemma, the uniform decay of $\hat{q}(-k,t)$ for large k is precisely the condition required for the integral to vanish. Thus

$$q(x,t) = \frac{1}{2\pi}\int_{-\infty}^{\infty} e^{ikx-\omega(k)t}\hat{q}_0(k)dk - \frac{1}{2\pi}\int_{\partial D^+} e^{ikx-\omega(k)t}\left[\hat{q}_0(-k) + 2ik\tilde{g}_0(\omega(k),t)\right]dk \tag{15}$$

is the solution to the Dirichlet problem for the heat equation on the half line.

The above calculation indicates that in solving equation (12) for $\tilde{g}_1$, the contribution of $\hat{q}(-k,t)$ vanishes from the final expression for the solution. In effect we have found a map from the given initial condition and Dirichlet data to the unknown Neumann condition.

Consider (12) with t replaced by T, multiply by $ike^{-\omega(k)t}$ and integrate along the contour ∂D^+ to obtain

$$\int_{\partial D^+} ike^{\omega(k)(T-t)}\hat{q}(-k,T)dk = \int_{\partial D^+} ike^{-\omega(k)t}\hat{q}_0(-k)dk - \int_{\partial D^+} ike^{-\omega(k)t}\tilde{g}_1(\omega(k),T)dk - \int_{\partial D^+} k^2 e^{-\omega(k)t}\tilde{g}_0(\omega(k),T)dk. \tag{16}$$

The left-hand side is zero, whereas the second term on the right-hand side equals $\pi q_x(0,t)$ using the change of variables $k^2 = il$ and the classical Fourier transform. The term involving $\tilde{g}_0$ requires more attention. Since $\omega(k) = k^2$, we have

$$\begin{aligned} -\int_{\partial D^+} k^2 e^{-\omega(k)t}\tilde{g}_0(\omega(k),T)dk &= -\int_{\partial D^+} k^2 \int_0^T e^{\omega(k)(s-t)} q(0,T)\, dsdk, \\ &= \int_{\partial D^+} \left(q(0,0)e^{-k^2 t} - e^{k^2(T-t)}q(0,T) + \int_0^T e^{k^2(s-t)}\dot{q}(0,s)ds \right) dk, \end{aligned}$$

after integration by parts. The dot denotes differentiation with respect to the s variable. The compatibility of initial and boundary condition at the corner $(x,t) = (0,0)$ implies $q(0,0) = g(0)$. The first integral on the right-hand side can be deformed back to the real line to obtain

$$\int_{\partial D^+} e^{-k^2 t} g(0)dk = \int_{-\infty}^{\infty} e^{-k^2 t} g(0)dk = \sqrt{\pi} g(0).$$

The integrand of the second term on the right-hand side is analytic, bounded and decaying in D^+. Hence it yields a zero contribution. The final integral on the right-hand side is split as follows

$$\begin{aligned} \int_{\partial D^+} \int_0^T e^{k^2(s-t)}\dot{q}(0,s)dsdk &= \int_{\partial D^+} \left(\int_0^t + \int_t^T \right) e^{k^2(s-t)}\dot{q}(0,s)dsdk \\ &= \int_{\partial D^+} \int_0^t e^{k^2(s-t)}\dot{q}(0,s)dsdk, \end{aligned}$$

since Cauchy's Theorem implies the second integral vanishes. Deforming this integral back to the real line and switching orders of integration, the k-integral can be computed directly to obtain

$$\int_{\partial D^+} \int_0^T e^{k^2(s-t)}\dot{q}(0,s)dsdk = \sqrt{\pi} \int_0^t \frac{\dot{q}(0,s)}{\sqrt{t-s}} ds.$$

Combining these results, we have

$$q_x(0,t) = -\int_{\partial D^+} ike^{-\omega(k)t}\hat{q}_0(-k)dk - \frac{g(0)}{\sqrt{\pi}} - \frac{1}{\sqrt{\pi}} \int_0^t \frac{\dot{g}(s)}{\sqrt{t-s}} ds, \quad t > 0.$$

Hence we obtain an explicit map from the given initial and boundary conditions to the unknown Neumann boundary value. Although, we did not require this explicit form in our solution (15), the respective integrals may be rearranged to see that the above expression is indeed present in the final solution. Thus, solving the global relation for the transform of the unknown boundary condition is equivalent to obtaining the Dirichlet→Neumann map. In other words, the global relation defines the map from the known to unknown boundary conditions.

Let us summarize the steps involved in solving boundary value problems on the half-line.

1. Using the dispersion relation $\omega(k)$ define the regions $D = \{k : \mathrm{Re}(\omega(k)) < 0\}$, $D^+ = D \cap \mathbb{C}^+$ and $D^- = D \cap \mathbb{C}^-$.

2. The PDE is rewritten as a one-parameter family of equations in divergence form. Applying Green's Theorem in the (x,t) plane, we obtain the global relation. By considering complex values for the spectral parameter k, extend the domain of definition of the global relation. For problems posed on the half line, the global relation is valid in $\mathrm{Im}(k) \leq 0$.

3. The global relation is solved for $\hat{q}(k,t)$. The integral expression for $q(x,t)$ is constructed by inverting the Fourier transform. The integral involving the boundary terms is deformed off the real line. For problems on the half line, we deform up to ∂D^+.

4. The discrete symmetries $\nu(k)$ of $\omega(k)$, $\omega(k) = \omega(\nu(k))$, are used to obtain additional versions of the global relation valid for k in certain regions of $\mathbb{C}^+$. These additional global relations are solved simultaneously for the transforms of the unknown boundary data. The expressions thus obtained are substituted into the integral expression for $q(x,t)$.

5. The integral expression for $q(x,t)$ now depends on $\hat{q}(\nu(k),t)$. Analyticity considerations are used to evaluate the contribution of $\hat{q}(\nu(k),t)$. Typically this contribution

vanishes. The functions $\hat{q}(\nu(k),t)$ and $\exp(ikx)$ are bounded and analytic in the upper-half plane. If the coefficient of $\exp(ikx)\hat{q}(\nu(k),t)$ in the integral expression is also analytic in D^+, then the contribution of this term is zero. For instance, this happens for the Dirichlet problem for the heat equation posed on the half line where this coefficient is a constant. Let us now consider the case when this coefficient has a simple pole at some point $k = k_0$ in D^+. An application of the Residue Theorem shows that we need the value of $\hat{q}(\nu(k_0),t)$. At this point, the global relation is used once more. The global relation connects the transform of the solution at time t to the transforms of both the known initial-boundary conditions and the unknown boundary conditions. Evaluating the global relation at $k = \nu(k_0)$, we obtain an expression for $\hat{q}(\nu(k_0),t)$. If this expression depends only on known initial-boundary conditions (*i.e.* the coefficients of the unknown terms add up to zero) we have solved the problem. The presence of unknown boundary conditions hints at an ill-posed problem. Note that we select only those transformations $\nu(k)$ whose image lies in the lower-half plane. Consequently $\hat{q}(\nu(k_0),t)$ is defined.

Remark 2.2.2 *For the Neumann problem, when $q_x(0,t)$ is supplied as the boundary condition, we can just as easily solve the global relation for $\tilde{g}_0$. The integral involving $\hat{q}(-k,t)$ vanishes for the same reason as for the Dirichlet problem [38]. Further, one may define the Neumann→Dirichlet map in an analogous manner to that described above for the Dirichlet problem.*

Remark 2.2.3 *The classical solution in terms of the sine transform may be recovered from the solution to the heat equation (15). Note that $\hat{q}_0(-k)$ is analytic and bounded in the upper-half plane and $\exp(-\omega(k)t)k\tilde{g}_0(\omega(k),t)$ is bounded and analytic in the region between D^+ and the real line. Thus the contour ∂D^+ may be deformed back to the real line:*

$$q(x,t) = \frac{1}{2\pi}\int_{-\infty}^{\infty} e^{ikx-\omega(k)t}\hat{q}_0(k)dk - \frac{1}{2\pi}\int_{-\infty}^{\infty} e^{ikx-\omega(k)t}(\hat{q}_0(-k) + 2ik\tilde{g}_0(\omega(k),t))dk.$$

By splitting the integral along the real line into integrals from $-\infty$ to 0 and from 0 to ∞,

and using the definition of sine in terms of exponentials, we obtain

$$q(x,t) = \frac{2}{\pi}\int_0^\infty e^{-\omega(k)t}\sin(kx)\left[\int_0^\infty \sin(ky)q(y,0)dy - k\tilde{g}_0(\omega(k),t)\right]dk.$$

This deformation back to the real line is not possible for all PDEs. In particular the deformation is possible only when a classical transform exists. Also note, that unlike the integral representation (15), the sine transform solution is not uniformly convergent at $x = 0$. Further, using methods like steepest descent or stationary phase, the contribution due to the boundary can be evaluated much more efficiently in (15) than in the classical sine transform solution, see [33].

Remark 2.2.4 *An alternative to the new method is the use of Laplace transforms in t. This results in multivalued integral kernels due to the presence of radicals. Consequently, the inversion of the Laplace transform involves contour integrals along branch cuts,* e.g *see example on pg.* 358 *of [68]. For spatial derivatives of order greater than two, this procedure quickly becomes far more involved. Further, the Laplace transform involves an integration over all time $t \geq 0$. This seems to contradict causality for evolution problems. For evolution equations we do not expect the solution at time $t = T$ to depend on times greater than T.*

2.2.2 A third-order PDE with Dirichlet boundary conditions

As a second example consider the following problem, posed again on the half line:

$$q_t + q_{xxx} = 0, \qquad x \geq 0,\ t \in (0,T], \tag{17a}$$

$$q(x,0) = q_0(x), \qquad x \geq 0, \tag{17b}$$

$$q(0,t) = g_0(t), \qquad t \in (0,T]. \tag{17c}$$

We follow the steps outlined in the previous section.

1. *Dispersion relation.* The dispersion relation for the PDE is $\omega(k) = -ik^3$. Using

$$\omega(k) = -i|k|^3[\cos(3\arg k) + i\sin(3\arg k)],$$

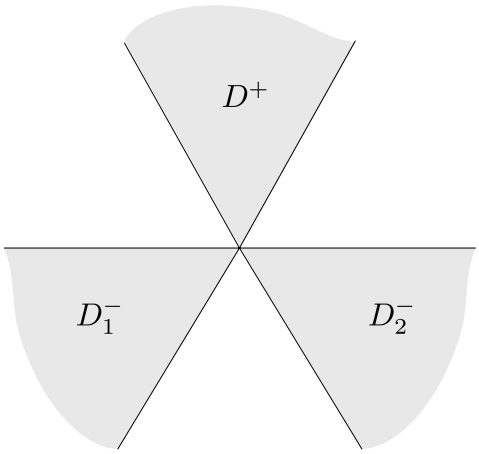

Figure 2.5: Domain $D = \{k : \mathrm{Re}(\omega(k)) < 0\}$ for the third-order PDE (17a).

we define the region D (where $\mathrm{Re}(\omega(k)) < 0$) as

$$D = \left\{ k : \arg k \in \left(\frac{\pi}{3}, \frac{2\pi}{3}\right) \cup \left(\pi, \frac{4\pi}{3}\right) \cup \left(\frac{5\pi}{3}, 2\pi\right) \right\},$$

so that

$$D^+ = \left\{ k : \arg k \in \left(\frac{\pi}{3}, \frac{2\pi}{3}\right) \right\},$$

and

$$D^- = D_1^- \cup D_2^-,$$

where

$$D_1^- = \left\{ k : \arg k \in \left(\pi, \frac{4\pi}{3}\right) \right\}, \quad D_2^- = \left\{ k : \arg k \in \left(\frac{5\pi}{3}, 2\pi\right) \right\}.$$

See Figure 2.5 for a depiction of these regions.

2. *Global relation.* Using the same method as before, we find the local relation

$$\left(e^{-ikx+\omega(k)t}q\right)_t + \left(e^{-ikx+\omega(k)t}(q_{xx} + ikq_x + (ik)^2 q)\right)_x = 0,$$

which is easily verified. Integrating the above equation over the domain

$$\mathcal{R} = \{0 \le x < \infty, 0 < t \le T\}$$

and applying Green's Theorem, we obtain

$$\begin{aligned}
&\iint_{\mathcal{R}} \left(\left[e^{-ikx+\omega(k)s} q(x,s) \right]_s - \left[e^{-ikx+\omega(k)t} (-q_{xx} - ikq_x - (ik)^2 q) \right]_x \right) dsdx = 0 \\
\Rightarrow &\int_{\partial\mathcal{R}} \Big(e^{-ikx+\omega(k)s} q(x,s)dx + e^{-ikx+\omega(k)s} (-q_{xx}(x,s) - ikq_x(x,s) - (ik)^2 q(x,s))dt \Big) \\
&\qquad = 0 \qquad (18) \\
\Rightarrow &\int_0^\infty e^{-ikx} q(x,0)dx - \int_0^T e^{\omega(k)s} (-q_{xx}(0,s) - ikq_x(0,s) - (ik)^2 q(0,s))ds \\
&\qquad = \int_0^\infty e^{-ikx+\omega(k)T} q(x,T)dx \\
\Rightarrow &\hat{q}_0(k) - [k^2 \tilde{g}_0(\omega(k),T) - ik\tilde{g}_1(\omega(k),T) - \tilde{g}_2(\omega(k),T)] = e^{\omega(k)T} \hat{q}(k,T), \qquad (19)
\end{aligned}$$

where, as before, $\hat{q}_0(k)$ and $\hat{q}(k,T)$ represent the Fourier transform of the solution at time $t = 0$ and time $t = T$. The time transforms of the boundary data are given by

$$\tilde{g}_i(\omega,T) = \int_0^T e^{\omega s} \partial_x^i q(0,s)ds, \ i = 0,1,2.$$

Equation (19) is the global relation for the third-order PDE (17a) posed on the positive half-line . Note that it is valid for $\mathrm{Im}(k) \leq 0$.

3. *Integral expression.* Let

$$\tilde{g}(k,t) = k^2 \tilde{g}_0(\omega(k),t) - ik\tilde{g}_1(\omega(k),t) - \tilde{g}_2(\omega(k),t).$$

Replacing T by t in the global relation (19) and applying the inverse Fourier transform, we obtain

$$\begin{aligned}
& e^{\omega(k)t} \hat{q}(k,t) = \hat{q}_0(k) - \tilde{g}(k,t) \\
\Rightarrow \ & \hat{q}(k,t) = e^{-\omega(k)t} \hat{q}_0(k) - e^{-\omega(k)t} \tilde{g}(k,t) \\
\Rightarrow \ & q(x,t) = \frac{1}{2\pi} \int_{-\infty}^{\infty} e^{ikx-\omega(k)t} \hat{q}_0(k)dk - \frac{1}{2\pi} \int_{-\infty}^{\infty} e^{ikx-\omega(k)t} \tilde{g}(k,t)dk \\
\Rightarrow \ & q(x,t) = \frac{1}{2\pi} \int_{-\infty}^{\infty} e^{ikx-\omega(k)t} \hat{q}_0(k)dk - \frac{1}{2\pi} \int_{\partial D^+} e^{ikx-\omega(k)t} \tilde{g}(k,t)dk,
\end{aligned}$$

where the second integral on the last line has been deformed into the upper-half complex plane up to the boundary of D^+.

4. *Solving for the unknown boundary data.* As for the heat equation, the integral expression for $q(x,t)$ does not represent a solution due to presence of unknown boundary terms, here $\tilde{g}_1, \tilde{g}_2$. As before we use the discrete symmetries of $\omega(k)$. In this case, these are $\nu_1(k) = e^{\frac{2\pi i}{3}}k$ and $\nu_2(k) = e^{\frac{4\pi i}{3}}k$.

   Observe that for $k \in D^+$, $\nu_1(k) \in D_1^-$ and $\nu_2(k) \in D_2^-$. Applying these transformations to the global relation, for $k \in D^+$ with $\alpha = e^{\frac{2\pi i}{3}}$ we find

$$\begin{aligned}
\hat{q}_0(\alpha k) - \alpha^2 k^2 \tilde{g}_0(\omega(k),t) + i\alpha k \tilde{g}_1(\omega(k),t) + \tilde{g}_2(\omega(k),t) &= e^{\omega(k)t}\hat{q}(\alpha k,t), \\
\hat{q}_0(\alpha^2 k) - \alpha k^2 \tilde{g}_0(\omega(k),t) + i\alpha^2 k \tilde{g}_1(\omega(k),t) + \tilde{g}_2(\omega(k),t) &= e^{\omega(k)t}\hat{q}(\alpha^2 k,t).
\end{aligned}$$

   Given $q(x,0)$ and $q(0,t)$ (or $\hat{q}_0(k)$ and $\tilde{g}_0(\omega,t)$) we may solve the above two equations for the two unknowns $\tilde{g}_1$ and $\tilde{g}_2$, for k in D^+ to obtain

$$\begin{aligned}
ik\tilde{g}_1(\omega(k),t) &= -k^2\tilde{g}_0(\omega(k),t) + \frac{1}{\alpha(1-\alpha)}\left[\hat{q}_0(\alpha^2 k) - \hat{q}_0(\alpha k)\right] \\
&\quad + \frac{e^{\omega(k)t}}{\alpha(1-\alpha)}\left[\hat{q}(\alpha k,t) - \hat{q}(\alpha^2 k,t)\right], \\
\tilde{g}_2(\omega(k),t) &= -k^2\tilde{g}_0(\omega(k),t) + \frac{1}{\alpha(1-\alpha)}\left[\alpha^2\hat{q}_0(\alpha k) - \alpha\hat{q}_0(\alpha^2 k)\right] \\
&\quad + \frac{e^{\omega(k)t}}{\alpha(1-\alpha)}\left[-\alpha^2\hat{q}(\alpha k,t) + \alpha\hat{q}(\alpha^2 k,t)\right].
\end{aligned}$$

   These expressions are substituted into the integral expression for $q(x,t)$, resulting in

$$q(x,t) = \frac{1}{2\pi}\int_{-\infty}^{\infty} e^{ikx-\omega(k)t}\hat{q}_0(k)dk - \frac{1}{2\pi}\int_{\partial D^+} H(k,x,t)dk, \tag{20}$$

$$\begin{aligned}
H(k,x,t) =& e^{ikx-\omega(k)t}\left[3k^2\tilde{g}_0(\omega(k),t) - \alpha\hat{q}_0(\alpha k) - \alpha^2\hat{q}_0(\alpha^2 k)\right] \\
&+ e^{ikx}\left[-\alpha\hat{q}(\alpha k,t) - \alpha^2\hat{q}(\alpha^2 k,t)\right].
\end{aligned}$$

   Since α is the cube root of unity note that $\alpha^3 = 1$ and $1 + \alpha + \alpha^2 = 0$.

5. *Contribution of $\hat{q}(\nu(k),t)$.* The functions $\hat{q}(\alpha k,t)$ and $\hat{q}(\alpha^2 k,t)$ are bounded and analytic in D^+ and decay to zero uniformly as $k \to \infty$. Once again Jordan's Lemma

implies that these terms do not contribute to the final solution, which is given by

$$\begin{aligned} q(x,t) &= \frac{1}{2\pi}\int_{-\infty}^{\infty} e^{ikx-\omega(k)t}\hat{q}_0(k)dk - \frac{1}{2\pi}\int_{\partial D^+} 3k^2 e^{ikx-\omega(k)t}\tilde{g}_0(\omega(k),t)dk \\ &\quad + \frac{1}{2\pi}\int_{\partial D^+} e^{ikx-\omega(k)t}\left[\alpha\hat{q}_0(\alpha k) + \alpha^2\hat{q}_0(\alpha^2 k)\right]dk. \end{aligned} \tag{21}$$

The classical *method of images* approach, by which one obtains the sine transform solution to the heat equation, cannot be applied to this third-order PDE (or for any PDE which involves odd order derivatives in x). For the third-order problem considered here, since $\hat{q}(\alpha k)$ is not bounded in the region $\{\arg(k) \in [0, \pi/3]\}$, Jordan's Lemma may not be applied in order to justify the deformation of the contour integral back to the real line. This would seem to imply that an integral transform pair using integrals along the real line does not exist for this third-order PDE.

2.2.3 A (slightly) different third-order PDE

The two problems considered so far are well posed when only $q(0,t)$ is specified at the left boundary. Using a slight modification of the previous example I will illustrate what changes when more boundary conditions are required. Consider the following third-order PDE on the positive half-line:

$$q_t - q_{xxx} = 0. \tag{22}$$

Assume that an initial condition $q(x,0)$ has been given. The analysis of the global relation indicates the number and type of the boundary conditions that need to be prescribed in order for the problem to be well posed. The dispersion relation is

$$\omega(k) = ik^3, \tag{23}$$

and

$$D = \left\{k : \arg k \in \left(0, \frac{\pi}{3}\right) \cup \left(\frac{2\pi}{3}, \pi\right) \cup \left(\frac{4\pi}{3}, \frac{5\pi}{3}\right)\right\}. \tag{24}$$

Let $D^+ = D_1^+ \cup D_2^+$, where

$$D_1^+ = \left\{k : \arg k \in \left(\pi, \frac{\pi}{3}\right)\right\}, \quad D_2^+ = \left\{k : \arg k \in \left(\frac{2\pi}{3}, \pi\right)\right\}, \tag{25}$$

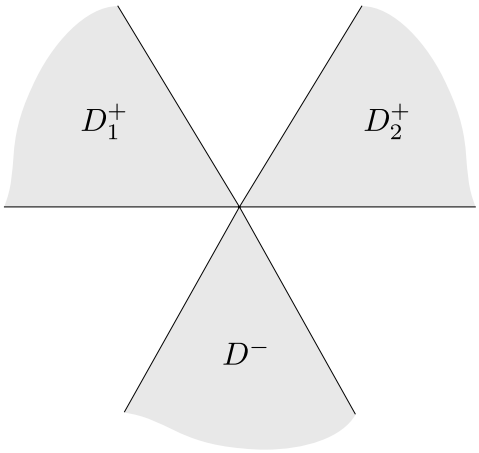

Figure 2.6: Domain $D = \{k : \mathrm{Re}(\omega(k)) < 0\}$ for the third-order PDE (22).

and

$$D^- = \left\{ k : \arg k \in \left(\frac{4\pi}{3}, \frac{5\pi}{3} \right) \right\},$$

see Figure 2.6.

The local relation is given by

$$(e^{-ikx+\omega(k)t}q)_t - \left(e^{-ikx+\omega(k)t}(q_{xx} + ikq_x - k^2 q)\right)_x = 0, \tag{26}$$

leading to the global relation (by integrating over the region $\mathcal{R} = \{x \geq 0,\ 0 < t \leq T\}$ and applying Green's theorem)

$$\hat{q}_0(k) - [-k^2\tilde{g}_0(\omega(k),t) + ik\tilde{g}_1(\omega(k),t) + \tilde{g}_2(\omega(k),t)] = e^{\omega(k)t}\hat{q}(k,t), \quad \mathrm{Im}(k) \leq 0. \tag{27}$$

The integral expression for the solution is

$$\begin{aligned} q(x,t) =& \frac{1}{2\pi}\int_{-\infty}^{\infty} e^{ikx-\omega(k)t}\hat{q}_0(k)dk - \frac{1}{2\pi}\int_{\partial D_1^+} e^{ikx-\omega(k)t}\tilde{g}(k,t)dk \\ & - \frac{1}{2\pi}\int_{\partial D_2^+} e^{ikx-\omega(k)t}\tilde{g}(k,t)dk, \end{aligned} \tag{28}$$

where

$$\tilde{g}(k,t) = -k^2\tilde{g}_0(\omega(k),t) + ik\tilde{g}_1(\omega(k),t) + \tilde{g}_2(\omega(k),t).$$

The symmetries of the global relation are as for the previous example. Hence if $k \in D_1^+, l \in D_2^+$ then $\alpha k, \alpha^2 l \in D^-$, where $\alpha = e^{\frac{2\pi i}{3}}$. We obtain the following versions of the global relation

$$\hat{q}_0(\alpha k) + \alpha^2 k^2 \tilde{g}_0(\omega(k), t) - i\alpha k \tilde{g}_1(\omega(k), t) - \tilde{g}_2(\omega(k), t) = e^{\omega(k)t} \hat{q}(\alpha k, t), \quad k \in D_1^+, \quad (29)$$

$$\hat{q}_0(\alpha^2 k) + \alpha k^2 \tilde{g}_0(\omega(k), t) - i\alpha^2 k \tilde{g}_1(\omega(k), t) - \tilde{g}_2(\omega(k), t) = e^{\omega(k)t} \hat{q}(\alpha^2 k, t), \quad k \in D_2^+. \quad (30)$$

Hence in each region, D_1^+ and D_2^+, there is one relation between the three quantities $\tilde{g}_i(\omega(k), t), i = 0, 1, 2$. Thus two boundary conditions are required at the left boundary in order to be able to solve the global relation for the unspecified boundary condition. For instance, given $q(0, t)$ and $q_x(0, t)$ we can calculate $\tilde{g}_0(\omega(k))$ and $\tilde{g}_1(\omega(k))$. The above relations can be used to obtain two expressions for $\tilde{g}_2(\omega(k))$, one valid for $k \in D_1^+$ and the other for $k \in D_2^+$. Substituting the resulting expressions into the integral expression for $q(x, t)$ we find the solution to (22) posed on the positive half-line.

2.2.4 A multi-term third-order PDE

For the problems above, the symmetries of the dispersion relation are easily found. With the present example I illustrate the use of Fokas's method if the symmetries are somewhat more complicated and the introduction of a branch cut is necessary. This method illustrates how to proceed in general, even if the symmetries cannot be written out explicitly. Consider

$$q_t = q_x + q_{xxx} = 0, \qquad x > 0, \quad (31)$$

where an initial condition $q(x, 0)$ is given. The previous example indicates that two boundary conditions are required on the left boundary, which we will verify in the process of solving the equation. As in the previous example, I shall skip some calculation details, which are similar to previous examples.

The dispersion relation is

$$\omega(k) = -ik + ik^3, \quad (32)$$

and

$$D = \left\{ k : k_I(1 + k_I^2 - 3k_R^2) < 0 \right\}, \quad (33)$$

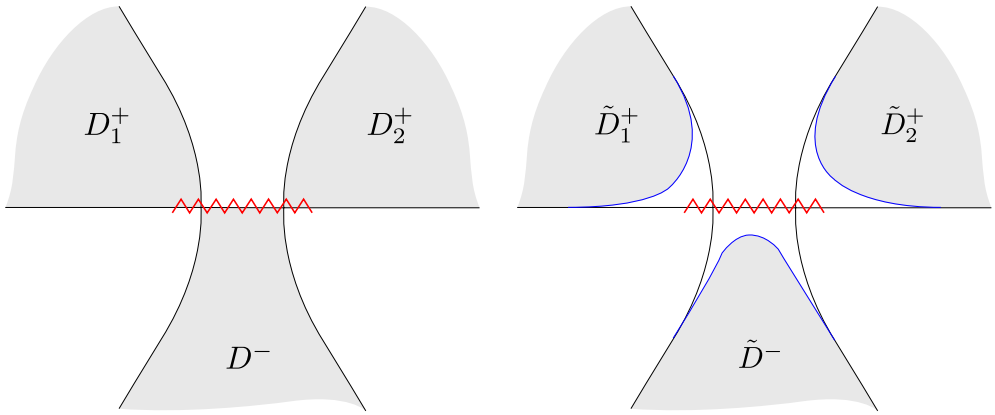

Figure 2.7: Domain $D = \{k : \mathrm{Re}(\omega(k)) < 0\}$ for the third-order PDE (left), and its deformation $\tilde{D}$ (right), for the third-order PDE (31). The branch cut $[-2/\sqrt{3}, 2/\sqrt{3}]$ is indicated by the jagged line.

where k_R and k_I denote the real and imaginary parts of k, respectively. The region D is shown on the left in Figure 2.7. The boundaries of the region consist of a hyperbola with asymptotes $k_I = \pm\sqrt{3}k_R$ and the real line. As above, define D^+ (D^-) to be the intersection of D with the upper (lower) half plane, and $D^+ = D_1^+ \cup D_2^+$, where

$$D_1^+ = \left\{k : D^+ \cap \text{second quadrant}\right\}, \quad D_2^+ = \left\{k : D^+ \cap \text{first quadrant}\right\}, \tag{34}$$

as indicated in Figure 2.7.

The local relation is given by

$$(e^{-ikx+\omega(k)t}q)_t - \left(e^{-ikx+\omega(k)t}(q_{xx} + ikq_x + (1-k^2)q)\right)_x = 0, \tag{35}$$

integrating over the region $\mathcal{R} = \{x \geq 0,\ 0 < t \leq T\}$ and using Green's theorem gives the global relation

$$\hat{q}_0(k) - \tilde{g}(k,t) = e^{\omega(k)t}\hat{q}(k,t), \quad \mathrm{Im}(k) \leq 0. \tag{36}$$

where $\tilde{g}(k,t) = (1-k^2)\tilde{g}_0(\omega(k),t) + ik\tilde{g}_1(\omega(k),t) + \tilde{g}_2(\omega(k),t)$. At this point, we might write an integral expression for $q(x,t)$ involving a contour integral over the boundary of D^+.

Before doing so, we examine the symmetries of the dispersion relation, as their functional form will influence what follows.

The discrete symmetries of $\omega(k)$ are found by solving $-ik + ik^3 = -i\nu(k) + i\nu^3(k)$ for $\nu(k)$. Eliminating the solution $\nu(k) = k$, we find

$$\nu = -\frac{k}{2} \pm \sqrt{1 - \frac{3k^2}{4}}.$$

This is a two-sheeted expression with branch points at $\pm\sqrt{3}/2$, leading to a choice of branch cut along $[-\sqrt{3}/2, \sqrt{3}/2]$. Define ν_1 to be the branch of ν which limits to $(-1/2+i\sqrt{3}/2)k = k\exp(2\pi i/3)$, and let ν_2 be the other branch, limiting to $k\exp(4\pi i/3)$. Our standard procedure would be to deform the integration over the real k axis to one along ∂D^+, leading to the expression

$$\begin{aligned} q(x,t) =& \frac{1}{2\pi}\int_{-\infty}^{\infty} e^{ikx-\omega(k)t}\hat{q}_0(k)dk - \frac{1}{2\pi}\int_{\partial D_1^+} e^{ikx-\omega(k)t}\tilde{g}(k,t)dk \\ &- \frac{1}{2\pi}\int_{\partial D_2^+} e^{ikx-\omega(k)t}\tilde{g}(k,t)dk, \end{aligned} \tag{37}$$

where

$$\tilde{g}(k,t) = (1-k^2)\tilde{g}_0(\omega(k),t) + ik\tilde{g}_1(\omega(k),t) + \tilde{g}_2(\omega(k),t).$$

This is problematic, since the integration paths ∂D_1^+ and ∂D_2^- contain the branch points and part of the branch cut. Instead, deform D to $\tilde{D}$ with its constituent parts $\tilde{D}_1^+$, $\tilde{D}_2^+$ and $\tilde{D}^-$, so that the boundary of these domains is separated from the branch cut. Although the integrands are growing as $k \to \infty$ in D, they are analytic in any bounded region, and this deformation has no overall effect, due to Cauchy's Theorem. The deformation from D to $\tilde{D}$ can be chosen in many ways, as long as $\tilde{D}$ has the same asymptotic form as D. Specifically, we may deform D_1^+ to $\tilde{D}_1^+$ and induce deformations on D_2^+ and D^- using $\tilde{D}_2^+ = \nu_2(\tilde{D}_1^+)$, $D^- = \nu_1(\tilde{D}_1^+)$, respectively. This leads to the solution formula

$$\begin{aligned} q(x,t) =& \frac{1}{2\pi}\int_{-\infty}^{\infty} e^{ikx-\omega(k)t}\hat{q}_0(k)dk - \frac{1}{2\pi}\int_{\partial \tilde{D}_1^+} e^{ikx-\omega(k)t}\tilde{g}(k,t)dk \\ &- \frac{1}{2\pi}\int_{\partial \tilde{D}_2^+} e^{ikx-\omega(k)t}\tilde{g}(k,t)dk. \end{aligned} \tag{38}$$

Next, we eliminate the dependence on unnecessary boundary conditions. In addition to (36), we have the following versions of the global relation:

$$\hat{q}_0(\nu_1(k)) - (1-\nu_1(k)^2)\tilde{g}_0(\omega(k),t) - i\nu_1(k)\tilde{g}_1(\omega(k),t) - \tilde{g}_2(\omega(k),t) = e^{\omega(k)t}\hat{q}(\nu_1(k),t), \qquad k \in \tilde{D}_1^+, \tag{39}$$

$$\hat{q}_0(\nu_2(k)) - (1-\nu_2(k)^2)\tilde{g}_0(\omega(k),t) - i\nu_2(k)\tilde{g}_1(\omega(k),t) - \tilde{g}_2(\omega(k),t) = e^{\omega(k)t}\hat{q}(\nu_2(k),t), \qquad k \in \tilde{D}_2^+. \tag{40}$$

As for the previous example, in each region, $\tilde{D}_1^+$ and $\tilde{D}_2^+$, there is one relation between the three quantities $\tilde{g}_i(\omega(k),t), i = 0,1,2$. Thus two boundary conditions are required at the left boundary in order to be able to solve the global relation for whichever boundary condition is unspecified.

2.2.5 A general evolution PDE

Fokas's method is also applicable to the general constant coefficient linear evolution PDE

$$q_t + \omega(-i\partial_x)q = 0, \quad x \geq 0,\ t \in (0,T]. \tag{41}$$

Here $\omega(k)$ is a polynomial of degree n. To ensure that solutions do not grow in time, let us impose that $\mathrm{Re}(\omega(k)) \geq 0$ for real k. Let

$$\omega(k) = \alpha_n k^n + \alpha_{n-1}k^{n-1} + \ldots + \alpha_0.$$

The large k limit of the condition $\mathrm{Re}(\omega(k)) \geq 0, k \in \mathbb{R}$ implies that if n is odd then $\alpha_n = \pm i$. For n even, $\mathrm{Re}(\alpha_n) \geq 0$. Using the dispersion relation, define the following regions in the complex k plane

$$D = \{k : \mathrm{Re}(\omega(k)) < 0\},$$

and

$$D^+ = D \cap \mathbb{C}^+, \quad D^- = D \cap \mathbb{C}^-.$$

The local relation is given by

$$\partial_t \left(e^{-ikx+\omega(k)t} q(x,t) \right) - \partial_x \left(e^{-ikx+\omega(k)t} \sum_{j=0}^{n-1} c_j(k) \partial_x^j q(x,t) \right) = 0,$$

where

$$\sum_{j=0}^{n-1} c_j(k)\partial_x^j q(x,t) = i\left(\frac{\omega(k)-\omega(l)}{k-l}\right)\Big|_{l=-i\partial_x} q(x,t). \tag{42}$$

The proof is straightforward [38]. Equation (42) implies the global relation

$$e^{\omega(k)T}\hat{q}(k,T) = \hat{q}_0(k) - \sum_{j=0}^{n-1} c_j(k)\tilde{g}_j(\omega(k),T), \quad \mathrm{Im}(k)\leq 0,$$

where

$$\tilde{g}_j(\omega,T) = \int_0^T e^{\omega s}\partial_x^j q(0,s)ds.$$

Applying the inverse Fourier transform to the global relation we obtain the integral expression for the solution

$$q(x,t) = \frac{1}{2\pi}\int_{-\infty}^{\infty} e^{-ikx+\omega(k)t}\hat{q}_0(k)dk - \frac{1}{2\pi}\int_{\partial D^+}\left(e^{-ikx+\omega(k)t}\sum_{j=0}^{n-1} c_j(k)\tilde{g}_j(\omega(k),t)\right)dk. \tag{43}$$

In order to obtain a solution, we require expressions for the time transforms of the unknown boundary data valid for $k\in\partial D^+$. As with the previous examples, we use the discrete symmetries of the equation

$$\omega(k) = \omega_0.$$

This relation is a polynomial or order n and thus has n roots in the complex plane. The mappings from one root to another are precisely the transformations $k\to\nu(k)$ which leave $\omega(k)$ invariant. We employ the induced versions of the global relation to solve for the transforms of the unknown boundary data. The solution proceeds as before. Having eliminated the unknown boundary data, we obtain an expression that depends on $\hat{q}(\nu(k),t)$. The transformation ν is such that $\hat{q}(\nu(k),t)$ is analytic and bounded in the region D^+. Hence we may use the Cauchy Integral Theorem to eliminate the contribution of the term involving $\hat{q}(\nu(k),t)$ to the integral along ∂D^+.

It is possible to predict how many boundary conditions are required for a well-posed problem by considering the large k behavior of $\omega(k)$. For large values of k, $\omega(k)\sim\alpha_n k^n$ and the region D approaches

$$D_R = \left\{k : \arg\alpha_n + n\arg k \in \left(\frac{\pi}{2},\frac{3\pi}{2}\right) + 2m\pi, \quad m=0,\ldots,n-1\right\}.$$

Indeed for large k, $\mathrm{Re}(\omega(k)) \sim |k|^n \cos(\arg \alpha_n + n \arg k)$ which is negative for k in D_R. The region D_R consists of n unbounded equal-angled sectors in the complex-k plane. Let N represent the number of unbounded sectors of D_R in the upper-half plane. It is easily seen that

$$N = \begin{cases} n/2 & n \text{ even;} \\ (n+1)/2 & n \text{ odd and } \alpha_n = -i; \\ (n-1)/2 & n \text{ odd and } \alpha_n = i. \end{cases} \tag{44}$$

The reader is encouraged to verify the formulas for D_R and N for the examples presented above. Indeed Figures 2.3, 2.5 and 2.6 are examples of the three possible cases for N. In these examples, the regions D_R and D coincide.

In the integral expression for $q(x,t)$, the contour ∂D^+ may be deformed to $\partial D_R^+ = \partial D_R \cap \mathbb{C}^+$, since the integrands are entire functions. Thus we require expressions for the time transform of the n boundary data, valid in the unbounded sectors of D_R in the upper-half plane.

Assume we are given p boundary conditions at the boundary at $x = 0$. This implies we require, for each of the N sectors in $\mathbb{C}^+$, expressions for the transforms of the $n - p$ unknown boundary data. For each of the N sectors in $\mathbb{C}^+$, the discrete symmetries of $\omega(k)$ allow us to choose $n - N$ transformations $\nu_i(k), i = 0, 1 \ldots n - N - 1$ which map that sector to the $n - N$ remaining sectors. Hence, by substituting $\nu_i(k)$ for k, there are $n - N$ versions of the global relation valid in each of the N sectors in $\mathbb{C}^+$. Thus we have $n - p$ unknowns with $n - N$ equations in each sector. Thus we need N boundary conditions at $x = 0$ for a well-posed problem or in other words a well-posed problem on the positive half-line requires as many boundary conditions as there are sectors of D_R in the upper-half plane.

Remark 2.2.5 *A canonical problem is one for which $q(0,t)$ and its first $N-1$ derivatives are provided as boundary conditions. An example of a non-canonical problem is the Neumann problem for the heat equation. Providing N linear combinations with constant coefficients of a subset of the boundary values is another example (Robin problem). In this case, versions of the global relation valid in D_R^+ and the N linear combinations form a system of equations which can be solved for the boundary data, provided a certain determinant*

is not identically zero. If the determinant has zeros in D_R^+, then the contribution of these zeros to the final solution is computed via the Residue Theorem.

2.3 Remarks

I have introduced Fokas's method for BVPs for linear evolution PDEs with constant coefficients on the half line. The main ideas behind the method are the use (i) of the analyticity properties of various functions, inherited from the global relation, and (ii) of the discrete symmetries of the dispersion relation. The method is more general than the standard methods used in the sense that it reproduces the results they provide, while being applicable to situations where the standard methods fail or are not applicable. The extension to problems on the finite interval is straightforward [29, 38].

The method of Fokas was inspired by techniques obtained from inverse scattering theory. Of particular relevance is the fact that a linear PDE with constant coefficients can be written as the compatibility condition of two first-order ordinary differential equations for an auxiliary function $\psi(x,t)$: one of these equations dictates how $\psi(x,t)$ changes as a function of x, with t as a parameter. The other equation has the roles of x and t reversed. Both equations may depend on $u(x,t)$ and its derivatives, thus they are not autonomous. In other words, one can associate Lax pairs to linear PDEs. As shown in [38], this approach leads to the solution of the PDE via a scalar Riemann-Hilbert problem, which may be solved explicitly using the Plemelj formula [1]. Using this route, it is not necessary to introduce even the Fourier transform!

The method of Fokas is far more general than I have discussed. For instance, it can be extended to apply to evolution equations with periodic boundary conditions [64], to evolution equations with more than one spatial dimension, or to systems of evolution equations. It is applicable also to some linear PDEs with nonconstant coefficients, and, as already stated, to so-called integrable nonlinear equations. These topics are beyond the scope of this short introduction, but the reader can find more details and additional references in [38]. The method continues to be extended. Recently, I applied the method of Fokas to PDEs with mixed partial derivatives, see Appendix A.

Chapter 3

THE FORWARD PROBLEM

The forward problem describes the evolution of an inviscid, irrotational, incompressible fluid with a free surface under the influence of gravity. The study of water waves has been the object of numerous theoretical and numerical investigations and is particularly relevant in understanding near-shore ocean dynamics. In this chapter, I present a method to numerically solve the water-wave equations that is inspired by the global relation for the water-wave equations. Existing methods to solve the forward problem include methods based on finite-element methods [51], Taylor expansions of the Dirichlet→Neumann operator [25, 44, 70], boundary integral methods as well as conformal mapping techniques [51, 52]. Amongst these methods, only Taylor expansions and finite-element methods extend in a straightforward manner to the three-dimensional problem. The boundary-integral methods do apply to three-dimensional problems, however, they involve inverting singular integral operators which is computationally challenging.

The numerical procedure to solve the Forward Problem presented in this chapter includes the Taylor expansion techniques of [25, 44] as a special case. I present sample simulations to justify the use of this method. Although, the forward problem is of considerable importance in its own right, our interest in the forward problem is motivated by our desire to solve a certain inverse problem in Chapter 4. In Section 3.1 I derive the equations of motion for water waves. Section 3.2 presents a rederivation of the results in [3]. I obtain a dual formulation of the Dirichlet→Neumann operator and highlight the connection of this formulation to the Taylor expansion method of [25] and the nonlocal equation of Ablowitz *et al.* [2]. Next, in Section 3.3 I present example simulations to test our new method for the forward problem. Finally, in Section 3.4 I review the method presented and discuss an example due to Jon Wilkening which hints at the range of validity of the present method.

3.1 The water-wave equations

The equations governing the motion of the free surface of a fluid, such as water, are simply a restatement of conservation of mass and momentum with suitable boundary conditions to define the free surface [15]. Consider an inviscid incompressible fluid with constant density ρ. The two conservation laws lead to

$$\mathbf{u}_t + (\mathbf{u}\cdot\nabla)\,\mathbf{u} = -\frac{\nabla p}{\rho} + \mathbf{g}, \tag{1}$$

$$\nabla\cdot\mathbf{u} = 0, \tag{2}$$

where $\mathbf{u}$ is the fluid velocity vector field, p is the local pressure of the fluid and $\mathbf{g} = -g\hat{\mathbf{z}}$ is the force due to gravity per unit mass in the vertical direction (taken as the $z-$coordinate). Aside from these equations we are also given the following boundary conditions

$$\eta_t + \mathbf{u}\cdot[\nabla\eta, -1] = 0, \qquad z = \eta(x,y,t) \tag{3}$$

$$p = p_0, \qquad z = \eta(x,y,t), \tag{4}$$

$$\mathbf{u}\cdot[\nabla H, 1] = 0, \qquad z = -h - H(x,y), \tag{5}$$

where η is the free surface of the fluid, p_0 is the constant pressure at the surface $z = \eta(x,y,t)$ and $z = -h - H(x,y)$ gives the profile of the solid surface bounding the fluid. The notation $[\nabla\eta, -1]$ and $[\nabla H, 1]$ refers to the normal vectors at the free surface $z = \eta(x,y,t)$ and solid boundary $z = -h - H(x,y)$ respectively. Condition (3) expresses the fact that fluid particles on the surface remain on the surface. An alternate interpretation is that the fluid surface $z = \eta$ moves in accordance to the velocity in the direction of the local normal. The second condition (4) is required as the surface η is itself an unknown. Thus two conditions are imposed at the unknown boundary. The final condition (5) is used to impose that the solid boundary $z = -h - H(x,y)$ is impermeable and rigid. Thus the velocity of the fluid in the normal direction is set to zero. In this chapter, I consider only flows which are periodic in the horizontal directions (x,y) with periods (L_1, L_2) respectively. Overall there are five unknowns: $\mathbf{u}$, p and η.

Water waves are often modeled by irrotational flows, *i.e.* $\nabla\times\mathbf{u} = 0$. For such flows there exists a scalar real-valued function Φ such that $\mathbf{u} = \nabla\Phi$. The incompressibility of the

fluid is expressed by the zero divergence condition. This implies Φ is a harmonic function since

$$\Delta\Phi = \nabla \cdot \nabla \mathbf{u} = 0.$$

The nonlinear term in (1) can be rewritten as

$$(\mathbf{u} \cdot \nabla)\,\mathbf{u} = \nabla\left(\frac{|\mathbf{u}|^2}{2}\right) - \mathbf{u} \times (\nabla \times \mathbf{u})\,.$$

The above vector identity reduces for irrotational flows to

$$(\mathbf{u} \cdot \nabla)\,\mathbf{u} = \nabla\left(\frac{|\mathbf{u}|^2}{2}\right) = \nabla\left(\frac{|\nabla\Phi|^2}{2}\right).$$

Substituting this into equation (1) and integrating over all space we obtain

$$\Phi_t + \frac{|\nabla\Phi|^2}{2} = -\frac{p}{\rho} - gz + c(t), \tag{6}$$

where $c(t)$ is an arbitrary function of time.

As mentioned above, we assume the fluid velocity (*i.e.* the gradient of Φ) is periodic in the horizontal directions. Hence the velocity potential is of the form

$$\Phi = A(t)x + B(t)y + \phi(x, y, z, t), \tag{7}$$

where ϕ is a periodic function in (x, y) with periods (L_1, L_2) respectively. As the fluid velocity $\mathbf{u} = \nabla\Phi$, we may add any constant function of space to Φ without changing the fluid velocities. Let us impose

$$\frac{1}{L_1 L_2}\int_0^{L_1}\int_0^{L_2} \phi(x, y, \eta, t)dxdy = 0.$$

Of course this assumes the existence and uniqueness of solutions to the water-wave problem. Happily the results of [49, 69] justify (7).

Combining (4) and (6) we have at $z = \eta$

$$\Phi_t + \frac{|\nabla\Phi|^2}{2} = -\frac{p_0}{\rho} - g\eta + c(t).$$

Substituting for Φ from (7) we obtain

$$A'(t)x + B'(t)y + \phi_t + \frac{|\nabla\Phi|^2}{2} = -\frac{p_0}{\rho} - g\eta + c(t), \quad z = \eta.$$

Define $q = \phi(x, y, \eta, t)$. Hence $q_t = \phi_t + \eta_t \phi_z$ and

$$A'(t)x + B'(t)y + q_t - \eta_t \phi_z + \frac{|\nabla \Phi|^2}{2} = -\frac{p_0}{\rho} - g\eta + c(t), \quad z = \eta.$$

We integrate over x, y and choose $c(t)$ such that

$$c(t) = \frac{p_0}{\rho} + \frac{1}{L_1 L_2} \int_0^{L_1} \int_0^{L_2} \left(\frac{|\nabla \Phi|^2}{2} + g\eta - \eta_t \phi_z \right) dxdy,$$

which implies

$$\frac{A'(t)L_1}{2} + \frac{B'(t)L_2}{2} = 0.$$

In other words

$$A(t) = -B(t)\frac{L_2}{L_1} + \alpha,$$

where α is a constant. Substituting this in (7) we obtain

$$\Phi = -B(t)\frac{L_2}{L_1}x + \alpha x + B(t)y + \phi.$$

If we take the average of the Dirichlet potential $\Phi(x, y, \eta, t)$ at $t = 0$ to be zero, we obtain $\alpha = 0$. Thus when we limit ourselves to one-dimensional fluid surfaces (*i.e.* $B(t) \equiv 0$) we observe that we can eliminate the drift term entirely and we may consider an equivalent problem for a periodic potential ϕ. In the more general case for a two-dimensional surface, we see that the drift is limited to one direction. Repeating the previous calculations assuming only a term proportional to x (say) in (7) we obtain the same conclusion as for the one-dimensional surface, namely that the zero average for the Dirichlet value at the free surface initially will be maintained throughout the time evolution. In general, the period lattice need not be rectangular for the two-dimensional surface as assumed above, but the results remain true. For the remainder of this chapter I shall assume the drift term has been eliminated and enforce periodicity of the velocity potential ϕ as the boundary condition in the horizontal directions. Summarizing, the velocity potential ϕ satisfies the following free

boundary-value problem:

$$\Delta\phi = 0, \quad -h - H(x,z) < z < \eta(x,y,t), \tag{8a}$$

$$\phi(x,y,\eta,t) = q, \tag{8b}$$

$$q_t = \mathcal{P}\left[-g\eta - \frac{1}{2}\left(\phi_x^2 + \phi_y^2 + \phi_z^2\right) + \eta_t\phi_z\right], \qquad z = \eta(x,y,t), \tag{8c}$$

$$\eta_t = \phi_z - \eta_x\phi_x - \eta_y\phi_y, \qquad z = \eta(x,y,t), \tag{8d}$$

$$\phi_z + H_x\phi_z + H_y\phi_y = 0, \qquad z = -h - H(x,y), \tag{8e}$$

where $\mathcal{P}$ is the projection on to the space of functions with zero average. Further, ϕ, η and H are functions periodic in the horizontal directions.

3.2 A weak formulation of Laplace's equation

In the previous section we derived the equations governing the motion of a water wave. To obtain the time evolution of the surface η, we require the solution to Laplace's equation in the fluid domain. In this section I present one possible method of obtaining the solution to Laplace's equation. For simplicity I shall assume no y dependence below. Further I suppress the dependence on t since the discussion below pertains only to Laplace's equation. The method described below provides an alternate derivation of the global relation for Laplace's equation we saw in the Introduction. Further, this alternate derivation provides a means to compute the Dirichlet→Neumann operator. The presentation below largely follows that of Ablowitz & Haut [3] with minor changes to emphasize the connections to the Ablowitz-Fokas-Musslimani (AFM) approach in particular and global relations in general.

Consider Laplace's equation

$$\phi_{xx} + \phi_{zz} = 0,$$

posed on the domain $D = \{(x,z) \in \mathbb{R}^2 : 0 < x < L, -h < z < \eta(x)\}$, where η is a smooth periodic function with period L. Further assume that ϕ is periodic in the horizontal variable x with period L, and

$$\phi_z(x,-h) = 0, \quad z = -h.$$

Thus we are restricting ourselves to a flat bottom boundary. Later we shall see how to generalize the arguments presented here to varying bottom boundaries. Let $\mathscr{D}(x)$ and

$\mathscr{N}(x)$ be the Dirichlet and Neumann values of the function ϕ at $z = \eta(x)$. If either $\mathscr{D}(x)$ or $\mathscr{N}(x)$ is provided to us, the problem is well posed in the Hadamard sense for $\mathscr{D}(x)$, $\mathscr{N}(x)$ in appropriate function spaces.

Following [3], consider a smooth function ψ which also satisfies Laplace's equation in D and the boundary condition at $z = -h$. Thus

$$\psi_{xx} + \psi_{zz} = 0, \text{ in } D,$$

and $\psi_z(x, -h) = 0$. Formally, ψ can be expressed as

$$\psi(x,z) = \frac{1}{2\pi} \sum_{k_n} e^{ik_n x} \cosh(k_n(z+h)) \hat{\Psi}_{k_n}, \quad k_n = \frac{2\pi n}{L}, n = 0, \pm 1, \pm 2 \dots \tag{9}$$

Indeed, if $\hat{\Psi}_k$ decays sufficiently fast as a function of k (at some exponential order), then ψ is defined for $z > \eta(x)$. The function $\hat{\Psi}_{k_n}$ has a natural interpretation as the Fourier transform of $\psi(x, -h)$. That it decays exponentially implies the function $\psi(x, -h)$ is holomorphic in a strip around the real x axis. Note that the function ψ has a harmonic extension to $z < -h$ through a reflection. Consequently, $\psi(x, -h)$ is an evaluation of the function in the interior of the domain of harmonicity, therefore it is real analytic in x.

Using Green's Identity, we have

$$\begin{aligned}
0 &= \int_D (\psi(\phi_{xx} + \phi_{zz}) - \phi(\psi_{xx} + \psi_{zz}))\, dxdz, \\
&= \int_{\partial D} \left(\psi \frac{\partial \phi}{\partial n} - \phi \frac{\partial \psi}{\partial n} \right) dS, \\
&= \int_0^L \psi(x,\eta) \left[\phi_z(x,\eta) - \eta_x \phi_x(x,\eta) \right] dx - \int_0^L \phi(x,\eta) \left[\psi_z(x,\eta) - \eta_x \psi_x(x,\eta) \right] dx, \\
&= \int_0^L \psi(x,\eta) \mathscr{N}(x) dx - \int_0^L \mathscr{D}(x) \left[\psi_z(x,\eta) - \eta_x \psi_x(x,\eta) \right] dx,
\end{aligned} \tag{10}$$

where $\partial/\partial n$ is the normal derivative to the surface. Hence ϕ may be regarded as a weak solution to Laplace's equation. Using the representation (9) for ψ and noting that

$$e^{ik_n x} \left(ik_n \sinh(k_n(\eta+h)) + k_n \eta_x \cosh(k_n(\eta+h)) \right) = \partial_x \left(e^{ik_n x} \sinh(k_n(\eta+h)) \right),$$

we obtain after an integration by parts

$$\sum_{k_n} \hat{\Psi}_{k_n} \left(\int_0^L e^{ik_n x} \left[\cosh(k_n(\eta+h)) \mathscr{N}(x) - i \sinh(k_n(\eta+h)) \mathscr{D}'(x) \right] dx \right) = 0. \tag{11}$$

Since this relation is valid for arbitrary $\hat{\Psi}_{k_n}$, we obtain

$$\int_0^L e^{ik_n x}\left[\cosh(k_n(\eta+h))\mathscr{N}(x) - i\sinh(k_n(\eta+h))\mathscr{D}'(x)\right]dx = 0, \quad \forall k_n = \frac{2\pi n}{L},$$

with $n = \pm 1, \pm 2, \ldots$, which is the Ablowitz-Fokas-Musslimani (AFM) global relation [2] for Laplace's equation. In light of this derivation, we arrive at an alternative interpretation: the global relation holds as a distribution. Further, note that the global relation as obtained through the AFM approach (see equation (4a) in the Introduction) is but a rephrasing of Green's Identity. That this is the case is not unexpected. Indeed the global relation extends the notion of Green's Identity to other PDEs besides Laplace's equation, as described in Chapter 2.

The insight that the global relation holds as a distribution, provides a way to compute the Dirichlet→Neumann operator. Notice that expressions such as

$$\int_0^L e^{ikx}\cosh(k(\eta+h))\mathscr{N}(x)dx, \quad \int_0^L e^{ikx}\sinh(k(\eta+h))\mathscr{D}'(x)dx,$$

define a functional over a suitable space of functions, namely those that decay at least like $e^{-M|k|}$ where $M = \max(|\eta+h|)$ as is easily seen by applying the Cauchy-Schwarz inequality. As Ablowitz & Haut [3] point out, the expressions above are themselves linear operators that map the Dirichlet and Neumann values on the boundary to distributions. The authors take an inverse Fourier transform of the AFM global relation to obtain a dual formulation for the water-wave problem. The Fourier transform is *defined* through duality using the inner-product (11), as the distributions involved are certainly not classical ones. However, progress can be made by rewriting equation (11) as

$$\begin{aligned}\int_0^L \mathscr{N}(x)\left(\sum_{k_n}\hat{\Psi}_{k_n}e^{ik_n x}\cosh(k_n(\eta+h))\right)dx \\ + i\int_0^L \mathscr{D}(x)\partial_x\left(\sum_{k_n}\hat{\Psi}_{k_n}e^{ik_n x}\sinh(k_n(\eta+h))\right)dx = 0.\end{aligned} \tag{12}$$

The above relation is an equality between two inner-products. Since the Dirichlet problem for the Laplace equation is well posed for all suitable $\mathscr{D}(x)$, the above equation implies

$$\sum_{k_n}\hat{\Psi}_{k_n}e^{ik_n x}\cosh(k_n(\eta+h)) = \mathscr{D}(x), \tag{13}$$

and

$$-i\partial_x\left(\sum_{k_n}\hat{\Psi}_{k_n}e^{ik_nx}\sinh(k_n(\eta+h))\right)=\mathscr{N}(x). \tag{14}$$

This is equivalent to choosing $\psi=\phi$ in (10). Note that the normal derivative to (9) is indeed given by the expression (14). The above pair of equations defines the Dirichlet→Neumann operator in terms of the "parameter" $\hat{\Psi}_{k_n}$. This same pair appears in [3] in the dual formulation of the water-wave problem. The Fourier transform of (13-14) leads to

$$\sum_{k_n}\hat{\Psi}_{k_n}A_{nl}=\hat{\mathscr{D}}_l,\quad \sum_{k_n}\hat{\Psi}_{k_n}B_{nl}=\hat{\mathscr{N}}_l,$$

with

$$A_{nl}=\int_0^L e^{ik_nx-ik_lx}\cosh(k_n(\eta+h))dx,\quad B_{nl}=l\int_0^L e^{ik_nx-ik_lx}\sinh(k_n(\eta+h))dx.$$

As noted by Craig *et al.* [24], the operator A_{nl} is invertible. Hence equations (13-14) define the Dirichlet→Neumann operator. It should be noted that this is not a perturbative or small amplitude in η representation for the operator. Indeed, one can simulate large amplitude water waves using this form of the operator. In section (3.4) I discuss further details about the range of validity of this formulation. Lastly, note the Taylor series for the operator derived by Craig & Sulem [25] may be obtained from the above definition in a straightforward manner by expanding terms in powers of η.

The Dirichlet→Neumann operator for Laplace's equation with a varying bottom boundary is obtained as follows. At the bottom boundary, now we have the Neumann condition

$$\phi_z+H_x\phi_x+H_y\phi_y=0,\quad z=-h-H(x),$$

where H is a continuously differentiable periodic function of x with period L. Starting with Green's Identity as before we obtain the appropriate generalization of the previous dual formulation. Alternately, we may start with the following global relations, see [2]:

$$\int_0^L e^{ik_nx}\left(\cosh(k_n(\eta+h))\mathscr{N}(x)-i\sinh(k_n(\eta+h))\mathscr{D}'(x)-i\sinh(k_nH)Q_x\right)dx=0, \tag{15}$$

$$\int_0^L e^{ik_nx}\left(i\sinh(k_n(\eta+h))\mathscr{N}(x)+\cosh(k_n(\eta+h))\mathscr{D}'(x)-\cosh(k_nH)Q_x\right)dx=0, \tag{16}$$

where $Q(x) = \phi(x, -h - H)$. Taking the inner product of the first equation with $\hat{\Psi}^1_{k_n}$, the second with $\hat{\Psi}^2_{k_n}$ and adding the resulting equations, we obtain after an integration by parts

$$\int_0^L \sum_{k_n} e^{ik_n x} \left(\hat{\Psi}^1_{k_n} \cosh(k_n(\eta + h)) + i\hat{\Psi}^2_{k_n} \sinh(k_n(\eta + h)) \right) \mathscr{N}(x) dx$$
$$+ \int_0^L \partial_x \sum_{k_n} e^{ik_n x} \left(i\hat{\Psi}^1_{k_n} \sinh(k_n(\eta + h)) - \hat{\Psi}^2_{k_n} \cosh(k_n(\eta + h)) \right) \mathscr{D}(x) dx$$
$$+ \int_0^L \partial_x \sum_{k_n} e^{ik_n x} \left(i\hat{\Psi}^1_{k_n} \sinh(k_n H) + \hat{\Psi}^2_{k_n} \cosh(k_n H) \right) Q(x) dx = 0.$$

The above equation can be obtained from Green's Identity (10) with the choice

$$\psi = \sum_{k_n} e^{ik_n x} \left(\hat{\Psi}^1_{k_n} \cosh(k_n(z + h)) + i\hat{\Psi}^2_{k_n} \sinh(k_n(z + h)) \right).$$

Imposing the boundary conditions, we obtain the following system of equations for $\hat{\Psi}^1_{k_n}$ and $\hat{\Psi}^2_{k_n}$

$$\sum_{k_n} e^{ik_n x} \left(\hat{\Psi}^1_{k_n} \cosh(k_n(\eta + h)) + i\hat{\Psi}^2_{k_n} \sinh(k_n(\eta + h)) \right) = \mathscr{D}(x), \tag{17}$$

$$\partial_x \sum_{k_n} e^{ik_n x} \left(i\hat{\Psi}^1_{k_n} \sinh(k_n H) + \hat{\Psi}^2_{k_n} \cosh(k_n H) \right) = 0. \tag{18}$$

On taking the Fourier transform of these equations, we arrive at a linear system of equations for $\hat{\Psi}^1_{k_n}$ and $\hat{\Psi}^2_{k_n}$. Finally the Neumann condition at the surface $z = \eta$ is given by

$$\mathscr{N}(x) = -i\partial_x \sum_{k_n} e^{ik_n x} \left(\hat{\Psi}^1_{k_n} \sinh(k_n(\eta + h)) + i\hat{\Psi}^2_{k_n} \cosh(k_n(\eta + h)) \right).$$

The arguments in this section may be generalized to two-dimensional free surfaces in the obvious way. Indeed Ablowitz & Haut [3] obtain this alternate formulation of the Dirichlet→Neumann operator in three-dimensions in their original derivation. In this chapter, I employ this alternate formulation to compute the Dirichlet→Neumann operator.

3.3 The numerical method

In this section I describe the numerical method adopted to simulate the time-dependent motion of the free surface of a water wave. The equations of motion for a one-dimensional free surface are given below. The fluid is assumed to be periodic in the $x-$direction and I

assume the bottom solid boundary to be flat, *i.e.* $z = -h$ represents the bottom boundary of the fluid. Thus we have

$$\phi_{xx} + \phi_{zz} = 0, \qquad (x,z) \in D, \tag{19a}$$

$$\phi_z = 0, \qquad z = -\tilde{h}, \tag{19b}$$

$$\phi = q, \qquad z = \eta(x,t), \tag{19c}$$

$$\eta_t = \phi_z - \eta_x \phi_x, \qquad z = \eta(x,t), \tag{19d}$$

$$q_t = \mathcal{P}\left[-\frac{1}{2}\left(\phi_x^2 + \phi_z^2\right) - g\eta + \eta_t \phi_z\right], \qquad z = \eta(x,t), \tag{19e}$$

$$\phi(x,z) = \phi(x+L,z), \qquad (x,z) \in D, L = ml\pi, \tag{19f}$$

where $D = \{(x,z) \in \mathbb{R}^2 : -\tilde{h} < z < \eta(x,t), 0 < x < L\}$ represents the fluid domain, L is the period of the flow, m is a positive integer, g is the acceleration due to gravity, l is the length-scale in the x direction and $\mathcal{P}$ is the projection on to the space of functions with zero average. The above equations may be rewritten in non-dimensional form using the scaling relations

$$\phi = l\sqrt{gl}\phi^*, \quad \eta = l\eta^*, \quad z = lz^*, \quad x = lx^*, \quad t = \sqrt{\frac{l}{g}}t^*, \tag{20}$$

where stars indicate non-dimensional quantities. The equations of motion are now given as

$$\phi_{xx} + \phi_{zz} = 0, \qquad (x,z) \in D, \tag{21a}$$

$$\phi_z = 0, \qquad z = -h, \tag{21b}$$

$$\phi = q, \qquad z = \eta(x,t), \tag{21c}$$

$$\eta_t = \phi_z - \eta_x \phi_x, \qquad z = \eta(x,t), \tag{21d}$$

$$q_t = \mathcal{P}\left[-\frac{1}{2}\left(\phi_x^2 + \phi_z^2\right) - \eta + \eta_t \phi_z\right], \qquad z = \eta(x,t), \tag{21e}$$

$$\phi(x,z) = \phi(x+m\pi,z), \qquad (x,z) \in D, \tag{21f}$$

where $D = \{(x,z) \in \mathbb{R}^2 : -h < z < \eta(x,t), 0 < x < m\pi\}$ and the stars are dropped. The relevant non-dimensional parameters for the given problem are the shallowness parameter $\mu = h/(m\pi)$ and the smallness parameter $\epsilon = \max |\eta|/h$. The above set of equations are

seen as a system of evolution equations for the surface quantities η and q. Evidently, to integrate these equations in time, we require expressions for the gradient of ϕ at $z = \eta$. We use the alternate formulation of the Dirichlet→Neumann operator established in the previous section to rewrite the equations of motion as

$$\sum_{k_n} e^{ik_n x} \cosh(k_n(\eta + h))\hat{\Psi}_{k_n} = q, \quad k_n = \frac{2n}{m}, n = 0, \pm 1, \pm 2 \tag{22a}$$

$$\eta_t = \phi_z - \eta_x \phi_x, \tag{22b}$$

$$q_t = \mathcal{P}\left[-\frac{1}{2}\left(\phi_x^2 + \phi_z^2\right) - \eta + (\phi_z - \eta_x\phi_x)\phi_z\right], \tag{22c}$$

where

$$\phi_x = \sum_{k_n} ik_n e^{ik_n x} \cosh(k_n(\eta + h))\hat{\Psi}_{k_n}, \quad \phi_z = \sum_{k_n} k_n e^{ik_n x} \sinh(k_n(\eta + h))\hat{\Psi}_{k_n}.$$

Due to the spatial periodicity of the flow I use a pseudospectral method for the spatial discretization. The quantities η and q are approximated by truncating their Fourier series with the same number of modes K_{max}. Derivatives are obtained by applying Fourier multipliers in Fourier space, while nonlinear products are computed in physical space on a discrete set of equally spaced grid points. Aliasing errors were removed by the zero-padding technique [63, 13]. Typically this entailed taking $2K_{max}$ modes if K_{max} modes of accuracy are required. Time integration is carried out in Fourier space. This allows us to readily implement the projection operator $\mathcal{P}$. I use a fourth-order Runge-Kutta scheme to advance the surface quantities to the next time step.

I present two example simulations using the method described above. The examples are those of Craig & Sulem [25]. Our goal is not to present detailed computations, rather it is establish that the numerical method introduced in this section produces satisfactory results. The first is a simulation of unsteady flow. For the second example I use an approximate Stokes wave as the initial condition.

3.3.1 Unsteady flow

Our first simulation is to compute the evolution of the free surface with initial condition

$$\eta_0(x) = 0.01e^{-4(x-\pi)^2}\cos(4x),$$

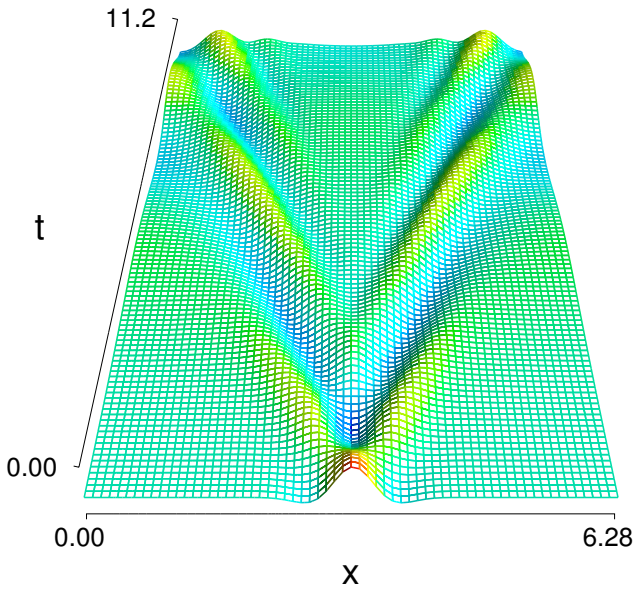

Figure 3.1: Evolution of an unsteady wave.

with zero initial velocity potential. The spatial period of the flow is 2π (hence $m = 2$). Figure 3.1 shows the evolution of the surface up to $t = 11.25$. The simulation is stable and could have continued longer. The computation was performed with 64 collocation points and full dealiasing was accomplished using zero-padding. Figure 3.2 depicts the time series for the relative error in the Hamiltonian and the absolute error in the momentum. Evidently, these quantities are conserved well for the duration of the simulation.

3.3.2 An approximate Stokes wave

Our second simulation uses the following second-order approximation to a Stokes wave as initial conditions:

$$\eta_0(x) = a\cos(kx) + \mu_2 a^2 \cos(2kx),$$
$$q_0(x) = \nu_1 a \cosh(k(\eta_0 + h))\sin(kx) + \nu_2 a^2 \cosh(2k(\eta_0 + h))\sin(2kx),$$

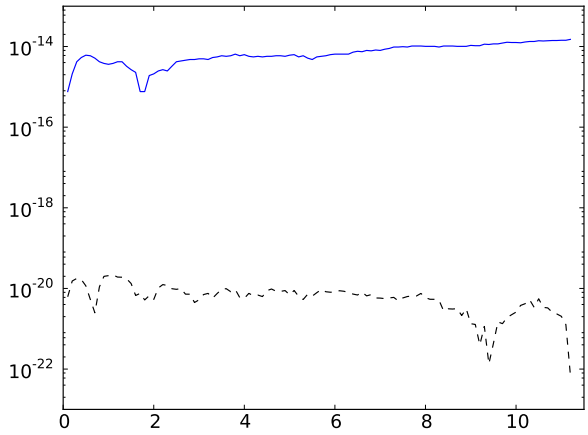

Figure 3.2: Time series of Hamiltonian and momentum for unsteady wave. Relative error in the Hamiltonian is shown in blue and the absolute error in the momentum is shown in black.

with

$$\mu_2 = \frac{1}{2}k\coth(kh)\left(1+\frac{3}{2\sinh^2(kh)}\right),$$
$$\nu_1 = \frac{\omega}{k\sinh(kh)}, \quad \nu_2 = \frac{3}{8}\frac{\omega}{\sinh^4(kh)},$$

where $\omega^2 = k\tanh(kh)$. Figure 3.3 displays the evolution of a 2π-periodic wave with $k = 2$, $a = 0.065$ and $h = 1$. The wave is near the linear regime and the Stokes expansion above is seen to be a fairly accurate representation of the full wave. We see in Figure 3.3 the wave translating over two full periods. The calculation was carried out further in time with almost no change in the profile. Since the initial condition is only an approximation to a Stokes wave, the peaks of the wave profile show a small amount of wobble as the wave translates. Again the Hamiltonian and momentum are conserved (Figure 3.4).

3.4 Discussion and remarks about the method

In this chapter, a new method to solve the Forward Problem is proposed. The method is valid for both one- and two-dimensional surfaces. The method produces satisfactory results

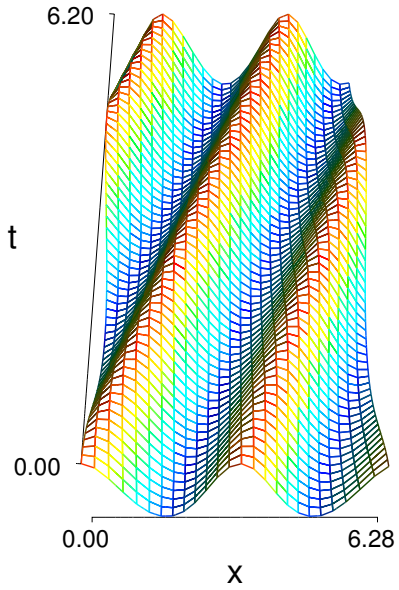

Figure 3.3: Evolution of an approximate Stokes wave.

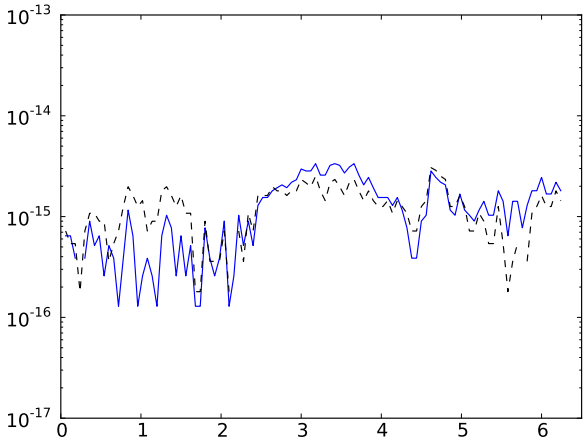

Figure 3.4: Time series of the Hamiltonian and the momentum for an approximate Stokes wave. Relative error in the Hamiltonian is shown in blue and in the momentum is shown in black.

and captures essential features of the water-wave problem. Further, the method can be viewed as an extension of Taylor-series expansion methods of [25, 53, 44]. Some theoretical questions regarding the numerical procedure discussed in this chapter need investigating. Indeed, one would like to know the function spaces for which expressions such as

$$\sum_{k_n} e^{ik_n x} \cosh(k_n(\eta(x)+h))\hat{\Psi}_{k_n} = q(x), \tag{23}$$

may be solved for $\hat{\Psi}_{k_n}$ given η and q. As the linearization of the above expression is involved in obtaining the Taylor-series formulae of [25, 44, 53], the invertibility of the operator on the left-hand side above (*i.e.*, the operator A_{nl} in Section 3.2) warrants study. In the next chapter, I use the data obtained from the Forward Problem to solve a particular inverse problem. As the inverse problem is solved successfully, the numerical procedure introduced in this chapter seems, at least in some regimes, to produce an accurate solution of the full water-wave problem. Thus for the purposes of investigating the problems of relevance to this thesis, the formulation of this chapter is sufficient.

I shall now present an example due to Jon Wilkening that explicitly shows equation (23) *cannot* be solved in general, even for analytic η and q. Consider the function

$$\begin{aligned}\phi(x,z) &= \frac{1}{2}\mathrm{Im}\left\{\cot\left(\frac{x+iz-i}{2}\right) - \cot\left(\frac{x-iz+i}{2}\right)\right\},\\ &= \mathrm{Re}\left\{\frac{\sinh(1)}{\cosh(1)-\cos(x+iz)}\right\}.\end{aligned} \tag{24}$$

The function ϕ is harmonic for all x, z except at $(x,z) = (0, \pm 1)$ and is periodic in x with period 2π. Further, $\phi(x,-z) = \phi(x,z)$ and hence $\phi_z(x,0) = 0$ for all x. Evaluating at $z = 0$, we obtain

$$\phi(x,0) = \frac{\sinh(1)}{\cosh(1)-\cos(x)},$$

which has a Fourier series representation

$$\phi(x,0) = \sum_{n=-\infty}^{\infty} e^{inx}e^{-|n|}.$$

Let $\eta(x) = 1 - \cos(x)/2$ and $q(x) = \phi(x,\eta(x))$. The function $q(x)$ is real analytic and 2π-periodic. Consider, the equation

$$\sum_{n=-\infty}^{\infty} e^{inx}\cosh(n\eta(x))c_n = q(x),$$

which is the analog of (23) for the example considered here. We wish to solve the above equation for the coeffients c_n. Of course, we know that $c_n = e^{-|n|}$ by construction, but the above equation cannot be solved for c_n in any obvious sense as the series on the left diverges for all $\pi/2 < x < 3\pi/2$. This is due to the fact that the representation

$$\phi(x,y) = \sum_{n=-\infty}^{\infty} e^{inx}\cosh(nz)e^{-|n|}, \tag{25}$$

holds only for $|z| < 1$ (essentially due to the singularity in ϕ). Thus even when η and q are analytic functions, it may not be possible to solve equation (23). However, it may still be the case that there does exist a harmonic function derived from a well posed problem for Laplace's equation with q as the Dirichlet condition at the surface $\eta(x)$

$$\begin{aligned}
\phi_{xx} + \phi_{zz} &= 0, \\
\phi(x,\eta(x)) &= q(x), & \eta(x) &= 1 - \cos(x)/2, \\
\phi_z(x,0) &= 0, \\
\phi(x,z) &= \phi(x+2\pi,z), & 0 \le x < 2\pi, 0 < z < \eta(x).
\end{aligned}$$

This leads us to conclude that the method to evaluate the Dirichlet→Neumann operator discussed here is not suitable for generic problems for Laplace's equation. Figure 3.5 shows the reconstruction of the Neumann value at $\eta(x) = 1 - \cos(x)/2$ for the example discussed here which clearly shows the failure of the representation (25).

A key point to note in the above example is that η was chosen independently of q (or equivalently ϕ). Indeed, $\eta = 1 - \cos(x)/2$ was chosen precisely so that representation (25) fails for some interval in x. However, if one chooses η such that $\|\eta\|_\infty < 1$, then representation (25) is valid and one can compute the Dirichlet→Neumann map accurately. Thus a necessary condition for the method to compute the Dirichlet→Neumann map presented here is that η and q be such that there are no obstructions to the harmonic extension of $\phi(x,z)$ to the region $-h < z < \|\eta\|_\infty$. This is not as artificial an assumption as it may seem, for the water-wave problem is a free-boundary problem. Thus η and q are not independent of one another. Of course, the exact relation between η and q for the Forward Problem is not a simple one and more work is required before we can rigorously establish the numerical procedure of this chapter.

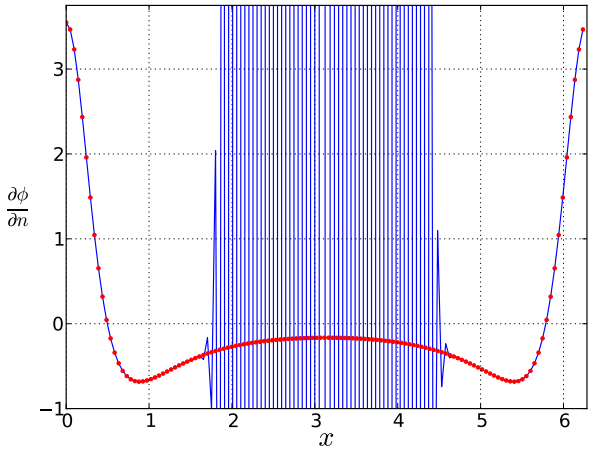

Figure 3.5: A comparison of the normal derivative computed using (13-14) and the true solution (24). True solution is shown in red dots.

Chapter 4

AN INVERSE PROBLEM

The problem addressed in this chapter is that of recovering the shape of the solid boundary bounding an inviscid, irrotational, incompressible fluid from measurements of the free surface alone. This problem is an idealization of the ocean bathymetry detection problem which arises naturally in the study of coastal dynamics [18, 42, 58, 62]. Further, knowledge of the ocean bathymetry is crucial for safe underwater navigation. The current work considers fluid-mechanical principles to determine the shape and location of the bottom surface. Other approaches to the bathymetry detection problem exist [18, 42, 58, 62]. Perhaps the most significant and popular ones are based on reflection of acoustic signals from the bottom surface [18, 62]. Other methods are based on nonlinear properties of ocean waves such as variations in the dispersion relation of shoaling waves [58] and further corrections to these formulas [42]. A recent approach that takes into account the entire flow field is due to Nicholls & Taber [54]. Their method is based on expansions of a nonlinear operator that accounts for the bottom surface (the Dirichlet→Neumann operator or DNO). However, Nicholls & Taber [54] restrict their approach to working with standing wave profiles on the surface. The extension to generic surfaces is not obvious.

The method I propose stands apart from the methods mentioned above in that I make no assumptions on the nature of the free surface (such as small amplitude waves, standing waves, *etc.*). The method allows us to accurately recover the bottom surface from only measurements of the free-surface deviation from rest at several times. In particular, the method can recover the average depth of the bottom surface *i.e.*, we do not require this as input as is required for linear and perturbative theories [18, 42, 58, 62] or by Nicholls & Taber [54]. I assume the flow is periodic in the horizontal directions without the presence of a vertically uniform horizontal current. In other words, I assume the velocity potential itself is periodic (see section 3.1 of Chapter 3 for a related discussion). Although the equations I

derive are valid for one- and two-dimensional surface water-waves, the numerical examples presented are limited to one-dimensional surfaces, due to the computational effort required to solve both the forward time-dependent evolution and the inverse bathymetry detection problem for two-dimensional surfaces.

The principal question I seek to address is that of what minimal input surface data is required to recover the bottom surface. In theory, to recover the bottom surface the method of reconstruction requires the surface elevation and its first two derivatives with respect to time as functions of the horizontal variable at one particular instant of time. In practice, it suffices to require the surface elevation at several successive instances of time as a function of the horizontal variable: the time derivatives may be obtained through finite differences. Although the input requirements made in this work could be considered a challenge in and of themselves, advances in remote sensing technology suggest these are reasonable assumptions [58].

The organization of this chapter is as follows: Section 4.1 contains the derivation of the exact, nonlinear equations to be solved for the bottom surface. These equations are a necessary condition of the full set of equations modeling water waves. As a result, it is possible to reconstruct large amplitude, nonlinear bottom surfaces from large amplitude, nonlinear free-surface deviations. In Section 4.2 I present several example calculations of bottom surface recovery assuming the surface elevation and its first two derivatives with respect to time as functions of the horizontal variable are provided. Following the examples, in Section 4.3 I discuss in detail several numerical issues involved in the reconstruction of the bottom surface. Bathymetry detection is a challenging inverse problem and I delineate features of the method which exhibit the ill-posed character of the problem. In short, many of the challenges can be explained by the fact that the velocity field decays exponentially with depth for an inviscid, irrotational fluid. This behavior is manifested mathematically through the presence of hyperbolic functions in the nonlinear equations to be solved, whose exponential growth inhibits accurate representation in finite-precision arithmetic. Finally in Section 4.4, I repeat the examples in Section 4.2 with finite-difference approximations to the time derivatives of the surface elevation. There I show that the bottom surface may be recovered from measurements of the surface deviation from rest alone. The error introduced

by the finite-difference approximation is negligible and the bottom surface is recovered accurately in certain parameter regimes, specifically in the shallow water regime. In this chapter I obtain the bottom surface from numerically generated free-surface elevations. Bathymetry recovery from experimental data will not be discussed. The input data for the inverse problem discussed here is obtained from the numerical solution of the Forward Problem. See Chapter 3 for details.

4.1 The bathymetry reconstruction equation

Euler's equations for the dynamics of an inviscid, irrotational periodic flow in a two ($N = 1$) or three ($N = 2$) dimensional domain $D = \{(x, z) \in \mathbb{R}^N \times \mathbb{R} : \zeta < z < \eta,\ 0 < x_i < L_i, i = 1, \ldots, N\}$ are

$$\Delta\phi + \phi_{zz} = 0, \qquad (x, z) \in D, \tag{1a}$$

$$\phi_z - \nabla\zeta \cdot \nabla\phi = 0, \qquad z = \zeta(x), \tag{1b}$$

$$\phi_z - \nabla\eta \cdot \nabla\phi = \eta_t, \qquad z = \eta(x, t), \tag{1c}$$

$$\phi_t + \frac{1}{2}\left(|\nabla\phi|^2 + \phi_z^2\right) + g\eta = 0, \qquad z = \eta(x, t), \tag{1d}$$

Here ϕ is the velocity potential, η is the surface displacement, g is the acceleration due to gravity and L_i is the period in the x_i direction. I use the convention that the Laplacian and gradient refer to those in $\mathbb{R}^N$, *i.e.* they refer to the horizontal Laplacian and horizontal gradient.

In this section I show how one can reconstruct the bottom topography ζ from only measurements at the surface. In particular, I state what is meant by surface measurements. Ideally, this would entail a snapshot of η at some instant of time. However, this is readily seen to be insufficient since Laplace's equation has a unique solution for every η and ζ suitably smooth, with prescribed boundary conditions. On the other hand, if we are given the complete solution of the free-boundary value problem (1a-1d) then this is (by definition) sufficient information. My definition of surface measurements lies in between these two extremes: I shall require $\eta(x, t_0)$, $\eta_t(x, t_0)$ and $\eta_{tt}(x, t_0)$, *i.e.*, the surface deviation from the undisturbed level and its first two $t-$derivatives as functions of the horizontal variable at

one particular instant $t = t_0$. The following paragraphs indicate why this is the case. The functions $\eta(x, t_0)$, $\eta_t(x, t_0)$ and $\eta_{tt}(x, t_0)$ can be considered the first three terms of the Taylor series of $\eta(x, t)$ at some time $t = t_0$ and hence represent independent pieces of information. Note that equation (1c) implies $\eta_t(x, t_0)$ is the normal velocity of the fluid at $z = \eta(x, t)$.

If we are given the surface quantities $\eta(x, t)$ and $q = \phi(x, \eta)$, the Hamiltonian formulation of the water-wave problem due to Zakharov [71] indicates that these surface quantities fully determine the solution to the water-wave problem (1a-1d). Instead, for now assume that at some instant of time t_0 the velocity potential at the surface $q(x, t_0)$, the shape of the surface $\eta(x, t_0)$ and the normal velocity $\eta_t(x, t_0)$ are given. This is sufficient information to pose the following initial-value problem for the Laplace equation with periodic boundary conditions in the horizontal directions.

$$\Delta\phi + \phi_{zz} = 0, \qquad z < \eta, \tag{2a}$$

$$\phi_z - \nabla\eta \cdot \nabla\phi = \eta_t, \qquad z = \eta, \tag{2b}$$

$$\phi = q, \qquad z = \eta. \tag{2c}$$

The question of bottom topography reconstruction involves finding a surface ζ such that (1b) is satisfied by the solution of the above problem. Several issues arise. First, we want to obtain an exact expression for the solution of (2a-2c) in terms of known quantities so that (1b) becomes a (nonlinear) equation for the unknown surface. Indeed solving the initial-value problem for the Laplace equation is numerically challenging. Second, the general initial-value problem (in z) for the Laplace equation may not have a solution far from $z = \eta(x, t_0)$. The Cauchy-Kowalevski Theorem [32] only guarantees a solution in the neighborhood of the initial condition *i.e* near $z = \eta(x, t_0)$. However, the true bottom surface ζ may be outside of this neighborhood. Third, measurements of the velocity potential at the surface $q(x, t_0)$ are impractical compared to measurements of the surface elevation itself and it is desirable to eliminate $q(x, t_0)$ from the problem. I proceed to address these issues below.

The expression

$$\phi = \frac{1}{(2\pi)^N} \sum_k e^{ik\cdot x} \cosh(|k|z)\hat{q}(k) + \frac{1}{(2\pi)^N} \sum_k e^{ik\cdot x} \frac{\sinh(|k|z)}{|k|} \hat{\eta}_t(k), \tag{3}$$

is a formal solution of (2a-2c) when $\eta(x,t_0) \equiv 0$. Here $\hat{q}(k)$ and $\hat{\eta}_t(k)$ are the Fourier transforms of $q(x,t_0)$ and $\eta_t(x,t_0)$ respectively. Thus

$$\hat{q}(k) = \int_R e^{-ik\cdot x} q(x)dx, \quad \hat{\eta}_t(k) = \int_R e^{-ik\cdot x} \eta_t(x)dx,$$

where

$$R = \{x \in \mathbb{R}^N : 0 < x_i < L_i, i = 1, \ldots, N\}$$

is the horizontal domain. The summation extends over all k in the lattice dual to the period lattice *i.e.*, over all possible wavenumbers.

To find ζ, evaluate the left-hand side of equation (1b) using (3) for ϕ. This results in the nonlinear function whose zero is the surface ζ. If the given Cauchy data (the Dirichlet data $q(x,t_0)$ and the Neumann data $\eta_t(x,t_0)$) are consistent with a well-posed *boundary-value problem* for Laplace's equation (for instance a Dirichlet condition at $z = 0$ and the Neumann condition (1c) at $z = \zeta$), then the solution exists outside of a small neighborhood of the surface $z = 0$. For the specific form of the solution (3) to be valid at $z = \zeta$ we require additional hypotheses. This is related to the issues discussed in section 3.4 of Chapter 3.

The expression (3) for ϕ may be generalized to $\eta(x,t_0) = h_0$ where h_0 is a constant. Fourier transform methods are cumbersome when initial conditions are given on surfaces, as in (2a-2c). Therefore we reduce this initial-value problem (IVP) to a problem posed on $z = -h_0$.

The reformulation of the water-wave problem due to Ablowitz *et al.* [2] introduces a global relation for the Laplace equation. The global relation connects the boundary information on the surface η and on the bottom topography ζ. We limit ourself to applying the nonlocal relation of Ablowitz *et al.* [2] on the region $-h_0 < z < \eta(x,t_0)$. This allows us to transfer the data on $z = \eta(x,t_0)$ to equivalent data on $z = -h_0$.

Let ϕ be a harmonic function in $0 < x_i < L_i$, $-h_0 < z < \eta$, periodic in the horizontal variables x_i with period L_i. Following Ablowitz *et al.* [2],

$$\nabla \cdot \mathscr{F}_H + \frac{\partial \mathscr{F}_V}{\partial z} = 0,$$

where

$$\mathscr{F}_H = (-ik\phi_z + \omega\nabla\phi)\, E,$$
$$\mathscr{F}_V = (\omega\phi_z + ik\cdot\nabla\phi)\, E,$$

with $E = \exp(-ik\cdot\vec{x} + \omega z)$ and $\omega = \pm|k|$. Integrating this divergence form and applying Green's Theorem we obtain the global relations

$$\begin{aligned}&\int_R e^{-ik\cdot x+|k|\eta}\left[|k|(-\nabla\phi\cdot\nabla\eta+\phi_z)+ik\cdot(\nabla\phi+\phi_z\nabla\eta)\right]_{z=\eta}dx\\ &=\int_R e^{-ik\cdot x-|k|h_0}\left[|k|(-\nabla\phi\cdot\nabla\eta+\phi_z)+ik\cdot(\nabla\phi+\phi_z\nabla\eta)\right]_{z=-h_0}dx,\end{aligned}\tag{4}$$

and

$$\begin{aligned}&\int_R e^{-ik\cdot x-|k|\eta}\left[-|k|(-\nabla\phi\cdot\nabla\eta+\phi_z)+ik\cdot(\nabla\phi+\phi_z\nabla\eta)\right]_{z=\eta}dx\\ &=\int_R e^{-ik\cdot x+|k|h_0}\left[-|k|(-\nabla\phi\cdot\nabla\eta+\phi_z)+ik\cdot(\nabla\phi+\phi_z\nabla\eta)\right]_{z=-h_0}dx,\end{aligned}\tag{5}$$

where

$$R = \{x\in\mathbb{R}^N : 0 < x_i < L_i, i = 1,\dots,N\}.$$

The relations (4), (5) hold for all k in

$$\Lambda = \left\{\left[\frac{2\pi n_1}{L_1}, \frac{2\pi n_2}{L_2}\right]^T \;:\; n_j\in\mathbb{Z},\; n_1^2+n_2^2>0\right\},$$

which defines the lattice dual to the physical period lattice and disregards the zero mode, see [28] for details. Using

$$[-\nabla\phi\cdot\nabla\eta+\phi_z]_{z=\eta} = \eta_t,$$

and

$$[\nabla\phi+\phi_z\nabla\eta]_{z=\eta} = \nabla q,$$

where $\eta_t(x,t_0)$ and $q(x,t_0)$ are the Neumann and Dirichlet values imposed at $z=\eta(x,t_0)$, we may rewrite the global relations (4) and (5) as

$$\int_R e^{-ik\cdot x+|k|\eta}\left[|k|\eta_t + ik\cdot\nabla q\right]dx = \int_R e^{-ik\cdot x-|k|h_0}\left[|k|\tilde{\phi}_z + ik\cdot\nabla\tilde{\phi}\right]dx,\tag{6}$$

$$\int_R e^{-ik\cdot x-|k|\eta}\left[-|k|\eta_t + ik\cdot\nabla q\right]dx = \int_R e^{-ik\cdot x+|k|h_0}\left[-|k|\tilde{\phi}_z + ik\cdot\nabla\tilde{\phi}\right]dx.\tag{7}$$

where $\tilde{\phi} = \phi(x, -h_0)$. Multiplying (6) by $e^{|k|h_0}$ and (7) by $e^{-|k|h_0}$, we can solve for the terms on the right-hand side to obtain

$$\int_R e^{-ik\cdot x}\tilde{\phi}_z dx = \int_R e^{-ik\cdot x}\left[\cosh(|k|(\eta+h_0))\eta_t + i\frac{\sinh(|k|(\eta+h_0))}{|k|}k\cdot\nabla q\right]dx, \tag{8}$$

$$-\int_R e^{-ik\cdot x}\tilde{\phi} dx = \int_R e^{-ik\cdot x}\left[\frac{\sinh(|k|(\eta+h_0))}{|k|}\eta_t + i\frac{\cosh(|k|(\eta+h_0))}{|k|^2}k\cdot\nabla q\right]dx. \tag{9}$$

In order to obtain the above equations, we impose that ϕ is periodic. In other words, we assume there is no mean current. This assumption is made throughout the present work.

Let us take a moment to discuss what we have accomplished. A well-posed problem for Laplace's equation is a boundary-value problem, not a Cauchy-problem. Given data at both $z = \eta(x, t_0)$ and $z = -h_0$, we may employ the above global relations to solve for the remaining unknown boundary conditions. Green's integral representation for a harmonic function in terms of its boundary data provides a solution to Laplace's equation. This solution depends continuously on the given boundary information, see [32]. For the problem of bathymetry reconstruction, we are given information only on the surface $z = \eta(x, t_0)$ and hence we need to solve the Cauchy problem (an initial-value problem) which is well known to be ill-posed [32, 43]. However, with the knowledge that our input data comes from a well-posed boundary-value problem and that the domain of harmonicity extends at least to $z = -h_0$, the global relation allows us to transfer the given information at $z = \eta$ to that at $z = -h_0$. Consequently, we have evaluated the harmonic function in the interior of the domain. Since harmonic functions are analytic in the interior of their domain of definition (and hence their Fourier transform decays exponentially as a consequence of a Paley-Wiener-type theorem [57]), the Cauchy problem can be solved off the line $z = -h_0$.

The discussion in the previous paragraph suggests that the definition

$$\phi(x, z) = \sum_k e^{ik\cdot x}\cosh(|k|(z+h_0))\,\widehat{\tilde{\phi}} + \sum_k e^{ik\cdot x}\frac{\sinh(|k|(z+h_0))}{|k|}\,\widehat{\tilde{\phi}_z}, \tag{10}$$

is reasonable, and further that ϕ is harmonic in a neighborhood of $z = -h_0$. In particular we may look for a surface ζ on which ϕ satisfies a homogeneous Neumann condition using this definition. Hence we consider

$$F(\zeta) = \left[\phi_z - \nabla\zeta\cdot\nabla\phi\right]_{z=\zeta(x)}, \tag{11}$$

where ϕ is given by (10). We have obtained a nonlinear function of ζ whose zero implies the bottom-boundary condition (1b) is satisfied. If we find such a ζ, then existence-uniqueness results for the Laplace equation (and the water-wave problem in particular [49, 69]) imply we have recovered the bottom topography. Notice however, that the numerical evaluation of the above expression for F is a formidable task. Considerable care must be taken in evaluating the hyperbolic functions. The exponential growth of such terms in (10) can cause numerical errors leading to errors in the overall solution.

Remark 4.1.1 *Under the assumption of the existence of h_0 such that*

$$\min_x \eta > -h_0 > \max_x \zeta,$$

equation (10) is an equally effective starting point for a boundary-value problem for Laplace's equation. Indeed, enforcing the given boundary conditions at $z = \eta$ and $z = \zeta$, we have two equations for the two unknowns $\widehat{\tilde{\phi}_z}$ and $\widehat{\tilde{\phi}}$. The right-hand side of (10) may be interpreted as a sum of linear operators acting on $\widehat{\tilde{\phi}_z}$ and $\widehat{\tilde{\phi}}$. Solving this system of equations effectively requires "dividing" by the hyperbolic terms. It is precisely this inversion that leads to the smoothness of the harmonic function in the interior as well as the well-posedness of the boundary-value problem. See Chapter 3 for further details regarding boundary-value problems for Laplace's equation and the forward problem of the time evolution of a water wave.

The nonlinear function F defined in (11) depends on both the Neumann and Dirichlet data at the surface $z = \eta(x, t_0)$. We may treat the Dirichlet data as an unknown if we can supplement the equation (11) with another. Indeed, equation (1b) holds for all time. Hence we consider the following system of nonlinear equations for ζ and q:

$$\begin{cases} F(\zeta, q) = [\phi_z - \nabla\zeta \cdot \nabla\phi]_{z=\zeta(x)} = 0, & \text{(12a)} \\ \dfrac{d}{dt}F(\zeta, q) = \dfrac{d}{dt}\left([\phi_z - \nabla\zeta \cdot \nabla\phi]_{z=\zeta(x)}\right) = 0, & \text{(12b)} \end{cases}$$

where

$$\begin{aligned} \nabla\phi(x, z) &= \sum_{k\in\Lambda} ike^{ik\cdot x}\left(\cosh(|k|(z + h_0))\widehat{\tilde{\phi}} + \frac{\sinh(|k|(z + h_0))}{|k|}\widehat{\tilde{\phi}_z}\right), \\ &= \sum_{k\in\Lambda} e^{ik\cdot x}\left(\cosh(|k|(z + h_0))\widehat{\nabla\tilde{\phi}} + \frac{ik}{|k|}\sinh(|k|(z + h_0))\widehat{\tilde{\phi}_z}\right), \end{aligned} \quad \text{(13)}$$

and

$$\begin{aligned}\phi_z(x,z) &= \sum_{k\in\Lambda} e^{ik\cdot x}\left(|k|\sinh(|k|(z+h_0))\widehat{\tilde{\phi}} + \cosh(|k|(z+h_0))\widehat{\tilde{\phi}_z}\right),\\ &= \sum_{k\in\Lambda} e^{ik\cdot x}\left(-\frac{ik}{|k|}\sinh(|k|(z+h_0))\widehat{\nabla\tilde{\phi}} + \cosh(|k|(z+h_0))\widehat{\tilde{\phi}_z}\right). \end{aligned} \tag{14}$$

The fluid velocities at $z=-h_0$ (the tilde variables) are given in terms of surface measurements by

$$\widehat{\tilde{\phi}_z} = \int_R e^{-ik\cdot x}\left[\cosh(|k|(\eta+h_0))\eta_t + i\frac{\sinh(|k|(\eta+h_0))}{|k|}k\cdot\nabla q\right]dx, \tag{15}$$

$$\widehat{\nabla\tilde{\phi}} = \int_R e^{-ik\cdot x}\left[\frac{-ik}{|k|}\sinh(|k|(\eta+h_0))\eta_t + \cosh(|k|(\eta+h_0))\frac{k}{|k|^2}k\cdot\nabla q\right]dx. \tag{16}$$

Finally, we supplement these equations with the time derivative of the surface velocity potential, namely

$$\frac{\partial q}{\partial t} = -g\eta - \frac{1}{2}|\nabla q|^2 + \frac{(\eta_t+\nabla q\cdot\nabla\eta)^2}{2(1+|\nabla\eta|^2)},$$

which is the equation of evolution for the surface potential [2]. As the velocity potential at the surface only appears through its spatial derivatives, we solve equations (12a) and (12b) for the unknowns ζ and ∇q.

Examining equation (12b), we observe that at some instant of time, we require the surface displacement $\eta(x,t_0)$, the normal velocity $\eta_t(x,t_0)$ and its rate of change $\eta_{tt}(x,t_0)$ as functions of the horizontal variable x. Figure 4.1 provides an overview of the algorithm to reconstruct the bottom boundary. Assume we are given the Dirichlet (rather its gradient *i.e.*, the tangential derivative of the velocity potential) and Neumann data (the normal velocity $\eta_t(x,t_0)$) at the surface $z=\eta(x,t_0)$. We use the AFM global relation to convert this data to corresponding data at some height $z=-h_0$. Using the information at the horizontal line $z=-h_0$, we solve the initial-value problem for Laplace's equation in the vertical direction (along z). Finally we look for a surface $z=\zeta$ such that the normal derivative of the potential (obtained through solving the initial-value problem) along the surface vanishes. Thus we have evaluated the nonlinear function F in equation (12a) assuming we know $q(x,t_0)$. However, as the boundary condition (1b) holds for all time, we impose relation (12b). This allows us to eliminate the Dirichlet data at $z=\eta(x,t_0)$. Although the

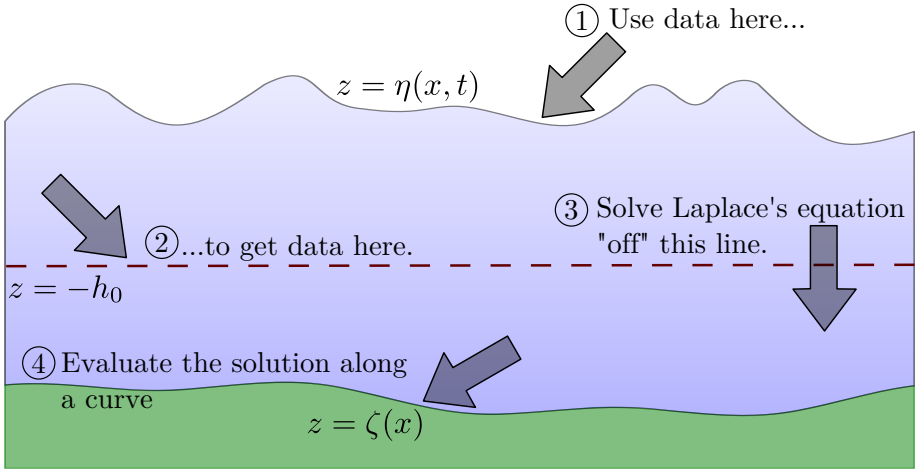

Figure 4.1: Algorithm for reconstruction of the bottom surface.

presentation above is valid for $N = 1, 2$, we restrict ourselves to $N = 1$ for the rest of the discussion.

Remark 4.1.2 *As shown by Lannes [49] and Wu [69], the water-wave problem* (1a-1d) *is well posed and has a unique solution. Since the set of nonlinear equations* (12a-12b) *are necessary conditions for the full water-wave problem, existence of solutions to these nonlinear equations is guaranteed. I do not investigate uniqueness of solutions to these equations.*

4.2 Examples

In this section I present example reconstructions carried out using the method proposed in the previous section. In all reconstructions presented here both the surface η and the normal velocity η_t are assumed to be given at some instant of time. Typically η and η_t are obtained from a simulation of the time-dependent evolution of the water-wave equations (see Chapter 3). The general inverse problem requires η_{tt} to be provided as well. In such cases, η_{tt} is computed from η_t using a five-point finite-difference stencil. In all the examples discussed below, I assume that the input data is obtained from the non-dimensional version

of equations (1a-1d). Assuming the scalings (20) from Section 3.3 of Chapter 3 we have

$$\phi_{xx} + \phi_{zz} = 0, \qquad (x,z) \in D, \tag{17a}$$

$$\phi_z - \zeta_x \phi_x = 0, \qquad z = \zeta(x), \tag{17b}$$

$$\eta_t + \eta_x \phi_x = \phi_z, \qquad z = \eta(x,t), \tag{17c}$$

$$\phi_t + \frac{1}{2}\left(\phi_x^2 + \phi_z^2\right) + \eta = 0, \qquad z = \eta(x,t), \tag{17d}$$

where $D = \{(x,z) \in \mathbb{R}^2 : \zeta < z < \eta,\ 0 < x < m\pi\}$ and m is a positive integer. To distinguish the different regimes of the fluid flow (*i.e.*, shallow water, large amplitude, *etc.*) we define the quantities

$$\mu = \frac{|\zeta|}{m\pi}, \quad \epsilon = \max_x \left|\frac{\eta}{h}\right|, \quad h = \frac{1}{m\pi}\int_0^{m\pi} \zeta dx.$$

Thus the larger ϵ (the amplitude parameter) is, the more nonlinear the fluid flow is. Values of μ near 1 indicate deep water, whereas smaller values indicate shallow water. Notice μ is a function of the spatial variable x.

To solve equations (12a-12b) numerically, we approximate both unknowns ζ and q_x by their truncated Fourier series

$$\zeta = \sum_{k=-K_\zeta}^{K_\zeta} e^{ikx}\hat{\zeta}_k, \quad q_x = \sum_{k=-K_{q_x}}^{K_{q_x}} e^{ikx}\hat{q_x}.$$

Here K_ζ and K_{q_x} define the resolution of the series for the bottom surface and the tangential velocity at the free surface η, respectively. The input data to the nonlinear equations (12a-12b) are η, η_t and η_{tt} as functions of x at one particular time t_0. These are obtained from a simulation of the time-dependent evolution of water waves with K_η the highest wavenumber resolved in the horizontal direction. Thus the incoming data has a maximum resolution corresponding to K_η. The expressions in (13) and (14) involve summations over all wavenumbers. These summations are truncated with highest mode number K_ϕ during the computations. The nonlinear functions are evaluated at several points in the physical grid and the problem is solved as a least-squares problem with the Fourier modes of the bottom surface and tangential velocity as the parameters. I used MINPACK's implementation of the Levenberg-Marquardt algorithm as the least-squares solver.

4.2.1 Flat bottom reconstruction using traveling wave solutions

As a first example, consider the case of a traveling-wave solution of Euler's equations. The exact nonlinear traveling-wave solutions corresponding to a particular value of the speed c are obtained from the work of Deconinck & Oliveras [28]. Given the surface profile η, computing η_t and η_{tt} is straightforward once the traveling-wave assumption is made. However, in this special case we know that the tangential velocity at the surface is related to the surface profile η through

$$q_x = c - \sqrt{(c^2 - 2g\eta)(1 + \eta_x^2)},$$

as described in [28]. Consequently, the second equation (12b) is *not* required for the bottom surface reconstruction. This dramatically reduces the computational effort. Furthermore, the bottom surface in the case of a traveling wave is known to be flat (for otherwise the bottom boundary ζ must be time-dependent) and we are in search of a single mode for the bottom surface. One may attempt to find the zero of the norm of the nonlinear function (12a). However I minimize the full function evaluated at various grid points in the horizontal variable. In fact, I do not assume the bottom surface to be flat, *i.e.*, I assume the bottom surface is parametrized by several modes, as in the general case.

Figure 4.2 depicts a 2π-periodic traveling-wave solution (solid line) with $\max|\eta| = 0.001$. The bottom boundary is given by $\zeta = -0.1$ and the speed of the wave $c = 0.31641443$. Thus $\epsilon = 0.01$ and $\mu = 0.016$. The initial guess for the bottom surface is shown as a dashed line. As mentioned earlier, the bottom surface is not assumed to be uniform. The true bottom surface is given by the thin solid line whereas the dotted line indicates the reconstructed bottom surface evaluated at select points. Because of the difference in magnitude of the free surface and bottom topography, I have used dual axes. The relative error in the reconstructed solution is $O(10^{-10})$. Note that all modes except the zero mode are reduced in magnitude from their initial value. Indeed, in our method, the solution converges precisely to the bottom surface without any *a priori* knowledge of the average depth. This is in contrast to other methods based on water-wave motion that have been suggested in the literature, for instance [54].

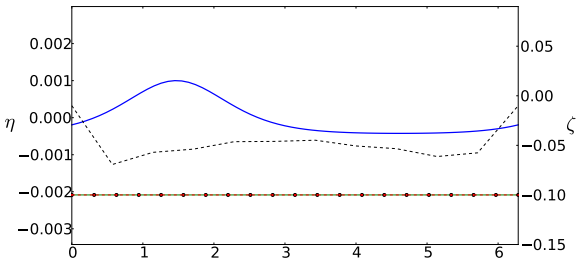

Figure 4.2: Flat bottom reconstruction using traveling wave solutions. Note the dual axes for this figure. The free surface η is shown with the solid bold line (with axis on the left). The true bottom surface and the reconstructed surface are shown in solid and dotted lines respectively, with the axis on the right. The initial guess for the least-squares solver is shown by the dashed line.

4.2.2 Flat bottom reconstruction using non-stationary waves

Using non-stationary waves, both equations (12a) and (12b) must be solved simultaneously. In this section I present the reconstruction of a flat bottom, as in the previous example. When the surface η and normal velocity η_t are given, we are able to reconstruct the flat bottom of $\zeta = -0.1$. At times $t = 0.5$ and $t = 1.0$ (Figure 4.3), the relative error in the tangential velocity at the surface is $O(10^{-8})$ and the relative error in the reconstruction of the bottom surface is $O(10^{-9})$. The shallowness parameter μ for these cases is 0.008 and $\epsilon = 1.25$ based on the initial condition for the forward problem. Thus the input data corresponds to very nonlinear flow in shallow water. Typically, both tangential velocity and bottom surface need to be well resolved to obtain a zero for the nonlinear functions (12a-12b).

Figure 4.4 depicts the reconstruction of the same flat surface, but at a later time. As seen in (4.4b), the normal velocity and its time rate of change are sharply peaked. This creates some numerical challenges when the fluid velocities at $z = -h_0$ (15-16) are computed using the same number of Fourier modes as are used for the surface quantities. To allow the least-squares solver to converge we need to smooth the data at $z = -h_0$ by reducing K_ϕ

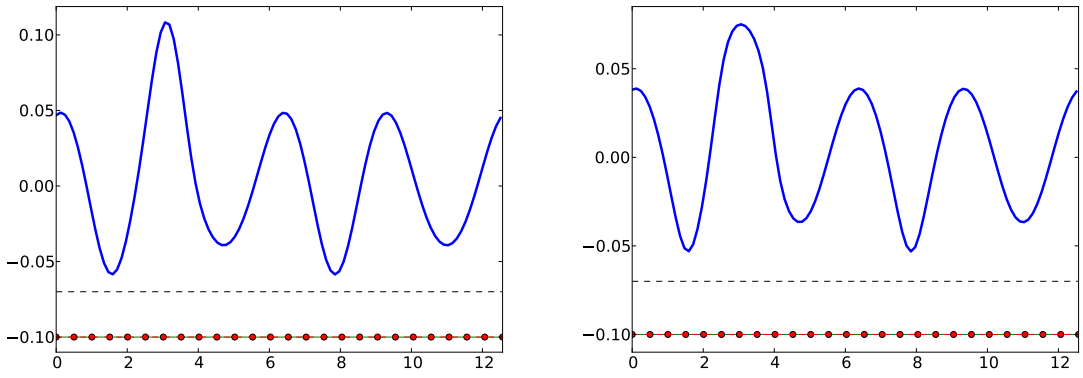

(a) $t = 0.5$ (b) $t = 1.0$

Figure 4.3: Reconstructing the flat bottom using non-stationary flow. The blue solid bold line shows the free surface η, the dashed line is the initial guess and red dots depict the final solution. The true solution is shown by the thin solid line. The true bottom surface and the reconstruction are indistinguishable on the scale of the figure.

appropriately. On truncating the modes, the solver converges to the true solution. Without truncation ($K_\phi = K_\eta$), the least-squares routine converges, however the nonlinear function has non-zero norm at the solution. This and other numerical issues are discussed in detail in Section 4.3.

4.2.3 x−dependent bathymetry

In this section I present the recovery of more complicated bottom surfaces. The first example is of a surface that is approximated by a finite number of Fourier modes whereas the remaining examples properly require an infinite number of modes. However in the latter cases, the bottom surface is well represented by a sufficiently large number of Fourier modes. In all cases both equations (12a) and (12b) were solved using a least-squares routine assuming the knowledge of $\eta(x, t_0)$ and $\eta_t(x, t_0)$ (obtained from a simulation of the time-dependent forward problem).

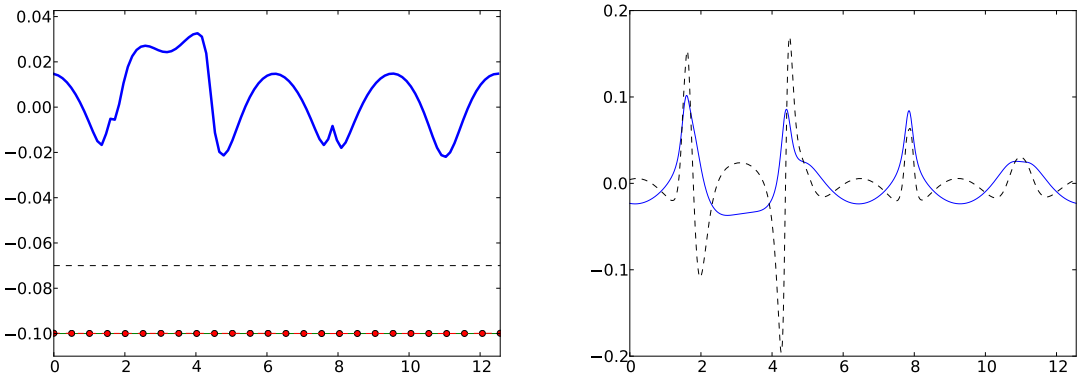

(a) $t = 2$.

(b) η_t (solid) and η_{tt} (dashed) vs. x at $t = 2$.

Figure 4.4: Reconstructing a flat bottom from non-stationary flow. Figure 4.4a is the same as Figure 4.3 but at $t = 2$. Notice the sharply peaked spatial profiles of η_t and η_{tt} in Figure 4.4b which poses difficulty in bottom surface reconstruction.

High-frequency wavy bottom

The following bottom surface

$$\zeta = -0.2 - (0.01 \sin 2x + 0.025 \sin x \cos 2x + 0.01 \sin 12x)\,, \tag{18}$$

which is represented by a finite number of Fourier modes, was recovered using data from a simulation of the forward problem. The shallowness parameter varies between 0.0134 and 0.0183 whereas ϵ is roughly 0.3 indicating moderate amplitude waves in shallow water. Here I present results from one instance t_0, but it should be noted that the same surface may be recovered from data at *any* instance. Figure 4.5 presents the bottom surface recovered for fixed K_{q_x} and increasing K_ζ. As seen from Figures (4.5a-4.5d), the bottom surface is progressively better approximated with increasing K_ζ. As K_ζ is increased, the norm of the nonlinear functions in (12a-12b) decreases, providing a check for convergence to the true solution. Figures 4.5e-4.5f show the bottom surface and tangential velocity at the free-surface for a suitably large value of K_{q_x}. The relative error in either ζ or q_x was observed to be $O(10^{-9})$. Note that the zero mode of the bottom surface was recovered from the

least-squares computation as well.

A Gaussian bump

Our next example is the recovery of a localized feature on an otherwise flat bottom-surface. The bottom surface is given by

$$\zeta = -0.2 + 0.025e^{-(x-L/2)^2}, \tag{19}$$

where L is the period in the horizontal direction. A localized feature such as a Gaussian is well represented in Fourier space by a suitably large number of modes. Consequently, as seen in Figure 4.6, $K_\zeta = 8$ is sufficient to recover the bottom surface accurately. The reduced amplitude in the surface deviation (as compared to the previous example, here $\epsilon = 0.03$) implies that large values of K_{q_x} are not required. Figure 4.6c is a plot of the relative error in the bottom surface ζ (dots) and the tangential velocity at the free-surface q_x (asterisks) versus K_{q_x}. We see a similar convergence to the true solution as K_{q_x} increases. Larger values of K_{q_x} do not result in any further reduction in the relative error. Possible reasons for this are discussed in the next section.

A sandbar

Consider the bottom surface given by

$$\zeta = -0.1 + 0.015\tanh(3(x - 0.3L)) + 0.015\tanh(3(x - 0.7L)), \tag{20}$$

which models a sandbar. Figure 4.7a presents recovery of this profile (shown with circle markers) and the true bottom surface (solid line). The free surface (bold solid line) and initial guess for the bottom surface (dashed line) are shown for reference. Alongside, in Figure 4.7b, we see the mode-by-mode relative error (dashes) between the computed bottom surface (dots) and the true bottom surface (solid line). As expected, the relative error is largest for modes with smallest amplitude. The overall relative error for the bottom surface in the infinity-norm is $O(10^{-7})$ and in the 2-norm is $O(10^{-8})$.

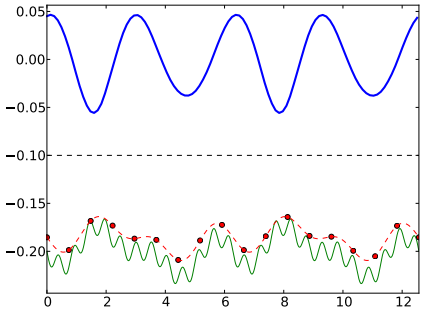

(a) $K_\zeta = 4$, $K_{q_x} = 48$

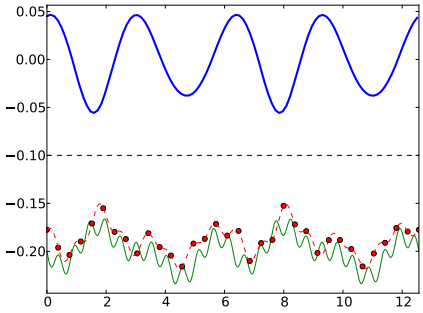

(b) $K_\zeta = 8$, $K_{q_x} = 48$

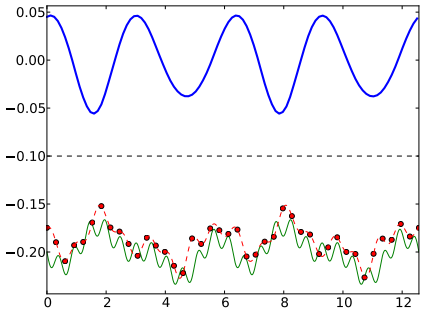

(c) $K_\zeta = 10$, $K_{q_x} = 48$

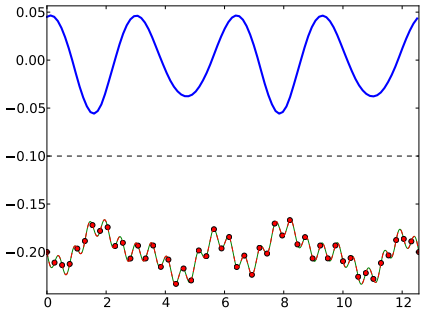

(d) $K_\zeta = 12$, $K_{q_x} = 48$

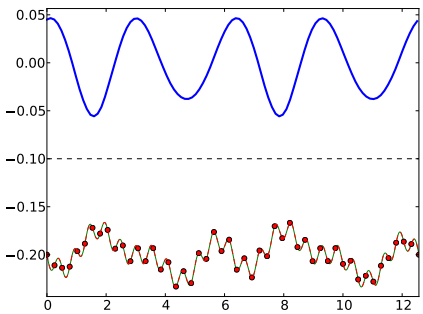

(e) $K_\zeta = 12$, $K_{q_x} = 62$

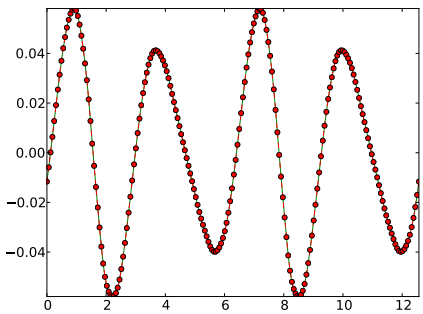

(f) $K_\zeta = 12$, $K_{q_x} = 62$

Figure 4.5: Bottom surface reconstruction with different resolutions. Figures 4.5a-4.5e depict the reconstructed surface (dots) and the true bottom surface (thin solid line) for different resolutions. The free surface is depicted by the solid bold line. Figure 4.5f shows the computed (dots) and true (solid) tangential velocity at the free surface.

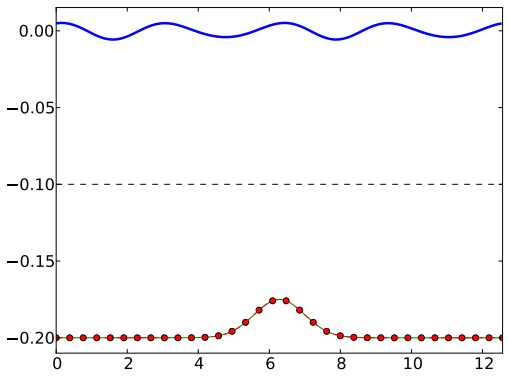

(a) Computed and true bottom surface

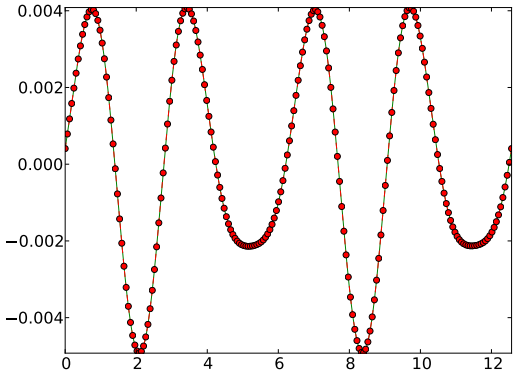

(b) Computed and true tangential velocity at free-surface

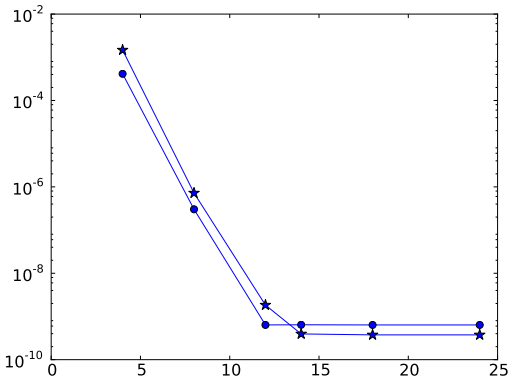

(c) Relative error vs. K_ζ for the bottom topography ζ shown in dots and for the tangential velocity at the free surface q_x shown in asterisks.

Figure 4.6: Reconstruction for the case of a Gaussian bump on bottom surface (19) with $K_\zeta = 8$, $K_{q_x} = 24$. Figure 4.6a-4.6b show the true solution (thin solid line) and the computed solution (dots). The bold solid line in 4.6a indicates the free surface η.

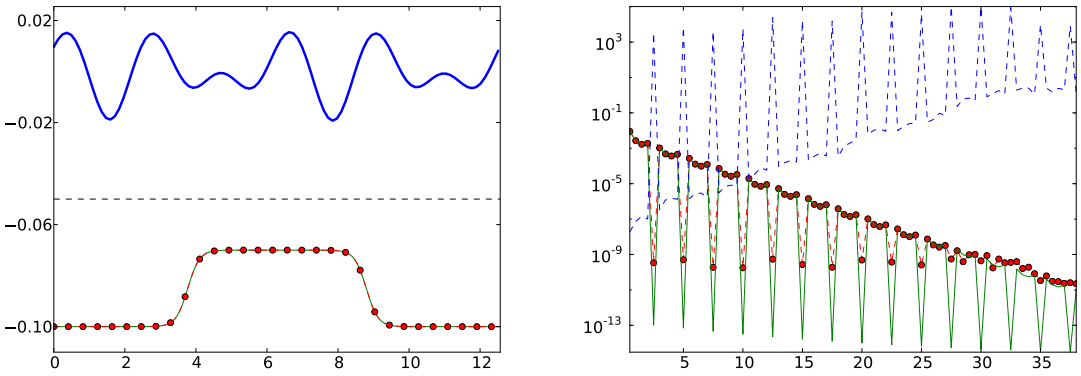

(a) (b)

Figure 4.7: Reconstruction of a sandbar profile. Figure 4.7a compares the true (thin solid) and computed (dots) bottom surfaces. Figure 4.7b is a mode-by-mode comparison of the amplitude in Fourier space of the true (solid line) and computed solution (dots). The dashed line indicates the relative error in the amplitude of each mode.

A multi-feature bottom surface

Our final example consists of recovering a more complex bottom surface consisting of two distinct isolated features: a smooth step and a ripple patch. The exact surface is given by

$$\begin{aligned}\zeta = &-0.2 + 0.02\tanh 10(x - L/8) - 0.02\tanh 10(x - L/4) \\ &+ 0.02\cos 6x\,(\tanh 10(x - 7L/8) - \tanh 10(x - 3L/4))\,. \end{aligned} \tag{21}$$

Figure 4.9 shows results for the bottom surface recovery for increasing K_ζ. The step-like condition properly requires an infinite number of Fourier modes, particularly to resolve the flat plateau between the features. Indeed the largest error is observed along the flat surface. Note the increased relative error in recovery of the bottom surface as compared to the other examples. The increased error is in part due to the fact that the bottom surface is not fully resolved in the forward simulation. The amplitudes of the Fourier modes of the bottom surface used in the forward simulation are shown in Figure 4.8. Ideally, the largest mode resolved should have amplitude on the order of machine precision (which is 10^{-15} for

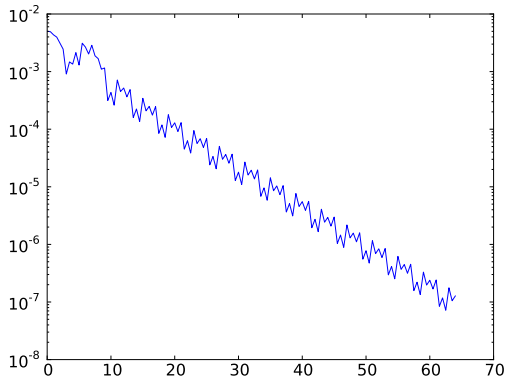

Figure 4.8: Amplitude of Fourier modes for the multi-feature bottom surface (21).

these calculations). As a result, the Hamiltonian for the time-dependent evolution of the water waves has a relative error of $O(10^{-6})$ compared to the desired $O(10^{-15})$ for the other simulations. In effect, this example illustrates the reconstruction of the bottom surface from data that is not an accurate solution to the water-wave problem. Of course, there are many issues to be separated before we can conclusively establish reconstruction from erroneous data. However, this example indicates some degree of reliability in bathymetry detection.

4.3 Discussion of numerical issues

Not unexpectedly, the majority of the numerical issues stem from the ill posed nature of the inverse problem, as expressed through the presence of the growing hyperbolic functions in our formulation. In this section I discuss various consequences of the hyperbolic functions on the reconstruction of the bottom surface.

4.3.1 Number of modes vs. length scales

Due to the exponential growth of the hyperbolic functions present in the nonlinear equations (12a) and (12b), numerical overflow is observed if the wavenumbers involved in the calculation are too large. Even when the overflow is avoided, due to the finite precision of the floating point representation, the accuracy in evaluating the expressions involved in

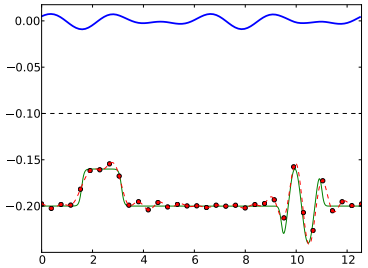

(a) $K_\zeta = 8$

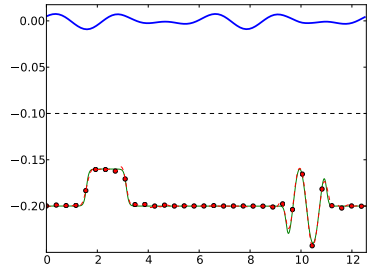

(b) $K_\zeta = 16$

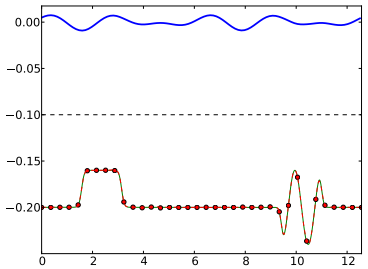

(c) $K_\zeta = 26$

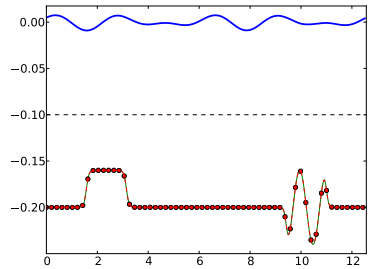

(d) $K_\zeta = 46$

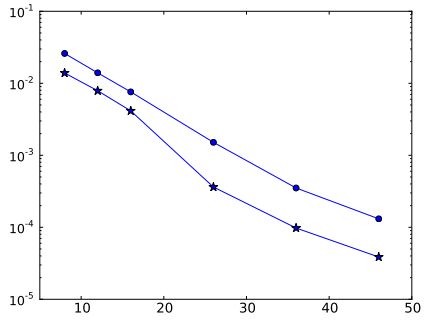

(e) Relative error vs. K_ζ for the bottom topography ζ (dots) and for the tangential velocity at the free surface q_x (asterisks).

Figure 4.9: Reconstruction of the multi-feature bottom surface (21) using different resolutions for the bottom surface. The thin solid line indicates the true solution and the dotted line shows the computed solution. The solid blue line is the free surface η and the dashed line is the initial guess for the least-squares solver.

the nonlinear functions is easily lost for larger wavenumbers. The inaccuracy in evaluating the left-hand side of the nonlinear equations results in inaccurate reconstructions. Large wavenumbers are required to reconstruct bottom surfaces corresponding to large amplitude waves, as well as to reconstruct fine detail of the bottom surface. To inhibit the size of the wavenumbers involved, we are forced to consider water waves with small μ values. The natural interpretation is that long waves enable easier reconstruction of bottom surfaces than short waves. A useful check on the inaccuracy of the function evaluation is to compare the relationship between the nonlinear function F and its derivative. If the function and its derivative are correctly evaluated then

$$\|F(\zeta + \Delta\zeta) - DF(\zeta)\Delta\zeta\| = O(\|\Delta\zeta\|^2). \tag{22}$$

Typically, with larger values for K_ζ, K_{q_x}, K_ϕ and K_η, this behavior is not observed. As a result, establishing convergence of the reconstructed bottom surface for larger values of these wavenumbers is not possible on a machine with finite precision. This is true particularly in the cases when the bottom surface properly requires an infinite number of modes to be accurately represented and to avoid the Gibbs phenomenon.

4.3.2 The problem of deep water

The equations describing water waves are such that, for large values of μ (*i.e.* deep water), the gradient of the velocity potential rapidly decreases in magnitude. To see why this may be the case, consider the following boundary-value problem

$$\phi_{xx} + \phi_{zz} = 0,$$

for ϕ periodic in x with period 2π and

$$\phi(x, 0) = f(x), \quad \phi_z(x, h) = 0.$$

The solution to this boundary-value problem is given by

$$\phi(x, z) = \sum_{n=-\infty}^{\infty} e^{inx} \frac{\cosh(n(z + h))\hat{f}_k}{\cosh(kh)}.$$

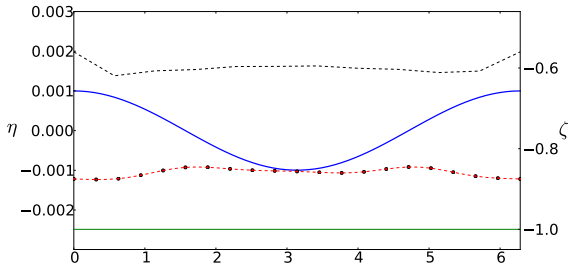

Figure 4.10: Reconstructing the bottom surface in "deep water". Note the dual axes for the free surface η (on the left) and the bottom surface ζ (on the right). The free surface is shown by the solid bold line whereas the reconstructed bottom surface is shown by the dotted line. The true bottom surface is give by the thin solid line and the initial guess for the least-squares solver is shown by the dashed line (both with axes on the right).

The $z-$derivative vanishes at $z = -h$ due to the boundary condition. The $x-$derivative at $z = -h$

$$\phi_x(x, -h) = \sum_{n=-\infty}^{\infty} e^{inx} \frac{ik\hat{f}_k}{\cosh(kh)},$$

is seen to decay uniformly in x as $h \to \infty$. Thus a consequence of terms such as $\cosh(kz)$ and $\sinh(kz)$ in (3) is that the solution decays exponentially in the vertical direction. The bottom surface we seek to reconstruct is defined as the zero of a function whose coefficients decay rapidly to zero. Hence on a finite-precision machine, finding the zero of this function is challenging. For sufficiently large depth, the function itself may evaluate identically to zero up to machine precision. At this point any function $\zeta(x)$ is a viable candidate for the bottom topography and the least-squares routine may converge to an incorrect solution. In the example shown in Figure 4.10, we try to reconstruct a flat bottom from a small (but nonzero) amplitude traveling wave in fairly deep water. Since the wave is a stationary solution, we may use (12a) alone to solve for the bottom surface as in section 4.2.1. The phrase "deep water" does not reflect the standard use in water-wave stability theory, as it is unrelated to the Benjamin-Feir instability. I use the word "deep" rather loosely to signify a regime where the fluid velocities are of the order of machine precision near the

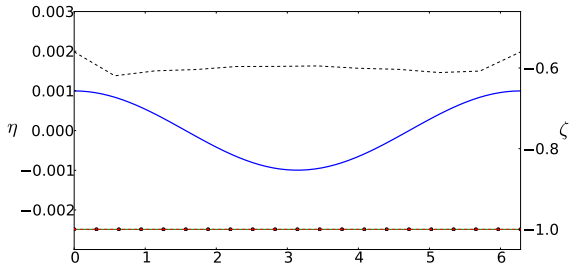

Figure 4.11: Reconstruction of the bottom surface in Section 4.3.2 using a lower resolution at $z = -h_0$ than that of Figure 4.10.

bottom boundary. Hence the phrase "deep water" refers to a *purely numerical effect* which is not distinguished by any physical phenomena. On any machine with finite precision, there are values of the shallowness parameter μ (typically much larger than 1) which imply the water is deep in our sense of the term and inhibit bottom-surface reconstruction. Certainly, computing the solution on a machine which supports arbitrary precision overcomes this issue. This paper does not discuss arbitrary precision computations. It should be remarked that the surface velocities are nonzero throughout the horizontal interval and they are not on the order of machine precision at the free surface. However, the velocities of the fluid are on the order of machine precision near $z = -0.9$. One possible fix to the situation described above on a machine with finite precision is to "lose" Fourier modes as we proceed deeper in the fluid. Instead of maintaining the number of modes for the fluid velocities at $z = -h_0$ (15-16), equal to those used at the surface, I reduce K_ϕ (in effect smooth the velocities) to a lower resolution. Figure 4.11 displays such a reconstruction with a relative error for the bottom surface reconstruction on the order of 10^{-11}. Thus, for deeper water (μ large) we can reconstruct only the large-scale features of the bottom topography effectively recovering the features corresponding to shallow water. Of course, for sufficiently deep water, bottom surface reconstruction is practically impossible.

The effect of deep water remains when considering non-stationary flow as is seen by considering the same bottom shape as given by equation (20) but at a deeper level. Figure 4.12 depicts this situation for a reduced value of K_ϕ (about half of K_η). The relative error

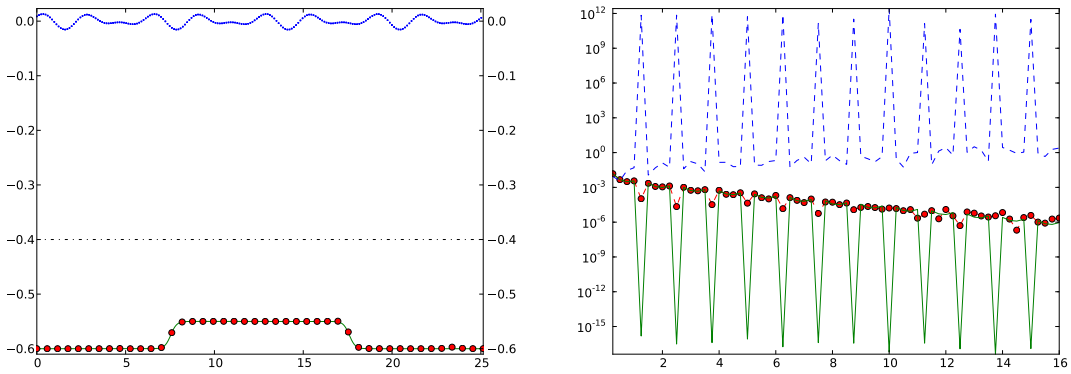

(a) (b)

Figure 4.12: Reconstruction of the sandbar profile (20) in deep water. Figure 4.12a compares the true (thin solid) and computed (dots) bottom surfaces. Figure 4.12b is a mode-by-mode comparison of the amplitude in Fourier space of the true (solid line) and computed solution (dots). The dashed line indicates the relative error in the amplitude of each mode.

in the reconstruction is $O(10^{-2})$ for both the 2-norm and the infinity norm. In this case, the situation is further compounded by the fact that the nonlinear function is harder to evaluate due to the loss of precision as the argument of the hyperbolic functions increases. Indeed, the nonlinear function and its derivative do not obey relationship (22) for this example.

4.3.3 Localized free-surfaces

It is intuitively obvious that still water (no surface deviation and zero surface velocities) can be bounded by any bottom surface. The difficulty in proving uniqueness of solutions to the set of equations (12a-12b) is in part due to this fact. Although the expressions are simpler when the surface deviation is zero, uniqueness of solutions does not hold. In this section I show this explicitly. Also I provide examples from simulations where this behavior can be observed.

Given the nature of water-wave motion, if the surface deviation is nonzero, then the normal velocity η_t at the surface must be nonzero as well. The method of reconstruction

presented in this chapter requires non-zero η, η_t and η_{tt}. In the case when $\eta = \eta_t = \eta_{tt} = 0$ the expressions for the nonlinear equations simplify considerably. They become

$$-i \sum_{k_n \in \Lambda} e^{ik_n x} \sinh(k_n \zeta) \widehat{q_x} - \zeta_x \sum_{k_n \in \Lambda} e^{ik_n x} \cosh(k_n \zeta) \widehat{q_x} = 0, \tag{23}$$

$$-i \sum_{k_n \in \Lambda} e^{ik_n x} \sinh(k_n \zeta) \widehat{q_x q_{xx}} - \zeta_x \sum_{k_n \in \Lambda} e^{ik_n x} \cosh(k_n \zeta) \widehat{q_x q_{xx}} = 0. \tag{24}$$

The periodicity of the function q implies these expressions can be rewritten as

$$\partial_x \sum_{k_n \in \Lambda} i e^{ik_n x} \sinh(k_n \zeta) \widehat{q} = 0, \tag{25}$$

$$\partial_x \sum_{k_n \in \Lambda} i e^{ik_n x} \sinh(k_n \zeta) \widehat{\frac{q_x^2}{2}} = 0. \tag{26}$$

These equations possess infinitely many non-trivial solutions as any ζ satisfies these equations for q constant since

$$\begin{aligned} \int_0^L e^{ik_n x} C dx &= C \int_0^L e^{ik_n x} dx, \\ &= C \delta_{k_n 0}, \end{aligned}$$

where $\delta_{k_n 0}$ is the Kronecker delta

$$\delta_{k_n 0} = \begin{cases} 1, & k_n = 0, \\ 0, & k_n \neq 0. \end{cases}$$

Following [24], equation (25) is a reformulation of the boundary-value problem

$$\phi_{xx} + \phi_{zz} = 0, \qquad 0 < x < L, \zeta < z < 0, \tag{27a}$$

$$\phi_z = 0, \qquad z = 0, \tag{27b}$$

$$\phi_z - \zeta_x \phi_x = 0, \qquad z = \zeta. \tag{27c}$$

The solution of this boundary-value problem may be written as

$$\phi = \sum_{k=-\infty}^{\infty} e^{ikx} \cosh(kz) \hat{\Phi}_k.$$

The boundary condition at $z = \zeta$ may be written in the form (25) with $\hat{\Phi}$ in the place of $\widehat{q}$. In other words, q is the Dirichlet value at the surface $z = 0$ for the boundary-value

problem associated with the first equation (23). The second equation (24) corresponds to a boundary-value problem with $q_x^2/2$ as the Dirichlet value at the surface $z = 0$. Further, nontrivial q that solve (23) imply nontrivial solutions for the above BVP (27a-27c). However, since the only nontrivial solutions for ϕ in the above boundary-value problem are constants, q is at most a constant in (23) and $q_x^2/2$ is at most a constant in (24). Hence $q = C$ for some constant C. It should be noted that ζ can be any continuously differentiable periodic function.

As a consequence of the arguments presented above, we do not expect the least-squares routine to capture the true bottom surface when $\eta = \eta_t = \eta_{tt} = 0$. In practice, the least-squares routine performs poorly when η, η_t and η_{tt} are near machine epsilon. Consider the example depicted in Figure 4.13 where I attempt to reconstruct the bottom surface using a localized free surface. Figure 4.13 shows three different positions of the localized surface deviation. The left column displays the free surface (bold solid line), reconstructed bottom surface (dashed line with dots) and true bottom surface (thin solid line). The right column compares the computed tangential velocity (dots) with the true tangential velocity (solid line). Of course, the localized free surface implies velocities (and consequently η_t and η_{tt}) are negligible far away from the localized disturbance. Clearly, the recovery is much better at those locations where the free-surface deviation is not negligible and poorer further away. It should be noted that the tangential velocity at the free surface is well resolved.

4.4 Examples revisited

To finish, I present results for bottom surface recovery using the surface deviation η (but not its $t-$derivative) as a function of the horizontal variable x at several times. A five-point finite-difference stencil is used to compute the time derivatives η_t and η_{tt}. Figure 4.14 shows the bottom surface recovered for the examples of Section 4.2.3. All errors reported are in the L_2-norm. In all cases, relation (22) holds for the given input data and choice of parameters (K_η and K_ϕ).

As seen in Figure 4.14, the error induced by the finite-difference approximation of η_t and η_{tt} does not significantly affect the bathymetry reconstruction. The relative error in bottom surface reconstruction is certainly greater than that observed earlier in Section 4.2.3

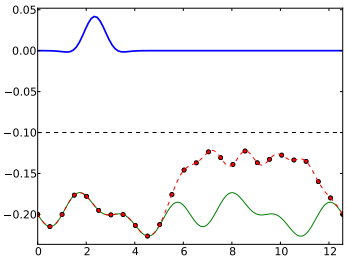

(a) True (thin solid line) and computed (dots) bottom surface.

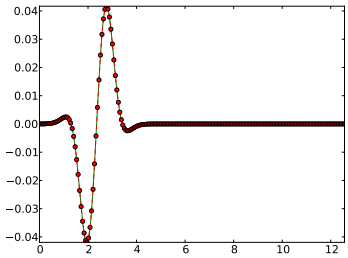

(b) True and computed tangential velocity at surface.

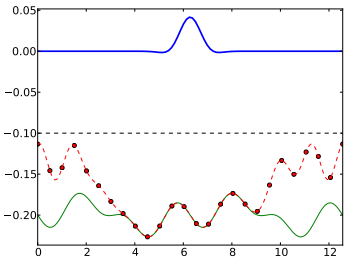

(c) True (thin solid line) and computed (dots) bottom surface.

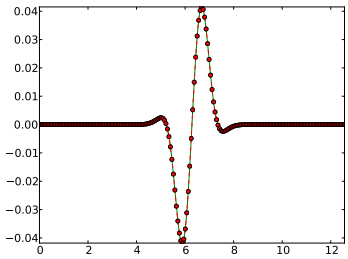

(d) True and computed tangential velocity at surface.

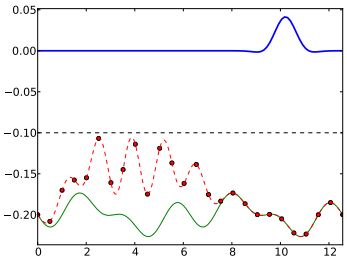

(e) True (thin solid line) and computed (dots) bottom surface.

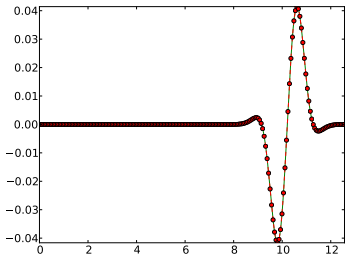

(f) True and computed tangential velocity at surface.

Figure 4.13: Recovering the bottom surface using localized surface deviations. Each row presents a reconstruction based on a different localized surface elevation profile (bold solid line in the left column). The left column shows true and computed bottom surfaces and the right column depicts the computed tangential velocity at the surface.

but not by much. As the reconstructions obtained using finite differences to compute time derivatives are remarkably accurate, I do not pursue more sophisticated methods to compute $t-$derivatives. Further, the finite-difference stencil uses the surface elevation η at five points in time and thus requires minimal input data.

To conclude, I have presented a technique to reconstruct the bottom boundary of an ideal incompressible irrotational fluid using only measurements of the free-surface elevation at several instances of time. The method makes no assumption on the magnitude or form of the surface elevation. It is valid for both one- and two-dimensional surface profiles and is accurate in the shallow-water regime.

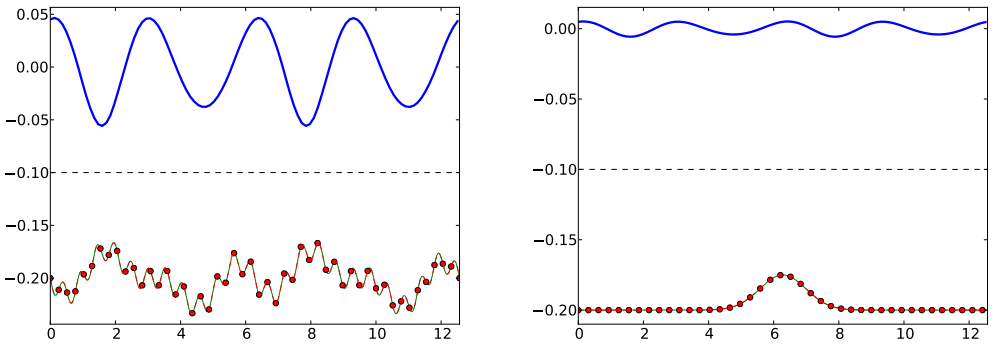

(a) Relative error in bottom surface: 8.22×10^{-7} (b) Relative error in bottom surface: 5.37×10^{-7}

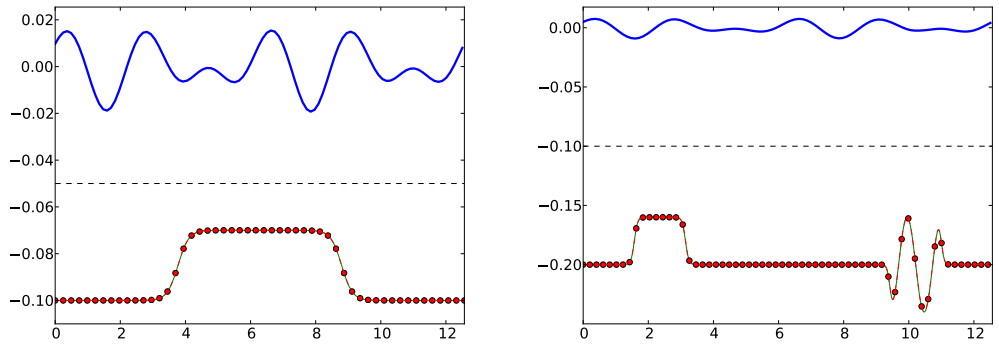

(c) Relative error in bottom surface: 1.27×10^{-7} (d) Relative error in bottom surface: 1.27×10^{-4}

Figure 4.14: Bottom surface reconstructions using finite differences to approximate time derivatives of the surface elevation η. I repeat the examples from Section 4.2.3 (bottom surfaces given by (18-21)) using only the surface elevation at several times as input data. A five-point finite-difference stencil is used to approximate the time derivatives. The true (thin solid line) and computed (dots) bottom surface cannot be distinguished on the scale of the figure. The free surface η is shown as a solid bold line and the initial condition for the least-squares solver is given by the dashed line.

Chapter 5

THE PRESSURE PROBLEM

I would like to acknowledge my collaborators Katie Oliveras and Diane Henderson. Their efforts are essential to obtain the results of this chapter. This chapter contains material published in SIAM Journal on Applied Mathematics.

In field experiments, the elevation of a surface water-wave in shallow water is often determined by measuring the pressure along the bottom of the fluid, see *e.g.* [7, 11, 47, 48, 66, 65]. A variety of approaches are used for this. The two most commonly used are the hydrostatic approximation and the transfer function approach. For the hydrostatic approximation [15, 27],

$$\eta(x,t) = \frac{P(x,-h,t)}{\rho g} - h, \tag{1}$$

where g is the acceleration due to gravity, h represents the average depth of the fluid, ρ is the fluid density, $P(x,-h,t)$ is the pressure as a function of space x and time t evaluated at the bottom of the fluid $z=-h$, and $\eta(x,t)$ is the zero-average surface elevation. Throughout, we assume that all wave motion is one-dimensional with only one horizontal spatial variable x. The hydrostatic approximation is used, for instance, in open-ocean buoys employed for tsunami detection by the National Data Bouy Center.

The transfer function approach uses a linear relationship between the Fourier transforms $\mathcal{F}$ of the dynamical part of the pressure and the elevation of the surface [15, 27, 31, 46]:

$$\mathcal{F}\{\eta(x,t)\}(k) = \cosh(kh)\mathcal{F}\{p(x,t)/g\}(k), \tag{2}$$

where $p(x,t) = (P(x,-h,t) - \rho g h)/\rho$ is the dynamic (or non-static) part of the pressure $P(x,z,t)$ evaluated at the bottom of the fluid $z=-h$, scaled by the fluid density ρ. In this relationship, η and p are regarded as functions of the spatial coordinate x, with parametric

dependence on time t. It is equally useful to let t vary for fixed x, as would be appropriate for a time series measurement, which results in extra factors of the wave speed $c(k)$, due to the presence of a temporal instead of a spatial Fourier transform.

It is well understood that nonlinear effects play a significant role when reconstructing the surface elevation for shallow-water waves or for waves in the surf zone (see [10, 11, 65], for instance). Since nonlinear effects are not captured by the linear transfer function (2), different modifications of (2) have been proposed. One approach is to modify the transfer function to incorporate extra parameters (*e.g.*, multiplicative factors, width scalings) that are tuned to fit data [47, 48, 65]. A less empirical approach is followed in [10] and [50] where corrections to the transfer function are proposed based on higher-order Stokes expansions. Bishop & Donelan [11] examine the empirical approaches and argue that the inclusion of the proposed parameters is not necessary as errors from inaccuracy in instrumentation and analysis are likely to outweigh the benefit of their presence. In this chapter, we do not include any of the modified transfer function approaches in the comparisons we make in section 5.4.

Bishop and Donelan [11] acknowledge that the linear response cannot accurately capture nonlinear effects. While both the hydrostatic model and the transfer function approach are accurate on some scales, they fail to reconstruct the surface elevation accurately in the case of large-amplitude waves, as might be expected. Errors of 15% or more are common, as is shown and discussed below. In order to address the inaccuracies of the linear models, nonlinear methods are required. With the exception of recent work by Escher & Schlurmann [31] and Constantin & Strauss [23], few nonlinear results are found in the literature. Escher & Schlurmann [31] provide a consistent derivation of (2) and offer some thoughts about the impact of nonlinear effects. Starting from a traveling wave assumption, Constantin & Strauss [23] obtain different properties and bounds relating the pressure and surface elevation. However, they do not present a reconstruction method to accurately determine one function in terms of the other. The paper [22] revisits the mathematical properties found by these authors, and examines them in an experimental setting. From a theoretical point of view the qualitative properties of the pressure play a central role in understanding the properties of irrotational traveling water waves such as in showing that their free surface

is the graph of a function [61, 67], and in discerning the patterns of particle paths beneath them [19, 21, 20].

One way to obtain an improved pressure-to-surface elevation map is to use perturbation methods to determine nonlinear correction terms to (2). Several such approaches are given below, and we include them when comparing the different methods. The main focus, however, is the presentation of a new nonlocal nonlinear relationship between the pressure at the bottom of the fluid, and the elevation of a traveling-wave surface that captures the full nonlinearity of Euler's Equations. The advantage of this approach is that

1. it allows for the surface to be reconstructed numerically from any given pressure data for a traveling wave,

2. it provides an environment for the direct analysis of the relationship between all physically relevant parameters such as depth and wave speed,

3. and it allows for the quick derivation of perturbation expansions such as the ones mentioned above.

4. Although the approach is formally limited to traveling waves, it can be applied with great success to more general wave profiles that are not merely traveling. This is illustrated and discussed below.

In what follows, we derive these nonlocal relations and demonstrate their practicality. We compare results from the nonlocal formulation with those from the linear approaches and different nonlinear perturbative models, using both numerical data for traveling waves in shallow water, and experimental data obtained at Penn State's Pritchard Fluid Mechanics Laboratory. We demonstrate the superiority of the nonlocal reconstruction formula for a large range of amplitudes. In addition, using the Implicit Function Theorem, we analyze the nonlocal formulation in order to demonstrate its solvability for the surface elevation given the pressure.

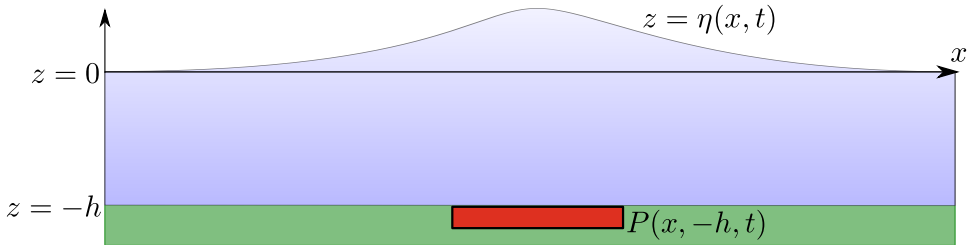

Figure 5.1: The fluid domain D for the water wave problem. An idealized pressure sensor is indicated at the bottom. In our calculations the pressure measurement is assumed to be a point measurement.

5.1 A nonlocal formula relating pressure and surface elevation

Consider Euler's equations describing the dynamics of the surface of an ideal irrotational fluid in two dimensions (with a one-dimensional surface):

$$\phi_{xx} + \phi_{zz} = 0, \qquad (x,z) \in D, \tag{3}$$

$$\phi_z = 0, \qquad z = -h, \tag{4}$$

$$\eta_t + \eta_x \phi_x = \phi_z, \qquad z = \eta(x,t), \tag{5}$$

$$\phi_t + \frac{1}{2}\left(\phi_x^2 + \phi_z^2\right) + g\eta = 0, \qquad z = \eta(x,t), \tag{6}$$

where $\phi(x,z,t)$ represents the velocity potential of the fluid with surface elevation $\eta(x,t)$. As posed, the equations require the solution of Laplace's equation inside the fluid domain D, see Figure 5.1. If the problem is posed on the whole line $x \in \mathbb{R}$, we require that all quantities approach zero at infinity. If periodic boundary conditions are used then all quantities at the right end of the fluid domain are equal to those at the left end. Below we work with the whole line problem, stating only the results for the periodic case.

Following [71], let $q(x,t)$ represent the velocity potential at the surface $z = \eta(x,t)$, so that

$$q(x,t) = \phi(x, \eta(x,t), t). \tag{7}$$

Combining the above with equation (5), we have

$$\phi_z = \eta_t + (q_x - \phi_z \eta_x)\,\eta_x,$$

obtained by taking an x-derivative of (7). This allows us to solve directly for ϕ_z in terms of η and q:

$$\phi_z = \frac{\eta_t + \eta_x q_x}{1 + \eta_x^2}. \tag{8}$$

Using (5) again gives an expression for ϕ_x, while taking a t-derivative of (7) leads to an expression for ϕ_t:

$$\phi_x = \frac{q_x - \eta_x \eta_t}{1 + \eta_x^2}, \quad \phi_t = q_t - \frac{\eta_t\,(\eta_t + \eta_x q_x)}{1 + \eta_x^2}. \tag{9}$$

Note that (8) and (9) are valid on the fluid surface only. Substituting these expressions into the dynamic boundary condition (6) we find

$$q_t + \frac{1}{2} q_x^2 + g\eta - \frac{1}{2}\,\frac{(\eta_t + q_x \eta_x)^2}{1 + \eta_x^2} = 0, \tag{10}$$

after some simplification.

Next, we restrict to the case of a traveling wave moving with velocity c. We introduce $\xi = x - ct$, so that x and t-derivatives become ξ-derivatives, the latter multiplied by $-c$. The Bernoulli equation (10) becomes a quadratic equation in q_ξ:

$$-cq_\xi + \frac{1}{2} q_\xi^2 + g\eta - \frac{1}{2}\,\frac{\eta_\xi^2 (q_\xi - c)^2}{1 + \eta_\xi^2} = 0. \tag{11}$$

Solving this quadratic equation, we find

$$q_\xi = c \pm \sqrt{(c^2 - 2g\eta)(1 + \eta_\xi^2)}, \tag{12}$$

where for $c > 0$ we choose the $-$ sign, to ensure that the local horizontal velocity is less than the wave speed [23]. Similarly, for $c < 0$ the $+$ sign should be chosen.

Substituting this result into (8) and (9), we find

$$\phi_\xi = c - \sqrt{\frac{c^2 - 2g\eta}{1+\eta_\xi^2}}, \qquad \phi_z = -\eta_\xi \sqrt{\frac{c^2 - 2g\eta}{1+\eta_\xi^2}}, \tag{13}$$

where we have chosen $c > 0$, without loss of generality. This simple calculations allows us to to express the gradient of the velocity potential at the surface directly in terms of the surface elevation.

Returning to the original coordinate system (x, z, t), let $Q(x,t) = \phi(x, -h, t)$, the velocity potential at the bottom of the fluid. Inside the fluid, we know that the Bernoulli equation holds:

$$\phi_t + \frac{1}{2}\left(\phi_x^2 + \phi_z^2\right) + gz + \frac{P(x,z,t)}{\rho} = 0, \quad -h \le z \le \eta(x,t). \tag{14}$$

Evaluating this equation at $z = -h$, we find

$$Q_t + \frac{1}{2}Q_x^2 - gh + \frac{P(x,-h,t)}{\rho} = 0. \tag{15}$$

Moving to a traveling coordinate frame as before, we obtain a quadratic equation for Q_ξ. Solving for Q_ξ we find

$$Q_\xi = c - \sqrt{c^2 - 2p}, \tag{16}$$

where $p(\xi)$ represents the non-static part of the pressure at the bottom in the traveling coordinate frame, scaled by the fluid density: $p(\xi) = P(x - ct, -h)/\rho - gh$. For consistency with our previous choice, we work with the $-$ sign again. Next, we connect the information at the surface with that at the bottom of the fluid.

Within the bulk of the fluid D,

$$\phi_{\xi\xi} + \phi_{zz} = 0, \tag{17}$$

where the boundary conditions given in (13) and (16) must also be satisfied. We can write the solution of this equation as

$$\phi(\xi, z) = \frac{1}{2\pi}\int_{-\infty}^{\infty} e^{ik\xi}\Psi(k)\cosh\left(k\left(z+h\right)\right)\, dk, \tag{18}$$

where the boundary condition for ϕ_z at $z = -h$ is satisfied. For the boundary condition at the bottom for ϕ_ξ we find

$$\frac{1}{2\pi}\int_{-\infty}^{\infty} ike^{ik\xi}\Psi(k)\,dk = c - \sqrt{c^2 - 2p}, \tag{19}$$

so that

$$ik\Psi(k) = 2\pi c\delta(k) - \mathcal{F}\left\{\sqrt{c^2 - 2p}\right\}(k), \tag{20}$$

where $\delta(k)$ is the Dirac delta function and $\mathcal{F}$ denotes the Fourier transform: $\mathcal{F}\{y(\xi)\}(k) = \int_{-\infty}^{\infty} y(\xi)\exp(-ik\xi)d\xi$. Evaluating $\phi_\xi(\xi, z)$ at the surface $z = \eta$, we have

$$\begin{aligned}\phi_\xi(\xi,\eta) &= \frac{1}{2\pi}\int_{-\infty}^{\infty} e^{ik\xi}ik\Psi(k)\cosh\left(k\left(\eta+h\right)\right)\,dk \\ &= c - \frac{1}{2\pi}\int_{-\infty}^{\infty} e^{ik\xi}\cosh\left(k\left(\eta+h\right)\right)\mathcal{F}\left\{\sqrt{c^2-2p}\right\}(k)\,dk.\end{aligned}$$

Using the boundary conditions given in (13), we find the nonlocal relationship

$$\sqrt{\frac{c^2 - 2g\eta}{1+\eta_\xi^2}} = \frac{1}{2\pi}\int_{-\infty}^{\infty} e^{ik\xi}\cosh\left(k\left(\eta+h\right)\right)\mathcal{F}\left\{\sqrt{c^2-2p}\right\}(k)\,dk. \tag{21}$$

Equation (21) is the main result of this chapter. It provides an implicit relationship between the surface elevation of a localized traveling wave $\eta(x)$ and the pressure measured at the bottom of the fluid $p(\xi)$. For the remainder of this chapter we investigate how this relationship may be used to compute $\eta(\xi)$ if $p(\xi)$ is known, and how different asymptotic formulas may be derived from it.

Remark 5.1.1 *In order to extend the above to periodic boundary conditions, we use the periodic generalization of the formulation of Ablowitz, Fokas, & Musslimani AFM, see [28]. Following the steps outlined above, this allows for the derivation of a relation between the surface elevation of a periodic traveling wave and the pressure at the bottom:*

$$\sqrt{\frac{c^2 - 2g\eta}{1+\eta_\xi^2}} = \frac{1}{2\pi}\sum_{k=-\infty}^{\infty} e^{ik\xi}\cosh\left(k\left(\eta+h\right)\right)\hat{P}_k, \tag{22}$$

where $\hat{P}_k = \int_0^{2\pi} e^{-ik\xi}\sqrt{c^2 - 2p(\xi)}\, d\xi$. *In what follows, we will use either (21) or (22).*

Remark 5.1.2 *In the above, we have assumed there exists a smooth solution to the water wave problem (3-6). Given a speed* c *and a non-hydrostatic pressure profile* p *as inputs, we aim to solve (21) for* η. *However, these inputs cannot be independent of each other: indeed arbitrary pressure profiles will not lead to surface elevations corresponding to solutions of (3-6). One expects that for a given speed* c, *there exists a surface elevations* η *and associated pressure profile* p. *In order to back up this intuition, we require another relation between* η, p *and* c. *Such a relation is found by taking a derivative with respect to* z *of (18) and equating the result to the right-hand side of the second equality in (13). Finally, (20) is used, resulting in*

$$\eta_x \sqrt{\frac{c^2 - 2g\eta}{1+\eta_x^2}} = \frac{-i}{2\pi}\int_{-\infty}^{\infty} e^{ikx}\sinh(k(\eta+h))\mathcal{F}\left\{c - \sqrt{c^2-2p}\right\}(k)dk. \tag{23}$$

The system of equations (21) and (23) may be solved to obtain both η *and* p, *given* c. *We will not pursue this issue further and content ourselves with establishing a map from* p *to* η.

For the purposes of the question considered here, the above is not an issue: we assume that the given pressure originates from experimental observations and hence corresponds to a solution of (3-6), to the extent that the Euler equations provide an accurate model for the water wave problem.

Remark 5.1.3 Obtaining the pressure at the bottom from the surface elevation. *An explicit nonlinear relationship for the pressure at the bottom in terms of the surface elevation may be obtained directly from the approach of Ablowitz, Fokas and Musslimani. Consider the relationship (the one-dimensional version of Equation* 1.11 *in [2])*

$$\int_{-\infty}^{\infty} e^{ikx\pm|k|(\eta+h)}\left(\mathrm{sgn}(k)\eta_t - i\, q_x\right) dx = -i\int_{-\infty}^{\infty} e^{ikx}\phi_x(x,-h,t)dx, \quad k\in\mathbb{R}_0. \tag{24}$$

Changing to a moving frame of reference and substituting the expressions (12,16) into this relation one obtains

$$\int_{-\infty}^{\infty} e^{ikx\pm|k|(\eta+h)}\left(\mp ic\,\eta_x+\left(c-\sqrt{(c^2-2g\eta)(1+\eta_x^2)}\right)\right)dx=\int_{-\infty}^{\infty} e^{ikx}\left(c-\sqrt{c^2-2p}\right)dx, \tag{25}$$

where top and bottom signs are selected consistently, and either choice is allowed. The right-hand side is essentially the Fourier transform of the quantity $c-\sqrt{c^2-2p}$. *Inverting this transform, one may solve for the pressure at the bottom in terms of the surface elevation. Equation (25) provides an alternative to (21) and can be used in its stead. The formula (25) is advantageous if one wishes to compute the pressure, given the surface elevation. A key point is that analyzing the global relation, one can formally derive suitable expressions to map data from one boundary to the other.*

Remark 5.1.4 *The explicit relation between (21) and (25) requires an understanding of the operators appearing in these equations. Such considerations are examined in [3] and [24]. Notice that these same operators appear when addressing the Forward Problem (Chapter 3) as well as the Inverse Problem (Chapter 4), emphasizing the relevance of adopting an approach that involves the global relation. Each of these problems is a different boundary-value problem for the same PDE (i.e., Laplace's equation) and each may be handled with equal ease using the associated global relations. The Pressure Problem is in a sense simpler than the Inverse Problem since we are given the information at a horizontal line, namely, the bottom* $z=-h$.

5.2 Existence and uniqueness of solutions to the nonlinear formula

In this section, we analyze (21). Among other results, using the Implicit Function Theorem, we show that the nonlocal relation (21) gives rise to a well-defined map from the pressure profile to the surface elevation: given the pressure profile p at the bottom, (21) defines a unique surface elevation η. In other words, we can expect the asymptotic and numerical methods employed in the next sections to produce faithful approximations to the true solution.

Define the operator F, parameterized by $c\in\mathbb{R}$, by

$$F(\eta,p)=c-\sqrt{\frac{c^2-2g\eta}{1+\eta_x^2}}-\frac{1}{2\pi}\int_{-\infty}^{\infty}e^{ikx}\cosh(k(\eta+h))\mathcal{F}\left\{c-\sqrt{c^2-2p}\right\}(k)dk. \tag{26}$$

Note that $F(\eta,p)=0$ is equivalent to (21). Using the Implicit Function Theorem, we wish to show that the equation $F(\eta,p)=0$ has a solution profile η, given sufficiently small pressure p. We have that $F(0,0)=0$. In order to apply the Implicit Function Theorem, we need to define appropriate Banach spaces for which the operator F is defined. First we seek a suitable space for η. An obvious choice is $\eta\in C^1[\mathbb{R},\mathbb{R}]$, *i.e.*, η is a continuously differentiable function which vanishes at infinity. This space is supplied with the usual norm:

$$\|\eta\|_{C^1}=\sup_{x\in\mathbb{R}}|\eta(x)|+\sup_{x\in\mathbb{R}}|\eta'(x)|. \tag{27}$$

If $\|\eta\|_{C^1}<c^2/2g$ then $c-\sqrt{(c^2-2g\eta)/(1+\eta_x^2)}$ represents a continuous function of x. Hence we are motivated to define the image of F in $C[\mathbb{R},\mathbb{R}]$. Consequently, we wish for

$$\int_{-\infty}^{\infty}e^{ikx}\cosh(k(\eta+h))\mathcal{F}\left\{c-\sqrt{c^2-2p}\right\}(k)dk,$$

to be a continuous function of x. For finite $\|\eta\|_{C^1}$, this nonlocal term is a continuous function of x if

$$\int_{-\infty}^{\infty}\cosh(k(\|\eta\|_{C^1}+h))\left|\mathcal{F}\left\{c-\sqrt{c^2-2p}\right\}(k)\right|dk<\infty, \tag{28}$$

and if the integrand of the nonlocal term is a continuous function of x for every k (see Theorem 2.27 on pg. 56 of [41]). Let us consider the second condition, namely, the continuity of the integrand. Since by assumption η is continuous, the continuity in x of the integrand requires

$$\sup_k\left|\mathcal{F}\left\{c-\sqrt{c^2-2p}\right\}(k)\right|<\infty. \tag{29}$$

An application of the Cauchy-Schwarz inequality gives

$$\left|\mathcal{F}\left\{c-\sqrt{c^2-2p}\right\}(k)\right|\leq\left(\int_{-\infty}^{\infty}\frac{1}{1+|x|^2}dx\right)^{\frac{1}{2}}\left(\int_{-\infty}^{\infty}(1+|x|^2)\left|c-\sqrt{c^2-2p}\right|^2dx\right)^{\frac{1}{2}}.$$

Hence, we impose the following condition on the pressure p:

$$\int_{-\infty}^{\infty}(1+|x|^2)\left|c-\sqrt{c^2-2p}\right|^2 dx<\infty. \tag{30}$$

Next, we return to the first condition (28). Due to the presence of the hyperbolic cosine, we expect that it is necessary for $\mathcal{F}\{c-\sqrt{c^2-2p}\}(k)$ to have sufficient decay for large $|k|$. Let $M>h+\|\eta\|_{C^1}$. Starting from the integral in (28), we apply the Cauchy-Schwarz inequality again to find

$$\begin{aligned}
&\int_{-\infty}^{\infty}\cosh(k(\|\eta\|_{C^1}+h))e^{-M|k|}e^{M|k|}\left|\mathcal{F}\left\{c-\sqrt{c^2-2p}\right\}(k)\right|dk\\
&\leq\left(\int_{-\infty}^{\infty}\left(\cosh(k(\|\eta\|_{C^1}+h))e^{-M|k|}\right)^2dk\right)^{\frac{1}{2}}\left(\int_{-\infty}^{\infty}e^{2M|k|}\left|\mathcal{F}\left\{c-\sqrt{c^2-2p}\right\}(k)\right|^2dk\right)^{\frac{1}{2}}\\
&\leq C\left(\int_{-\infty}^{\infty}e^{2M|k|}\left|\mathcal{F}\left\{c-\sqrt{c^2-2p}\right\}(k)\right|^2dk\right)^{\frac{1}{2}},
\end{aligned}$$

for some constant C. Thus, if the conditions

$$\int_{-\infty}^{\infty}e^{2M|k|}\left|\mathcal{F}\left\{c-\sqrt{c^2-2p}\right\}(k)\right|^2dk<\infty \tag{31}$$

and

$$\int_{-\infty}^{\infty}(1+|x|^2)\left|c-\sqrt{c^2-2p}\right|^2dx<\infty \tag{32}$$

hold, the function $F(\eta,p)(x)$ is continuous for $\eta\in C^1$.

Having found the conditions (31-32), we now determine an appropriate function space for p so that they are satisfied. The following theorem due to Paley and Wiener (Theorem 4 pg. 7 of [57]) is helpful.

Theorem 5.2.1 *If $w(z)$ (with $z=x+iy$) is an analytic function in the strip $-\lambda\leq y\leq\mu$ where $\lambda,\mu>0$ and*

$$\int_{-\infty}^{\infty}|w(x+iy)|^2dx<\infty,\quad -\lambda\leq y\leq\mu,$$

then there exists a measurable function $\hat{w}(k)$ such that

$$\int_{-\infty}^{\infty} |\hat{w}(k)|^2 e^{2\mu k} dk < \infty, \qquad \int_{-\infty}^{\infty} |\hat{w}(k)|^2 e^{-2\lambda k} dk < \infty,$$

and

$$w(x+iy) = \lim_{A\to\infty} \int_{-A}^{A} \frac{1}{2\pi} \hat{w}(k) e^{ik(x+iy)} dk, \quad -\lambda \le y \le \mu$$

where the limit is to be understood in the mean-square sense.

In other words, the Fourier transform of $w(x)$ exists and it has decay as specified above. In particular, for any $M < \min\{\lambda, \mu\}$

$$\begin{aligned}
\int_{-\infty}^{\infty} e^{2M|k|} |\hat{w}(k)|^2 dk &= \int_0^{\infty} e^{2Mk} |\hat{w}(k)|^2 dk + \int_{-\infty}^{0} e^{-2Mk} |\hat{w}(k)|^2 dk, \\
&= \int_0^{\infty} e^{2Mk} e^{-2\mu k} e^{2\mu k} |\hat{w}(k)|^2 dk + \int_{-\infty}^{0} e^{-2Mk} e^{2\lambda k} e^{-2\lambda k} |\hat{w}(k)|^2 dk, \\
&\le \int_0^{\infty} e^{2\mu k} |\hat{w}(k)|^2 dk + \int_{-\infty}^{0} e^{-2\lambda k} |\hat{w}(k)|^2 dk < \infty.
\end{aligned}$$

The theorem implies that a sufficient condition for (31) to hold is that $c - \sqrt{c^2 - 2p}$ is an analytic function of z within a strip of width at least $2M$ centered around the real axis and that it is square-integrable along lines parallel to the real axis within this strip. Of course, the presence of the square root is a hinderance to the analyticity of the function. Consequently, we require that $|p| < c^2/2$ everywhere in the strip. This condition also implies the square-integrability of the function if p is square-integrable. Indeed, the function

$$f(z) = c - \sqrt{c^2 - 2z},$$

is analytic (and hence Lipschitz) in a neighborhood of the origin for which $|z| < c^2/2$. Hence, for all z_1, z_2 in such a neighborhood of the origin we have

$$|f(z_1) - f(z_2)| \le C|z_1 - z_2|, \tag{33}$$

for some constant C. In particular, since $f(0) = 0$,

$$|f(z)| \leq C|z|, \tag{34}$$

uniformly for all $|z| \leq \delta < c^2/2$, *i.e.*, the constant C is independent of z. Next, consider the function $f(p(z))$, where $p(z)$ is a function which is analytic and bounded in the strip of width $2M$. This implies

$$|f(p(z))| \leq C|p(z)|. \tag{35}$$

As above, the constant C is independent of $p(z)$ and thus of z, provided $|p(z)| < c^2/2$. Thus the square-integrability of $p(z)$ implies the square-integrability of $c - \sqrt{c^2 - 2p}$ for $|p| \leq \delta < c^2/2$ for every z in the strip. Thus, if $p(z)$ is an analytic function in the strip of width at least $2M$, square-integrable along lines parallel to the real axis, and bounded in the strip, the first condition (31) holds.

Another theorem due to Paley and Wiener (Theorem 2 pg 5 of [57]) allows us to bound $|p|$ in terms of the L^2-norm.

Theorem 5.2.2 *Let $w(z)$ be analytic in the strip $-\lambda \leq y \leq \mu$ with $\mu, \lambda > 0$ and*

$$\int_{-\infty}^{\infty} |w(x+iy)|^2 dx < \infty, \quad -\lambda \leq y \leq \mu, \tag{36}$$

then for any z in the interior of the region

$$w(z) = \frac{1}{2\pi} \int_{-\infty}^{\infty} \frac{w(x+i\mu)}{x+i\mu-z} dx - \frac{1}{2\pi} \int_{-\infty}^{\infty} \frac{w(x-i\lambda)}{x-i\lambda-z} dx. \tag{37}$$

In particular, an application of the Cauchy-Schwarz inequality shows that for any $y \in [-\lambda + \epsilon, \mu - \epsilon]$ with $\epsilon > 0$, $w(z)$ is bounded in terms of the L^2 norms of $w(x+i\mu)$ and $w(x-i\lambda)$.

Collecting these ideas, we choose the pressure p to be in the space of analytic functions in the symmetric strip of width $2M$ about the real axis such that

$$\int_{-\infty}^{\infty} (1+|x|^2)|p(x+iy)|^2 dx < \infty, \quad -M \leq y \leq M. \tag{38}$$

Note that this complex-analytic extension of p to the strip around the real axis is not necessarily the dynamic pressure. Condition (38) guarantees that the second condition (32) is also satisfied. Let H_M denote the space defined by (38). It is endowed with the norm

$$\|p\|_{H_M} = \sup_{|y|\leq M} \left[\int_{-\infty}^{\infty} (1+|x|^2)|p(x+iy)|^2 dx\right]^{1/2}. \tag{39}$$

We claim that H_M is a Banach space. Indeed, with the obvious definitions of addition and scalar multiplication for elements $p \in H_M$, H_M is a vector space. It is straightforward to verify that (39) defines a norm. Thus, it remains to verify completeness. Let $\{f_k\}$ be a Cauchy sequence in H_M. With the norm above, this sequence converges to a complex-valued function f defined on the strip since for fixed y, $\{f_k\}$ defines a Cauchy sequence in the space L^2 with weight $(1+|x|^2)$ and has the limit $f(\cdot, y)$ in this space for each y. We define the function

$$f(x,y) = \lim_{k\to\infty} f_k(x+iy), \text{ y fixed.} \tag{40}$$

Since $\{f_k\}$ is a Cauchy sequence, for every $\epsilon > 0$ there exists an N such that for $n, k \geq N$

$$\|f_n - f_k\|_{H_M} \leq \epsilon. \tag{41}$$

This implies

$$\int_{-\infty}^{\infty} (1+|x|^2)|f_n(x+iy) - f_k(x+iy)|^2 dx \leq \epsilon, \tag{42}$$

for every $|y| \leq M$. Letting $k \to \infty$ in the above integral we obtain

$$\int_{-\infty}^{\infty} (1+|x|^2)|f_n(x+iy) - f(x,y)|^2 dx \leq \epsilon, \tag{43}$$

for every $|y| \leq M$ and thus $f_n \to f$ in the H_M norm. Theorem 5.2.2 implies the pointwise bound

$$|w(x+iy)| \leq C\|w(x+iy)\|_{H_M}, \tag{44}$$

for $x+iy$ in the interior of the strip. Consequently, convergence in H_M implies uniform convergence on compact subsets of the strip. From Morera's Theorem, it follows that the

Cauchy sequence of analytic functions f_k converges to an analytic function, thus the space H_M is complete.

We now state the theorem for the existence of a map from the pressure beneath a traveling wave to the surface elevation of the wave.

Theorem 5.2.3 *Let p and η be the bottom pressure and surface elevation, respectively, obtained by solving the Euler equations augmented with (14). Assume that $p \in H_{M+\epsilon}$ for some $M > h$, $\epsilon > 0$ and that $\|\eta\|_{C^1} < \min[M-h, c^2/2g]$. Then for fixed $c \neq 0$ and sufficiently small p, the equation*

$$c - \sqrt{\frac{c^2 - 2g\eta}{1+\eta_x^2}} = \frac{1}{2\pi}\int_{-\infty}^{\infty} e^{ikx}\cosh(k(\eta+h))\mathcal{F}\left\{c - \sqrt{c^2-2p}\right\}(k)dk,$$

has a solution $\tilde{\eta}$. Further, $\tilde{\eta} = \eta$, the surface water-wave profile of the stationary water wave problem with speed c.

Proof. Let $M > h$ and $\epsilon > 0$. By Theorem 5.2.2 there is a ball V around the origin in $H_{M+\epsilon}$ *i.e.*, $V = \{p \in H_{M+\epsilon} : \|p\|_{H_{M+\epsilon}} < \delta\}$, such that

$$\sup_{|y|\leq M+\epsilon/2} |p(x+iy)| \leq S < \frac{c^2}{2}.$$

By definition, $p \in V$ is bounded, analytic and square integrable along lines parallel to the real axis. Then the function $c - \sqrt{c^2-2p}$ is also analytic and square integrable along lines parallel to the real axis in a strip of width $2(M+\epsilon/2)$ symmetric with respect to the real axis. Using Theorem 5.2.1,

$$\int_{-\infty}^{\infty} e^{2M|k|}\left|\mathcal{F}\left\{c - \sqrt{c^2-2p}\right\}(k)\right|^2 dk < \infty.$$

For $p \in V$, following the discussion preceeding Theorem 5.2.1, define the reconstructed functions $\phi^{R,x}$ and $\phi^{R,z}$ as

$$\phi^{R,x}(x,z;p) = \frac{1}{2\pi}\int_{-\infty}^{\infty} e^{ikx}\cosh(k(z+h))\mathcal{F}\left\{c - \sqrt{c^2-2p}\right\}(k)dk, \tag{45}$$

$$\phi^{R,z}(x,z;p) = \frac{1}{2\pi}\int_{-\infty}^{\infty} -ie^{ikx}\sinh(k(z+h))\mathcal{F}\left\{c - \sqrt{c^2-2p}\right\}(k)dk. \tag{46}$$

Then $\phi^{R,x}$ and $\phi^{R,z}$ are harmonic (and thus smooth) for all $x \in \mathbb{R}$ and $|z+h| < M$. Let $R = \min\left(M-h, c^2/2g\right)$ and define the ball $U = \{\eta \in C^1 : \|\eta\|_{C^1} < R\}$. Then $G : U \times V \to C^1[\mathbb{R}, \mathbb{R}]$, defined as

$$G(\eta, p) = -\phi^{R,x}(x, \eta; p) + \frac{1}{2c}[\phi^{R,x}(x, \eta; p)]^2 + \frac{1}{2c}[\phi^{R,z}(x, \eta; p)]^2 + \frac{g}{c}\eta,$$

is a continuously differentiable function with $G(0,0) = 0$, as is readily verified by computing its second variation evaluated at $(\eta, p) = (0,0)$. The Fréchet derivative of G with respect to η at the origin is

$$G_\eta(0,0)v = \frac{g}{c}v, \qquad v \in C^1.$$

The Fréchet derivative $G_\eta(0,0)$ is an isomorphism on C^1. Hence the Implicit Function Theorem applies and there exists a continuously differentiable map $\nu : p \to \eta$ such that $G(\nu(p), p) = 0$ for all sufficiently small p.

Next, we show that if p is the pressure consistent with the traveling water wave problem with velocity c, then $\nu(p)$ is indeed the corresponding water wave surface elevation. This is achieved by establishing that the reconstructed functions $\phi^{R,x}$ and $\phi^{R,z}$ are the horizontal and vertical fluid velocities ϕ_x and ϕ_z, respectively.

Let $D = \{-\infty < x < \infty, -h < z < \eta\}$, as before, where η represents the solution for the surface elevation of the traveling water wave problem with velocity potential ϕ. Hence ϕ is harmonic in D. It is possible to harmonically extend ϕ to $\bar{D} = \{-\infty < x < \infty, -\eta - 2h < z < \eta\}$ by reflecting the problem across the mirror line $z = -h$. Thus ϕ_x is harmonic in $\bar{D}$.

If p is the pressure corresponding to the solution (ϕ, η) of the water wave problem through (14), then at $z = -h$, $\phi^{R,x}$ and its normal derivative take the same values as ϕ_x and its normal derivative, respectively. The Cauchy-Kowalevski Theorem for Laplace's equation [32] implies that $\phi_x = \phi^{R,x}$ in a region near $z = -h$. But then ϕ_x and $\phi^{R,x}$ and all their derivatives are equal in this region. This implies that $\phi_x = \phi^{R,x}$ in D, by analytic continuation. A similar argument shows that $\phi_z = \phi^{R,z}$ in D: to determine ϕ_{zz} at $z = -h$ we use the fact that due to the extension to $\bar{D}$, ϕ is harmonic on $z = -h$. In addition, from (45) and (46), $\phi^{R,x}$ and $\phi^{R,z}$ harmonically extend up to $z = M - h > \|\eta\|_\infty$. Since

$\phi_x = \phi^{R,x}$ and $\phi_z = \phi^{R,z}$ in D, we can harmonically extend ϕ_x and ϕ_z up to $z = M - h$. This implies that $\phi^{R,x} = \phi_x$ and $\phi^{R,z} = \phi_z$ at $z = \eta$. Hence, from (6) in the traveling frame of reference,

$$\begin{aligned} -c\phi_x + \frac{1}{2}\phi_x^2 + \frac{1}{2}\phi_z^2 + g\eta = 0, \quad z = \eta \\ \Rightarrow -c\phi^{R,x} + \frac{1}{2}(\phi^{R,x})^2 + \frac{1}{2}(\phi^{R,z})^2 + g\eta = 0, \quad z = \eta, \\ \Rightarrow G(\eta, p) = 0. \end{aligned}$$

From the Implicit Function Theorem, for small p all solutions η to $G(\eta, p) = 0$ are of the form $\eta = \nu(p)$, where $\nu : p \to \eta$ is a C^1 map. Hence

$$\phi^{R,x}(x, \nu(p); p) = \phi^{R,x}(x, \eta; p) = \phi_x(x, \eta) = c - \sqrt{\frac{c^2 - 2g\eta}{1 + \eta_x^2}} = c - \sqrt{\frac{c^2 - 2g\nu(p)}{1 + \nu_x^2(p)}},$$

where we used (13). In other words, there are functions η which depend continuously on the true pressure p such that (21) is true.

Next, assume there exists a different solution $\tilde{\eta} \in U \subset C^1, \tilde{\eta} \neq \eta$ such that

$$c - \sqrt{\frac{c^2 - 2g\tilde{\eta}}{1 + \tilde{\eta}_x^2}} = \phi^{R,x}(x, \tilde{\eta}; p),$$

for all x, where the pressure p is the pressure corresponding to the traveling water wave problem with velocity c. As before, $\phi^{R,x}(x, \tilde{\eta}; p) = \phi_x(x, \tilde{\eta})$ and thus

$$c - \sqrt{\frac{c^2 - 2g\tilde{\eta}}{1 + \tilde{\eta}_x^2}} = \phi_x(x, \tilde{\eta}),$$

for all x. However, for a fixed c, the water wave problem has a unique traveling wave solution, provided the amplitude is small [5]. This is contradicted by the statement that $\eta \neq \tilde{\eta}$. Thus the only solutions η of (21) associated with the pressure p are the traveling wave solutions of the Euler equations.

5.3 Asymptotic approximations

In this section we derive a variety of asymptotic approximations to the pressure as a function of the surface elevation. Given the complexity of (21), such approximations are especially useful. In the sections below, we compare the results for the pressure obtained using (21), with those obtained from (1) and (2), as well as some asymptotic formulas obtained here.

We introduce the nondimensional quantities ξ^*, z^*, η^* and k^*:

$$\xi^* = \xi/L, \quad z^* = z/h, \quad \eta^* = \eta/a, \quad k^* = Lk, \quad c^* = c/\sqrt{gh}, \quad p^* = p/ga, \tag{47}$$

where L is a typical horizontal length scale, and a is the amplitude of the surface wave. From (3–6), a nondimensional version of (21) is found to be

$$\sqrt{\frac{c^2 - 2\epsilon\eta}{1 + (\epsilon\mu\eta_\xi)^2}} = \frac{1}{2\pi}\int_{-\infty}^{\infty} e^{ik\xi}\mathcal{F}\left\{\sqrt{c^2 - 2\epsilon p(\xi)}\right\}(k)\cosh\left(\mu k\left(1+\epsilon\eta\right)\right)\,dk, \tag{48}$$

where $\epsilon = a/h$ and $\mu = h/L$. The *'s have been omitted to simplify the notation. This form of the nonlocal relation is our starting point to derive various approximate results. The two parameters ϵ and μ provide many options for different asymptotic expansions: we may assume small amplitude waves ($\epsilon \ll \mu$), or we may assume a long-wave approximation ($\mu \ll \epsilon$), or we may balance both effects as in a Korteweg-de Vries (KdV)-type approximation (see [4], for instance).

5.3.1 The small-amplitude approximation: SAO1 and SAO2

If we expand η in powers of $\epsilon \ll 1$, assuming that $\epsilon \ll \mu$, we recover at leading order the approximation

$$\eta(\xi) = \mathcal{F}^{-1}\left\{\cosh(\mu k)\widehat{p}(k)\right\} + \mathcal{O}\left(\epsilon\right), \tag{49}$$

where $\widehat{p}(k) = \mathcal{F}\{p\}(k)$. Ignoring the $\mathcal{O}\left(\epsilon\right)$ term, (49) is the nondimensional version of (2). This demonstrates that (21) is consistent with the frequently used (2), and we are able to recover such formulas in a consistent manner using the single equation (21), instead of

having to work with the full set of equations of motion. We refer to the model (49) (solved for the pressure) as SAO1 (Small-Amplitude, Order 1).

If we proceed to higher order in ϵ we find the presumably more accurate approximation

$$\eta(\xi) = \eta_0(\xi) + \epsilon\eta_1(\xi) + \mathcal{O}(\epsilon^2), \tag{50}$$

where

$$\eta_0(\xi) = \mathcal{F}^{-1}\big\{\cosh(\mu k)\widehat{p}(k)\big\}\big\}, \tag{51}$$

$$\eta_1(\xi) = -\frac{c^2\mu^2}{2}\eta_0\eta_{0\xi}^2 - \frac{1}{2c^2}\eta_0^2 + \mu\eta_0\mathcal{F}^{-1}\{k\widehat{p}(k)\sinh(\mu k)\} + \frac{1}{2c^2}\mathcal{F}^{-1}\{\widehat{p^2}(k)\cosh(\mu k)\}. \tag{52}$$

The formula (50) provides a new, explicit, higher-order approximation for the surface elevation $\eta(\xi)$ in terms of the pressure $p(\xi)$ and the traveling wave speed c, assuming a small-amplitude approximation. This order of approximation will henceforth be referred to as SAO2.

5.3.2 The KdV Approximation: SWO1 and SWO3

Alternatively, we can balance the parameters μ and ϵ so that $\mu = \sqrt{\epsilon}$. This is the KdV approximation, (see [2, 4]). At leading order, we recover the simplest approximation that the surface elevation equals the pressure:

$$\eta(\xi) = p(\xi) + \mathcal{O}(\epsilon). \tag{53}$$

This equation is exactly the hydrostatic approximation (1) in dimensionless variables; we will refer to this model as SWO1 (Shallow Water, Order 1). Continuing the aproximations to higher order (up to order ϵ^3), we find

$$\eta(\xi) = p - \frac{\epsilon}{2}\frac{\partial^2 p}{\partial\xi^2} + \epsilon^2\left(\frac{1}{24}\frac{\partial^4 p}{\partial\xi^4} - p\frac{\partial^2 p}{\partial\xi^2} - \frac{1}{2}\left(\frac{\partial p}{\partial\xi}\right)^2\left(c^2 + \frac{1}{c^2}\right)\right) + \mathcal{O}(\epsilon^3). \tag{54}$$

We refer to this approximation as SWO3 (Shallow Water, Order 3).

Remark 5.3.1 *For $\eta \in C^1$ and $p \in H_{M+\delta}$, it is possible to prove the analyticity of (48) in ϵ and μ. Here, as before, M is related to the size of a symmetric strip around the real ξ axis. This analyticity serves to validate the asymptotic approximations derived above, as being obtained through a process that gives the first few terms of a convergent series.*

Remark 5.3.2 *It appears to be a restriction that the nonlocal formula (21) and the approximations derived above require a traveling wave profile. As shown in the next section, good results are also obtained for waves that are not merely traveling at constant speed. For waves in shallow water, excellent agreement is often obtained by using $c = 1$ (or $c = \sqrt{gh}$, returning to the dimensional version), which may be regarded as the zero-order approximation of an asymptotic series for c in terms of ϵ.*

Remark 5.3.3 *Using the procedures outlined in this section, the reader will find it straightforward to derive yet different approximations for the surface elevation in terms of the pressure measured at the bottom. For instance, one may consider a shallow-water approximation without imposing that the waves are of small amplitude,* i.e., *$\mu \ll \epsilon < 1$,* etc.

5.3.3 A heuristic formula: SAO2h

The transfer function approach (2) is very successful for a variety of reasons: (i) it is quite accurate, as is illustrated in the next few sections. This statement remains true to a varying degree for waves of relatively high amplitude; (ii) the most complicated aspect of using the formula is the computation of two Fourier transforms; and (iii) the formula applies to waves that are not necessarily traveling with constant speed. This is a consequence of the linearization that led to (2): each individual linear wave is traveling at constant speed, but typically their superposition is not.

In this section we derive a different formula for the reconstruction of the surface elevation from the pressure at the bottom. This formula is obtained somewhat heuristically, and its justification rests on the fact that it agrees extremely well with both numerical and experimental data. Furthermore, its use requires the computation of only three Fourier transforms, and the velocity c does not appear in the final result. As a consequence, even though the derivation does not justify this, it is straightforward to apply to non-traveling

wave profiles, where it performs very well. As for the other formulas above, the numerical and experimental results are presented below.

An equivalent form of the nondimensional nonlocal equation (48) is

$$1-\sqrt{\frac{1-2\epsilon\eta/c^2}{1+(\epsilon\mu\eta_\xi/c)^2}}=\frac{1}{2\pi}\int_{-\infty}^{\infty}e^{ik\xi}\hat{P}(k,\epsilon)\cosh\left(\mu k\left(1+\epsilon\eta\right)\right)\,dk, \tag{55}$$

where

$$\hat{P}(k,\epsilon)=\mathcal{F}\left\{1-\sqrt{1-2\epsilon p(\xi)/c^2}\right\}(k). \tag{56}$$

So as to consider a small-amplitude approximation, we expand this equation in powers of ϵ. However, we do not expand $\hat{P}(k,\epsilon)$ at this point. Proceeding this way and retaining only first-order terms in $\epsilon\eta$ and $\epsilon\eta_\xi$, we find

$$\begin{aligned}
&\frac{\epsilon\eta}{c^2}=\frac{1}{2\pi}\int_{-\infty}^{\infty}e^{ik\xi}\hat{P}(k,\epsilon)\left(\cosh(\mu k)+\epsilon\mu\eta k\sinh(\mu k)\right)\,dk\\
\Rightarrow\qquad&\epsilon\eta=\frac{\frac{1}{2\pi}\int_{-\infty}^{\infty}e^{ik\xi}\hat{P}(k,\epsilon)\cosh(\mu k)\,dk}{\frac{1}{c^2}-\frac{\mu}{2\pi}\int_{-\infty}^{\infty}e^{ik\xi}\hat{P}(k,\epsilon)k\sinh(\mu k)\,dk}.
\end{aligned} \tag{57}$$

Next, we expand $\hat{P}(k,\epsilon)$ in ϵ, omitting terms of order ϵ^2 and higher. We obtain

$$\hat{P}(k,\epsilon)\sim\frac{\epsilon}{c^2}\hat{p}. \tag{58}$$

Substitution of (58) in (57) results in

$$\eta=\frac{\mathcal{F}^{-1}\left\{\hat{p}(k)\cosh(\mu k)\right\}}{1-\epsilon\mu\mathcal{F}^{-1}\left\{\hat{p}(k)\,k\sinh(\mu k)\right\}}, \tag{59}$$

or, reintroducing the physical dimensions,

$$\eta=\frac{\mathcal{F}^{-1}\left\{\hat{p}(k)\cosh(kh)\right\}/g}{1-\mathcal{F}^{-1}\left\{\hat{p}(k)\,k\sinh(kh)\right\}/g}. \tag{60}$$

As stated above, this reconstruction formula does not depend on c, and its application requires the computation of a mere three Fourier transforms. This can be contrasted, for instance, with the formula SAO2 which also uses a small-amplitude approximation. That formula requires the computation of five Fourier transforms and has explicit dependence on

c. In fact, if one were to expand (59) in powers of ϵ one would find at order ϵ^0 the transfer function formula (2), and at order ϵ^1 the result SAO2 with all c-dependent terms omitted. We refer to the results obtained using (59) as SAO2h.

5.4 Comparison of the different approaches

In this section, we present numerical results for the reconstruction of the surface elevation using the various relationships derived in Section 5.3 for both numerical and experimental pressure data. For the comparison using numerical data, we use previously computed periodic traveling waves solutions from [28]. By using the exact pressure underneath the traveling wave, we attempt to reconstruct the surface elevation. The same is done for various sets of experimental data obtained from the one-dimensional wave tank at the William Pritchard Fluids Laboratory at Penn State University.

5.4.1 Comparison of the Different Approaches Using Numerical Data

Using traveling wave solutions with periodic boundary conditions as calculated in [28], we determine the pressure at the bottom using (21) as follows. Without loss of generality, we assume that the solutions are 2π periodic. For a given traveling wave solution profile specified by $(\eta_{true}(\xi), c_{true})$, the pressure $p(\xi)$ is obtained by equating the k-th Fourier coefficient of both the right- and left-hand side of (21) for $k = -N, \ldots, N$, using a sufficiently high value of N. This results in a linear system of algebraic equations for the coefficients of the Fourier series of $\sqrt{c^2 - 2p}$. Using this truncated Fourier series, we may solve directly for $p(\xi)$ in terms of the given solution set $(\eta_{true}(\xi), c_{true})$. Note that (25) offers a numerically equivalent alternative for computing $p(\xi)$.

Our goal is to reconstruct the surface elevation from the thus computed pressure at the bottom, using the various formulas given above. The asymptotic formulas given in the previous section do not require anything more complicated than a fast Fourier transform. The solution of the nonlocal equation (21) is obtained using a pseudo-spectral method with differentiation carried out in Fourier space, while multiplication is carried out in physical space. We reconstruct η by using a nonlinear solver such as a Gauss-Newton or Dogleg method [30, 55] with an error tolerance of 10^{-14}. As an initial guess for our nonlinear

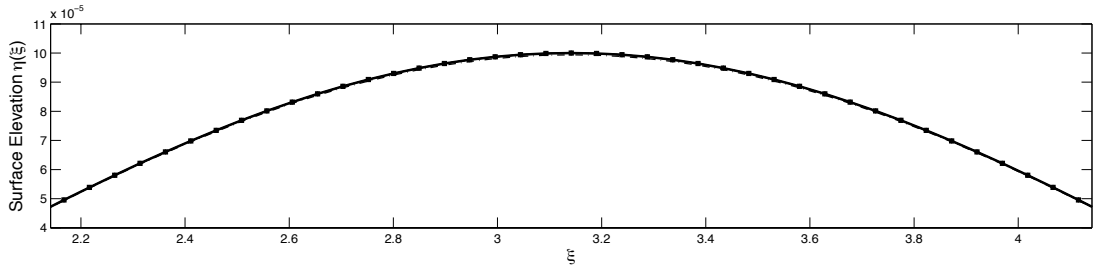

(a)

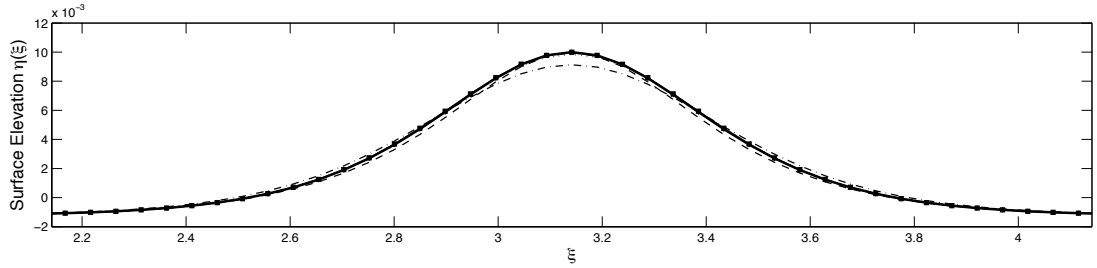

(b)

Figure 5.2: Reconstruction of the surface elevation from pressure data based on numerical experiments for $h = 0.1$, $g = 1$, $\rho = 1$ and $L = 2\pi$. Amplitudes are $a = 0.0001$ (a) and $a = 0.0056$. (b). No legend is included: all approximations including the nonlocal formula (21) result in indistinguishable curves, except for the hydrostatic approximation SWO1, which displays a significant discrepancy for the bottom numerical experiment.

solver, we use the approximation from (50). Of course, the result obtained from the nonlocal equation should return the original surface elevation profile used to generate the pressure data, within machine precision. This provides a validation for the various numerical methods used. Here we compare the results from the asymptotic formulas of the previous section and evaluate their different errors.

Using the parameter values $h = .1$, $g = 1$, $\rho = 1$ and $L = 2\pi$, we reconstruct the solution for various solution amplitudes and speeds. For solutions of small amplitude (say $ak = .0001$), we see that the reconstructions using all methods are in excellent agreement with the true surface wave elevation, see Figure 5.2a. However, even for waves with am-

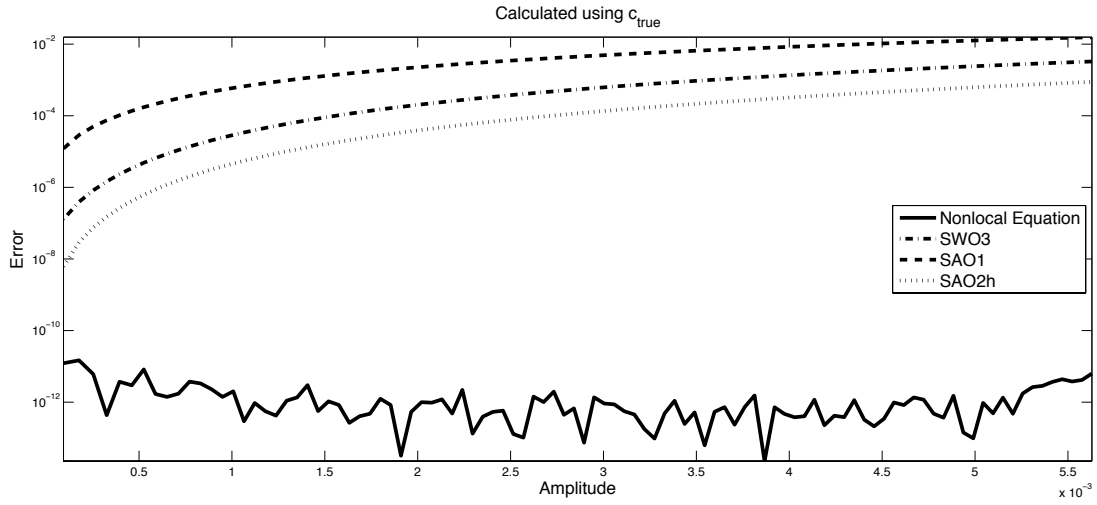

Figure 5.3: Plot of the relative error (61) in the reconstructed surface elevation η_r as a function of the amplitude of η_{true} using the true value of the wave speed c. The asymptotic approximation SAO2 is not included in this figure. It is more costly to compute than its heuristic counterpart SAO2h, which yields better results.

plitudes less than 15% of the limiting wave height as given by [17] it becomes clear that certain approximations yield better results than others, see Figure 5.2b. In particular, while the nonlocal formula and the higher-order asymptotic formula reconstruct the wave profile well, the hydrostatic approximation SWO1 reconstruction fails to reproduce an accurate reconstruction of the peak wave height.

To demonstrate how the error changes as a function of the wave amplitude (or nonlinearity), we compute the relative error

$$\text{error} = \frac{||\eta_{true} - \eta_r||_\infty}{||\eta_{true}||_\infty}, \tag{61}$$

where η_{true} represents the expected solution and η_r represents the reconstructed solution. For the same nondimensional parameters as before, we calculate the error as a function of increasing peak wave height demonstrated in Figure 5.3. As seen there, the error in all approximations grows as the amplitude of the Stokes wave increases. Figure 5.3 includes only solutions of small amplitude. If solutions of larger amplitude are considered, the

Percentage of Limiting Wave Height	SWO1	SAO1	SWO3	SAO2	SAO2h	Nonlocal
35	21.14	9.43	4.01	2.36	1.76	0.00
45	25.67	13.43	6.49	4.27	3.18	0.00
50	27.88	15.49	7.89	5.41	4.04	0.00
53	28.94	16.49	8.67	5.96	4.40	0.00
54	29.65	12.17	9.15	6.36	4.70	0.00
55	30.08	17.58	9.45	6.61	4.88	0.00

Table 5.1: Relative error (61) in percent, calculated comparing peak wave heights using various reconstruction formulas using numerical data.

discrepancies between the different approximations grow, as shown in Table 5.1.

This table illustrates the large error generated by the lower-order methods SAO1 and SW01 for waves which are no more than 55% of the limiting wave height as calculated in [17]. Even for waves which are 50% of the limiting wave height, the relative error (61) of the commonly used transfer function reconstruction SAO1 exceeds 15%. In contrast, the higher-order methods SA02, SWO3, and SA02h consistently yield more accurate results. It is also clear from the table that even for large amplitude waves, the nonlocal formula (21) (or more precisely for these numerical data sets, its periodic analogue (22)) provides a practical means to reconstruct the surface elevation from pressure data measured along the bottom of a fluid, at least in this numerical data setting. Below we establish the same using physical experiments.

One limitation of the nonlocal equation (21) and some of its asymptotic counterparts from the previous section is that they require the knowledge of the traveling wave speed c. In practice, this can be a difficult or impractical quantity to measure. One such impractical option is to include additional pressure sensors in order to measure the time it takes for the peak of the pressure data to travel from one sensor to another. A simpler option is to use approximations for the wave speed based on small-amplitude theory. For example, if we

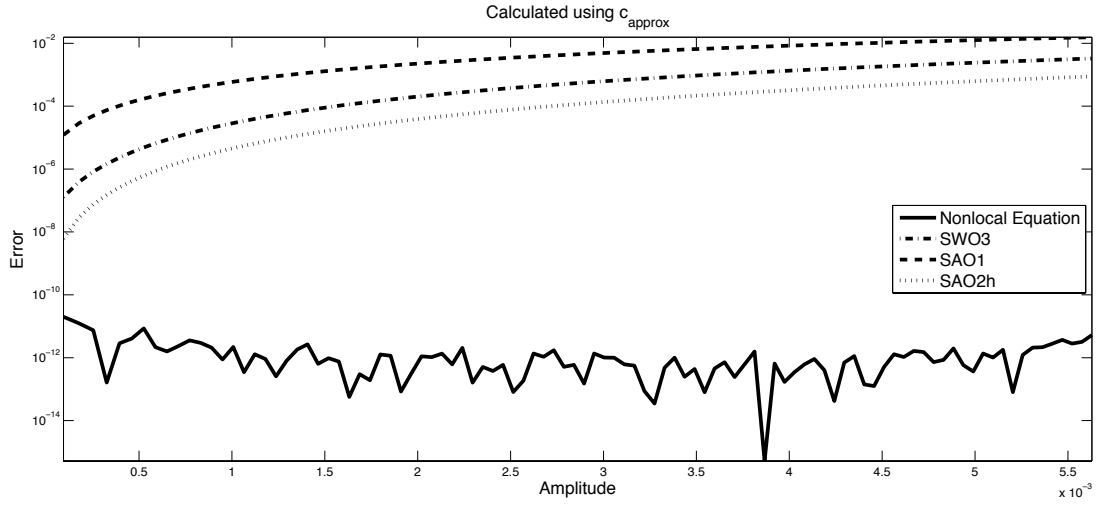

Figure 5.4: Plot of the error in the reconstructed surface elevation η_r as a function of the amplitude of η_{true} using an approximation for the wave-speed c. The SAO2 model is not included for the same reason as in Figure 5.3.

repeat the same error calculation as above, but with $c \approx \sqrt{gh}$, we obtain Figure 5.4. We might hope that the reconstruction of the surface elevation would not suffer much. In fact, it appears unchanged. As seen in Figure 5.4, the error in reconstructing the peak wave height does not suffer at all from using this simple approximate (and amplitude-independent) value of c. Surprisingly, the error in the nonlocal reconstruction remains consistent with the error calculated using the true wave speed c. This lack of sensitivity to the precise value of c yields hope that with experimental data a simple approximation of the wave speed will be sufficient to accurately reconstruct the surface elevation.

5.4.2 Comparison of the Different Approaches Using Data From Physical Experiments

Here we discuss comparisons of results from the nonlocal formula (21) and the asymptotic approaches with results from ten laboratory experiments performed at Penn State's Pritchard Fluid Mechanics Laboratory. In these experiments the pressure at the bottom of the fluid domain and the displacement of the air–water interface were measured simultaneously. The experimental facility consisted of the wave channel and water, the wavemaker,

bottom pressure transducers, and a surface displacement measurement system. The wave-tank is 50 ft long, 10 in wide and 1 ft deep. It is constructed of tempered glass. It was filled with tap water to a depth of h, as listed in Table 5.2. The pressure gauge was a SEN^{Z}ORS PL6T submersible level transducer with a range of 0–4 in. It provided a 0–5 V dc output, which was digitized with an NI PCI-6229 analog-to-digital converter using LabView software. We calibrated this transducer by raising and lowering the water level in the channel. The pressure measurements had a high-frequency noise component, and thus were low-pass filtered at 20 Hz. The still-water height was measured with a Lory Type C point gauge. The capacitance-type surface wave gauge consisted of a coated-wire probe connected to an oscillator. The difference frequency between this oscillator and a fixed oscillator was read by a Field Programmable Gate Array (FPGA), NI PCI-7833R. Thus, no D/A conversion, filtering, or A/D conversion was required. The surface capacitance gauge was held in a rack on wheels that are attached to a programmable belt. We calibrated the capacitance gauge by traversing the rack at a known speed over a precisely machined, trapezoidally-shaped "speed bump". The waves were created with a horizontal, piston-like motion of a paddle made from a Teflon plate (0.5 in thick) inserted in the channel cross-section. The paddle was machined to fit the channel precisely with a thin lip around its periphery that served as a wiper with the channel's glass perimeter. This wiper prevented any measurable leakage around the paddle during an experiment. The paddle was connected to the programmable belt and traveled in one direction. It was programmed with the horizontal velocity of a KdV soliton, which is given by

$$u(x,t) = u_0 \operatorname{sech}^2\left(\frac{3u_0}{4{h_0}^2 c_0}(x - c_0 t - u_0 t/2)\right), \tag{62}$$

where $c_0 = \sqrt{gh}$, a_0 is the wave amplitude, and $u_0 = a_0 c_0/h$ is the maximum horizontal velocity. The a_0 for the wavemaker displacement was varied between 2 cm and 3 cm. These values corresponded to large velocities and fluid displacements, outside of the regime of the KdV equation. The water adjusted to create a leading wave with a radiative tail. We compare results for the leading wave, where nonlinearity is likely to be important.

To convert the time series of pressure and surface displacement data into spatial data, we

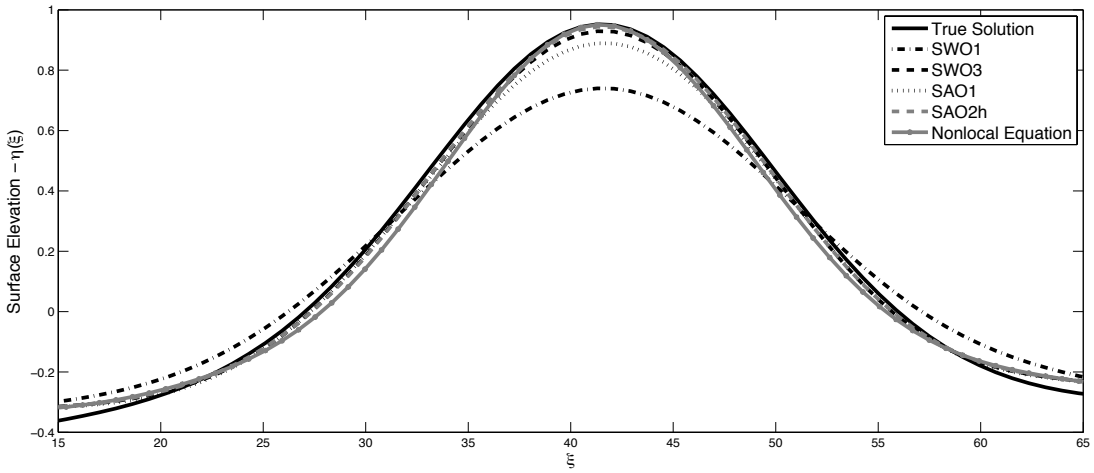

Figure 5.5: Wave tank comparisons of the reconstructed surface elevation with surface height measurements for $h = 5.05\,cm$. This corresponds to Experiment #1 in Table 5.2.

use a combination of the sampling frequency and the estimated wave speed c. Specifically, let p_j represents the measured pressure at time $t_j = j\,\Delta t$, where Δt is the time between pressure measurements. We assign a corresponding x value x_j to p_j so that $x_j = c\,(j\,\Delta t)$. From the pressure data measured from the physical experiments, we reconstruct the surface elevation using the same methods as in the previous section. For all experiments we use the admittedly simple approximation $c \approx \sqrt{gh}$. We use the measured pressure data to reconstruct the surface elevation using the nonlocal formula (21), as well as the asymptotic approximations SWO1 (hydrostatic), SAO1 (transfer function), SAO2, and SWO3.

As seen in Figure 5.5, the higher-order methods capture the peak wave height better than the lower-order methods, with the nonlocal equation yielding the most accurate representation of the peak wave height. The visual comparisons for all experiments is displayed in Figure 5.6. The nonlocal formula (21) consistently captures the peak wave height better than any of the approximate models derived in the previous section, and significantly better than the SWO1 (hydrostatic) and SAO1 (transfer function) models. This is quantified in Table 5.2, which displays the error (61) for the different approximations and the nonlocal equation (21). As is seen there, the result from (21) consistently produced the smallest

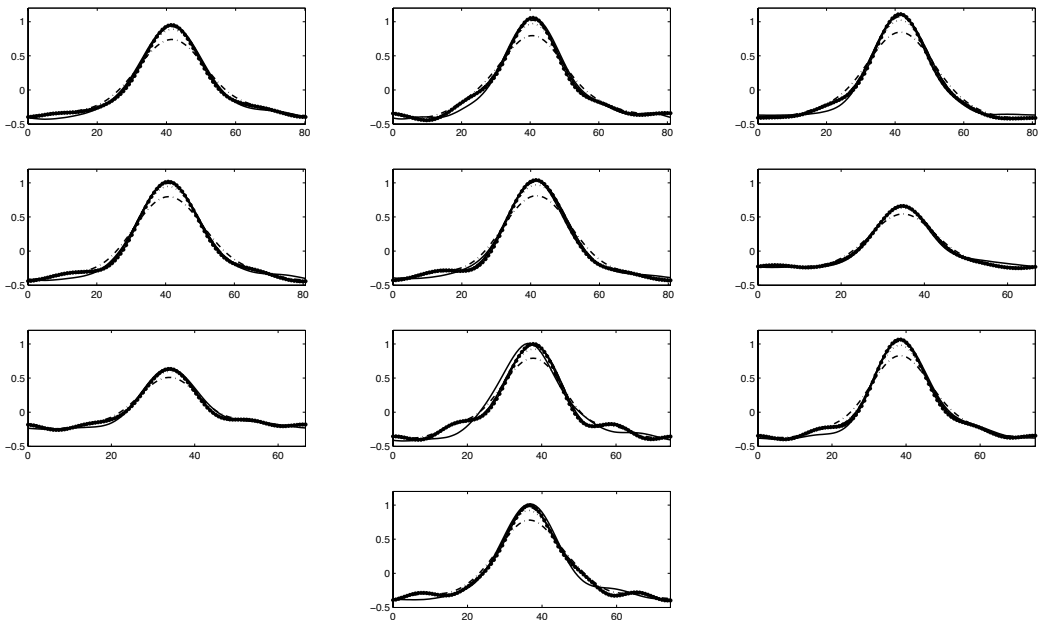

Figure 5.6: Wave tank comparisons of the reconstructed surface elevation with surface height measurements for various fluid depths. The experiments are ordered from left-to-right and top-to-bottom, corresponding to the experiment # in Table 5.2.

error among all the reconstruction formulas. It is noteworthy that the heuristic SAO2h approximation (59) consistently yields the second-lowest peak height error and consistently outperforms all other models except the nonlocal equation (21). Given the computational expense of solving the nonlocal equation, the approximation SAO2h apparently yields the best compromise between efficiency and accuracy.

5.5 Concluding remarks

We have presented a new equation (21) relating the pressure at the bottom of the fluid to the surface elevation of a traveling wave solution of the one-dimensional Euler equations without approximation. This equation is analyzed rigorously and the existence of solutions is proven using the Implicit Function Theorem. Solving the equation numerically is possible, but this is computationally relatively expensive when compared to currently-used approaches that require the computation of at most a few Fourier transforms. To this end, we derive

Experiment #	Depth (cm)	SWO1	SAO1	SWO3	SAO2	SAO2h	Nonlocal
1	5.05	22.29	6.51	2.35	0.84	0.45	0.20
2	5.05	24.66	8.05	3.30	1.13	0.56	0.01
3	5.05	23.56	7.75	2.90	0.95	0.41	0.18
4	5.05	21.98	7.18	2.80	1.29	0.89	0.66
5	5.05	22.00	6.63	2.10	0.48	0.05	0.03
6	3.55	18.11	5.21	1.65	0.65	0.43	0.36
7	3.55	20.81	7.04	3.33	2.22	1.95	1.52
8	4.10	21.59	8.39	3.50	2.18	1.73	0.93
9	4.10	22.13	7.65	2.29	0.33	0.31	0.05
10	4.10	23.32	9.25	4.60	2.91	2.44	2.13

Table 5.2: Relative error (61) in percent, calculated comparing peak wave heights using various reconstruction formulas using experimental data.

various new approximate formulas, starting from the new nonlocal formula. The canonical approaches (hydrostatic approximation and transfer function approach) are easily obtained from the nonlocal formula as well.

The different approximations and the nonlocal formula (21) are compared using numerical data, and their performance on physical laboratory data is examined. The nonlocal formula consistently outperforms its different approximations. For the numerical data this is by construction, as it was used to generate the numerical pressure data used for the comparison, starting from computed traveling wave solutions of the Euler equation. The higher-order approximate formulas result in a better reconstruction of the surface elevation compared to the hydrostatic or transfer function approaches. In the lab experiments, both the surface elevation and the bottom pressure are measured, allowing for an independent validation of the nonlocal equation (21). As expected, it outperforms the different approximations, where higher-order models perform better than lower-order ones. A good compromise between computational cost and obtained accuracy seems to be achieved by

the heuristic approximation SAO2h (59), which requires the computation of three Fourier transforms.

Our derivation of the nonlocal equation (21) requires the surface elevation profile to be traveling with constant speed c. Regardless, we show that the results are not sensitive to the exact value of c and even rough estimates (*i.e.*, $c = \sqrt{gh}$) provide excellent results, both for the nonlocal equation (21) and its various asymptotic approximations, most notably (59).

Appendix A

WELL-POSEDNESS OF THE LINEAR BENJAMIN-BONA-MAHONY EQUATION

As mentioned in Chapter 2, the method of Fokas (MoF) is applicable to many different kinds of PDEs. Here we apply the MoF to the linear Benjamin-Bona-Mahony (BBM) equation [9]:

$$u_t - u_{xxt} + u_x = 0. \tag{1}$$

The BBM equation is a well-known model for long waves in shallow water. Due to the presence of the mixed derivative, the linear BBM equation has a rational dispersion relation which tends to zero for large wave numbers. This non-polynomial nature of the dispersion relation means that a modification of the MoF is required in order to use the method. Although I do not consider examples other than the linear BBM equation, the procedure presented applies to problems of the form

$$M(-i\partial_x)u_t + L(-i\partial_x)u = 0, \tag{2}$$

where $M(k)$ and $L(k)$ are polynomials. Using the MoF, it is possible to find explicit solutions for various boundary-value problems associated with such PDEs. In fact, such equations may be analyzed with the same efficiency as those without mixed derivatives. Although, mixed derivative PDEs do not often appear in the classroom, they are important in many applications [34]. Indeed, inspired by problems in water-waves, Fokas and Pelloni discuss boundary-value problems for Boussinesq type systems [39]. However, those mixed-partial derivative equations do not demonstrate the behavior reported here. Specifically, for particular cases of the Robin boundary condition, the initial and boundary conditions cannot be imposed independently of one another. In this chapter, I shall obtain explicit solutions for Dirichlet, Neumann and Robin boundary conditions for the half-line and for the finite interval and also elaborate on the special cases of the Robin boundary condition.

As already stated, the non-polynomial nature of the dispersion relation for the linear BBM equation has a significant impact on the application of the MoF. It is the cause of the essential singularities that arise in the analysis which obstruct the deformation of contour integrals. Further, the global relation ceases to be valid at certain points in the finite complex plane. It is precisely this fact that results in the PDE being ill posed for specific cases of the Robin boundary condition. As a final remark, the results presented extend to the forced equation

$$u_t - u_{xxt} + u_x = F(x,t).$$

For small time, we may regard the nonlinear term in the full BBM equation as a forcing. Since BBM is a semi-linear equation, I conjecture that the ill-posedness results apply to the nonlinear problem as well.

A.1 The local relation and Lax pairs

In this section, an algorithmic procedure for deriving one-parameter divergence forms associated with linear PDEs is presented. As seen in Chapter 2 the divergence form, referred to as the *local relation*, is the starting point for the MoF. Further, this section highlights the connection of the method with techniques for nonlinear integrable PDEs through the existence of Lax pairs for linear PDEs.

Consider the linear constant-coefficient differential equation

$$u_t + \omega(-i\partial_x)u = 0. \tag{3}$$

This PDE has a Lax pair of the form

$$\mu_x - ik\mu = u,$$
$$\mu_t + \omega(k)\mu = Xu,$$

where X is a differential operator acting on $u(x,t)$ with coefficients depending on the spectral parameter k. Imposing the compatibility of these two equations and assuming that $u(x,t)$ solves (3) one obtains

$$X = i\,\frac{\omega(l)-\omega(k)}{l-k}\bigg|_{l=-i\partial_x}.$$

As an example, for the heat equation with "dispersion relation"[1] $\omega(k) = k^2$, we obtain the Lax pair

$$\mu_x - ik\mu = u,$$
$$\mu_t + k^2\mu = u_x + iku.$$

A one-parameter family of equations in divergence form, referred to as the *local relation* follows immediately. Indeed the above equations may be written as

$$(e^{-ikx+k^2t}\mu)_x = e^{-ikx+k^2t}u,$$
$$(e^{-ikx+k^2t}\mu)_t = e^{-ikx+k^2t}(u_x + iku),$$

which implies

$$\left[e^{-ikx+k^2t}u\right]_t - \left[e^{-ikx+k^2t}(u_x + iku)\right]_x = 0.$$

Equation (3) represents the evolution of $u(x,t)$ with dispersion relation $\omega(k)$. Similarly, one may consider (2) to represent the evolution of a quantity $u(x,t)$ with dispersion relation $L(k)/M(k)$. Consequently, we seek a Lax pair of the form

$$\mu_x - ik\mu = M(-i\partial_x)u,$$
$$\mu_t + \frac{L(k)}{M(k)}\mu = Xu.$$

Further, it is assumed that $M(k) > 0$ for $k \in \mathbb{R}$ and $L(k), M(k)$ do not share any roots. As before, imposing compatibility of the two ordinary differential equations for μ and imposing that $u(x,t)$ solves (2), we obtain that the appropriate differential operator is given by

$$X = i\left.\frac{L(l)M(k) - L(k)M(l)}{M(k)(l-k)}\right|_{l=-i\partial_x}.$$

For the specific case of the linear BBM equation with $L(k) = ik$ and $M(k) = 1 + k^2$, we obtain

$$X = \frac{-1 - ik\partial_x}{1+k^2},$$

resulting in the local relation

$$\left[e^{-ikx+\frac{ik}{1+k^2}t}(u - u_{xx})\right]_t - \left[e^{-ikx+\frac{ik}{1+k^2}t}\left(\frac{-u - iku_x}{1+k^2}\right)\right]_x = 0. \tag{4}$$

[1] I follow the notation for the dispersion relation that is typically used in the literature where the MoF is used. This differs by a factor of i from what is used in the literature on dispersive wave equations.

A.2 Solutions of the linear BBM equation on the half-line

The BBM equation models long waves in shallow water. It is natural to consider the boundary-value problem for the equation posed on the semi-infinite line:

$$u_t - u_{xxt} + u_x = 0, \qquad x \geq 0,\ t \in (0, T], \tag{5a}$$

$$u(x, 0) = u_0(x), \qquad x \geq 0, \tag{5b}$$

$$\alpha u(0, t) + \beta u_x(0, t) = g(t), \qquad t \in (0, T),\ \alpha, \beta \in \mathbb{R}. \tag{5c}$$

In what follows, I start with formal calculations assuming a smooth solution exists which has sufficiently rapid decay at infinity. These calculations lead us to a solution expression $u(x, t)$ for most values of α and β. Assuming sufficient regularity of the initial and boundary condition functions, I claim the solution expression is a classical solution to the above boundary-value problem. For the particular case when $\alpha = \beta$, the arguments below lead us to conclude the problem is ill posed in the sense that the initial and boundary condition functions may not be chosen arbitrarily. Instead, as we shall see at the end of this section, there exists a discontinuous relation between them in order for the problem to be solvable.

Integrating the local relation (4) over the region $\{(x, s) : x \geq 0, s \in (0, t)\}$, applying Green's Theorem and integrating by parts, we obtain the global relation

$$U_0(k) + \frac{\tilde{g}(k, t)}{1 + k^2} = e^{\omega t} U(k, t), \quad \text{Im}(k) \leq 0, k \neq -i, \tag{6}$$

with

$$\begin{aligned} U_0(k) &= (1 + k^2)\hat{u}_0(k) + u_x(0, 0) + iku(0, 0), \\ U(k, t) &= (1 + k^2)\hat{u}(k, t) + u_x(0, t) + iku(0, t), \\ \tilde{g}(k, t) &= \tilde{g}_0(\omega, t) + ik\tilde{g}_1(\omega, t), \\ \omega &= \frac{ik}{1 + k^2}, \end{aligned}$$

where $\hat{u}_0(k)$ and $\hat{u}(k, t)$ represent the Fourier transform of the initial condition and of the solution at time t respectively. They are defined by

$$\hat{u}_0(k) = \int_0^\infty e^{-ikx} u_0(x) dx, \quad \hat{u}(k, t) = \int_0^\infty e^{-ikx} u(x, t) dx,$$

with inverses

$$u_0(k) = \frac{1}{2\pi}\int_{-\infty}^{\infty} e^{ikx}\hat{u}_0(k)dk, \quad u(x,t) = \frac{1}{2\pi}\int_{-\infty}^{\infty} e^{ikx}\hat{u}(k,t)dk,$$

where $u_0(x)$ and $u(x,t)$ are defined to be zero for $x < 0$. Similarly, $\tilde{g}_0(\omega,t)$ and $\tilde{g}_1(\omega,t)$ are the finite-time transforms of the boundary data given by

$$\tilde{g}_0(\omega,t) = \int_0^t e^{\omega s}u(0,s)ds, \quad \tilde{g}_1(\omega,t) = \int_0^t e^{\omega s}u_x(0,s)ds.$$

Solving the global relation (6) for $\hat{u}(k,t)$ and applying the inverse Fourier transform, we obtain the following integral expression for the solution

$$\begin{aligned} u(x,t) =& \frac{1}{2\pi}\int_{-\infty}^{\infty} e^{ikx-\omega t}\frac{U_0(k)}{1+k^2}dk + \frac{1}{2\pi}\int_{-\infty}^{\infty} e^{ikx-\omega t}\frac{\tilde{g}(k,t)}{(1+k^2)^2}dk \\ & - \frac{1}{2\pi}\int_{-\infty}^{\infty} e^{ikx}\frac{u_x(0,t)+iku(0,t)}{1+k^2}dk, \\ \Rightarrow u(x,t) =& \frac{1}{2\pi}\int_{-\infty}^{\infty} e^{ikx-\omega t}\hat{u}_0(k)dk + \frac{1}{2\pi}\int_{\mathcal{C}} e^{ikx-\omega t}\frac{\tilde{g}(k,t)}{(1+k^2)^2}dk \\ & + \frac{1}{2\pi}\int_{\mathcal{C}} e^{ikx-\omega t}\frac{u_x(0,0)+iku(0,0)}{1+k^2}dk - \frac{1}{2\pi}\int_{\mathcal{C}} e^{ikx}\frac{u_x(0,t)+iku(0,t)}{1+k^2}dk, \end{aligned} \quad (7)$$

where the integral on the real line has been deformed to a closed contour $\mathcal{C}$ around $k = i$ as shown in Figure A.1. This is possible since the respective integrands are analytic functions which decay in the upper-half plane for large k.

The integral expression (7) depends on unprescribed boundary data. As is usual in the MoF, this is resolved by using the invariances of $\omega(k)$. Note that $\omega(k)$ is invariant under the transform $k \to 1/k$. Using this transformation, the global relation becomes

$$\begin{aligned} U_0(1/k) + \frac{\tilde{g}(1/k,t)}{1+1/k^2} &= e^{\omega t}U(1/k,t), \quad \mathrm{Im}(k) \geq 0,\ k \neq 0, i, \\ \tilde{g}(1/k,t) &= \tilde{g}_0(\omega,t) + \frac{i}{k}\tilde{g}_1(\omega,t). \end{aligned}$$

The time transform of the boundary condition (5c) is given by

$$\alpha\tilde{g}_0(\omega,t) + \beta\tilde{g}_1(\omega,t) = G(\omega,t) = \int_0^t e^{\omega s}g(s)ds.$$

Solving the above equations for $\tilde{g}_0(\omega,t)$ and $\tilde{g}_1(\omega,t)$, and substituting the result in (7) we

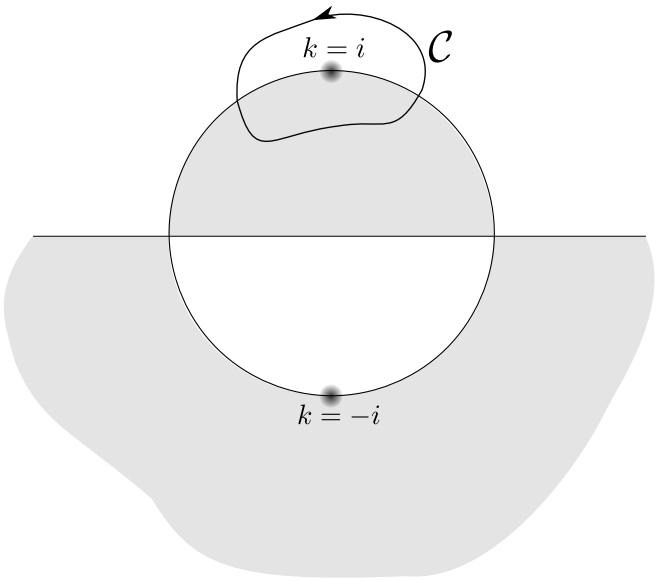

Figure A.1: The closed contour $\mathcal{C}$ and the region $D = \{k : \mathrm{Re}(\omega) < 0\}$, indicated in grey.

obtain

$$\begin{aligned} u(x,t) =& S(x,t) + \frac{1}{2\pi}\int_{\mathcal{C}} \frac{e^{ikx}}{k^3}\left(\frac{\alpha i k - \beta}{\alpha i - k\beta}\right)\hat{u}(1/k,t)dk \\ &+ \frac{1}{2\pi}\int_{\mathcal{C}} \frac{e^{ikx}}{1+k^2}\left[(u_x(0,t) + \frac{i}{k}u(0,t))\left(\frac{\alpha i k - \beta}{\alpha i k - k^2\beta}\right) - (u_x(0,t) + iku(0,t))\right]dk \end{aligned} \tag{8}$$

where

$$\begin{aligned} S(x,t) =& \frac{1}{2\pi}\int_{-\infty}^{\infty} e^{ikx-\omega t}\hat{u}_0(k)dk + \frac{1}{2\pi}\int_{\mathcal{C}} \frac{ie^{ikx-\omega t}}{(1+k^2)^2}\left(\frac{1-k^2}{\alpha i - k\beta}\right)G(\omega,t)dk \\ &- \frac{1}{2\pi}\int_{\mathcal{C}} \frac{e^{ikx-\omega t}}{k^3}\left(\frac{\alpha i k - \beta}{\alpha i - k\beta}\right)\hat{u}_0(1/k)dk \\ &+ \frac{1}{2\pi}\int_{\mathcal{C}} \frac{e^{ikx-\omega t}}{1+k^2}\left[(u_x(0,0) + iku(0,0)) - \left(\frac{\alpha i k - \beta}{\alpha i k - k^2\beta}\right)(u_x(0,0) + \frac{i}{k}u(0,0))\right]dk. \end{aligned}$$

The right-hand side of (8) depends on $u(x,t)$ itself, through the presence of $\hat{u}(1/k,t)$ in the second term. As such, (8) does not represent an explicit solution formula, and more work is required. Consider two possible cases.

- **Case 1.** $\boldsymbol{\alpha \neq \beta}$**.** By deforming the contour $\mathcal{C}$ as indicated in Figure A.1 *before* substitution of the transforms of the unknown boundary terms, we assure that the only singularity of the integrals in (8) enclosed by $\mathcal{C}$ is at $k = i$. Thus

$$\int_{\mathcal{C}} \frac{e^{ikx}}{k^3} \left(\frac{\alpha ik - \beta}{\alpha i - k\beta} \right) \hat{u}(1/k, t) dk = 0,$$

since the integrand is analytic in a neighborhood of $k = i$. Further, an application of the Residue Theorem for the third term in (8) leads to

$$\frac{1}{2\pi} \int_{\mathcal{C}} \frac{e^{ikx}}{1+k^2} \left[(u_x(0,t) + \frac{i}{k} u(0,t)) \left(\frac{\alpha ik - \beta}{\alpha ik - k^2 \beta} \right) - (u_x(0,t) + iku(0,t)) \right] dk = \frac{e^{-x} g(t)}{\alpha - \beta}.$$

Thus the solution $u(x,t)$ is given by

$$u(x,t) = S(x,t) + \frac{e^{-x} g(t)}{\alpha - \beta}. \tag{9}$$

In particular, the Dirichlet ($\beta = 0$) and Neumann ($\alpha = 0$) problems for this PDE have solutions given by the above expression. Since the term proportional to the exponential satisfies the boundary condition, it is necessary that

$$\alpha S(0,t) + \beta S_x(0,t) = 0,$$

which is assured by taking $g(0) = u_0(0) = 0$. Thus, the existence of a classical solution requires the compatibility of the boundary and initial conditions at the corner point $(x,t) = (0,0)$.

- **Case 2.** $\boldsymbol{\alpha = \beta = 1}$**.** The solution to the boundary-value problem given above is not valid when $\alpha = \beta$. Without loss of generality, we consider $\alpha = \beta = 1$. In this case, both integrals possess singularities at $k = i$. The residues are calculated to obtain

$$u(x,t) = S(x,t) + e^{-x} g(t) \left(x + \frac{1}{2} \right) + 2e^{-x} u(0,t) - 2e^{-x} \hat{u}(-i,t). \tag{10}$$

This may be interpreted as a linear integral equation for the solution $u(x,t)$ that depends on known initial-boundary data as well as on the unknowns $u(0,t)$ and $\hat{u}(-i,t)$.

If it is possible to express these unknowns in terms of the known initial- and boundary-condition functions then the above expression represents the solution to the problem. However, since by assumption $u(x,t)$ solves the PDE, we may substitute (10) into (5a) to obtain

$$g'(t) + \hat{u}(-i,t) = u(0,t). \tag{11}$$

If this relation holds for all time, we obtain the following solution to the problem on the half-line

$$u(x,t) = S(x,t) + e^{-x}g(t)\left(x + \frac{1}{2}\right) + 2e^{-x}g'(t). \tag{12}$$

Further, since the terms proportional to e^{-x} satisfy the boundary condition, the expression $S(x,t)$ has the same interpretation as in the case $\alpha \neq \beta$. Consequently we require $g(0) = u_0(0) = 0$. However, the initial condition is not satisfied unless

$$g'(0) + \hat{u}_0(-i) = 0, \tag{13}$$

as is readily seen by letting $t = 0$ in (12). It is noted that this expression may be obtained from (11) also.

Given a continuously differentiable function $g(t)$, the constraint (13) requires the initial condition $u_0(x)$ to be of the form

$$u_0(x) = -4xe^{-x}g'(0) + w(x), \tag{14}$$

where $w(x)$ is a function orthogonal to e^{-x} using the standard inner product on $[0,\infty)$, and $w(0) = 0$ with sufficient smoothness and decay for large x to justify the contour deformations in the previous section. Alternatively, given an initial condition $u_0(x)$ with $u_0(0) = 0$ and sufficient decay and smoothness, the above is a constraint on permissible boundary conditions $g(t)$.

The relation between initial and boundary conditions evidently restricts our freedom to arbitrarily choose initial and boundary functions for the case $\alpha = \beta$. Interestingly,

if $g(t)$ is identically zero, then $u_0(x)$ must be identically zero too, as we show below. Indeed, if $g(t) \equiv 0$, the solution expression is given by

$$u(x,t) = \frac{1}{2\pi}\int_{-\infty}^{\infty} e^{ikx-\omega t}\hat{u}_0(k)dk - \int_{\mathcal{C}} \frac{e^{ikx-\omega t}}{k^3}\left(\frac{ik-1}{i-k}\right)\hat{u}_0(1/k)dk. \tag{15}$$

Substituting this expression into (11), we find

$$\begin{aligned}\int_0^{\infty} e^{-x}u(x,t)dx =& u(0,t) \;\Rightarrow \\ \int_{-\infty}^{\infty}\frac{e^{-\omega t}\hat{u}_0(k)}{1-ik}dk + \int_{\mathcal{C}}\frac{e^{-\omega t}\hat{u}_0(1/k)}{i-k}dk =& \int_{-\infty}^{\infty} e^{-\omega t}\hat{u}_0(k)dk \\ &- \int_{\mathcal{C}}\frac{e^{-\omega t}(ik-1)\hat{u}_0(1/k)}{k^3(i-k)}dk. \end{aligned}\tag{16}$$

Using the transformation $k \to 1/k$ and replacing all contours $\mathcal{C}$ to contours $\tilde{\mathcal{C}}$ around $k=-i$, we obtain

$$\begin{aligned}&\int_{-\infty}^{\infty}\frac{e^{-\omega t}\hat{u}_0(k)}{1-ik}dk + \int_{\tilde{\mathcal{C}}}\frac{e^{-\omega t}\hat{u}_0(k)}{k(1-ik)}dk = \int_{-\infty}^{\infty} e^{-\omega t}\hat{u}_0(k)dk \\ &\qquad\qquad + \int_{\tilde{\mathcal{C}}}\frac{e^{-\omega t}k(i-k)\hat{u}_0(k)}{(ik-1)}dk \\ \Rightarrow\quad &-\int_{\tilde{\mathcal{C}}}\frac{e^{-\omega t}\hat{u}_0(k)}{1-ik}dk + \int_{\tilde{\mathcal{C}}}\frac{e^{-\omega t}\hat{u}_0(k)}{k(1-ik)}dk = -\int_{\tilde{\mathcal{C}}} e^{-\omega t}\hat{u}_0(k)dk \\ &\qquad\qquad + \int_{\tilde{\mathcal{C}}}\frac{e^{-\omega t}k(i-k)\hat{u}_0(k)}{(ik-1)}dk \\ \Rightarrow\quad &\int_{\tilde{\mathcal{C}}}\frac{e^{-\omega t}\hat{u}_0(k)(1-k)(k^2+k+1)}{k(1-ik)}dk = 0. \end{aligned}\tag{17}$$

Since this statement is valid for all t we may expand the exponential in a Taylor series in t, interchange order of summation and integration and equate the coefficient of every power of t to zero. This imposes the following set of conditions on the Fourier transform of the initial condition:

$$\text{Res}\left[\left(\frac{ik}{1+k^2}\right)^n \frac{(1-k)(k^2+k+1)}{(1-ik)k}\hat{u}_0(k)\right]_{k=-i} = 0, \quad n = 0,1,2\ldots,$$

hence

$$\frac{d^n}{dk^n}\hat{u}_0(k)\bigg|_{k=-i} = 0, \quad n = 0,1,2\ldots.$$

However, $\hat{u}_0(k)$ is an analytic function of k in the lower-half plane and is continuous up to the real line. Consequently, $\hat{u}_0(k) \equiv 0$ for k real and the initial condition $u_0(x)$

is identically zero. It follows that the initial condition is not a continuous function of the boundary data $g(t)$, at $g(t) \equiv 0$, since (14) shows that for $g(t) \not\equiv 0$, $u_0(x)$ can be arbitrarily large by choosing $w(x)$ large.

Finally I shall show that (11) holds for any classical solution to the PDE. Assuming $u(x,t)$ is a solution to the problem (5a-5c), we have

$$u_t - u_{xxt} + u_x = 0.$$

Multiplying this equation by e^{-x} and integrating over the domain $[0,\infty)$ yields after a few integrations by part

$$\frac{d}{dt}\left(u_x(0,t) + u(0,t)\right) + \int_0^\infty e^{-y} u(y,t) dy = u(0,t).$$

Noting that the first term on the left-hand side is the time derivative of the boundary condition, we obtain (13).

The identity (13), valid for any solution to the differential equation (11) is a constraint on the initial and boundary conditions when $\alpha = \beta = 1$. Indeed it may be verified that when $\alpha \neq \beta$, (11) is readily satisfied by the solution (9) to the problem.

A.3 Uniqueness of solutions to linear BBM on the half-line

In the previous section we constructed solutions to the linear BBM equation. The procedure was algorithmic. Depending on the values of the coefficients α and β, we obtained a solution expression (case 1) or we concluded additional constraints were required on the initial and boundary condition functions (case 2). In either case, it is necessary to investigate the uniqueness of the solution of the equation. If we can prove uniqueness, then in case 1, we may conclude that (9) is the unique solution to the given boundary-value problem. In particular, it follows that the Dirichlet and Neumann problems have unique solutions. Similarly, in case 2, where the initial and boundary conditions are required to satisfy the constraint (13), we conclude that the problem is ill posed in the sense that we cannot choose initial and boundary conditions arbitrarily.

It is typical to address uniqueness of solutions to evolution PDEs using energy integral arguments. The energy integral for the linear BBM equation is found as shown below.

$$
\begin{aligned}
& & u_t - u_{xxt} + u_x &= 0 \\
\Rightarrow & & uu_t - uu_{xxt} + uu_x &= 0 \\
\Rightarrow & & \int_0^\infty (uu_t - uu_{xxt} + uu_x)dx &= 0 \\
\Rightarrow & \frac{d}{dt}\int_0^\infty \frac{u^2}{2}dx - [uu_{xxt}]_0^\infty + \int_0^\infty u_x u_{xt}dx + \left[\frac{u^2}{2}\right]_0^\infty &= 0 \\
\Rightarrow & & \frac{d}{dt}\int_0^\infty \frac{1}{2}\left(u^2 + u_x^2\right)dx &= \frac{u^2(0,t)}{2} - u(0,t)u_{xt}(0,t).
\end{aligned}
$$

In the above expression, consider $u(x,t)$ as the difference of two distinct solutions to the BVP. Since the given initial and boundary conditions are linear, uniqueness follows if the right-hand side of the above expression is non-positive for homogeneous boundary conditions. Clearly this is the case for the Dirichlet problem. However, no direct conclusion is obtained for the Neumann or the Robin problem. We may consider the right-hand side of the last line above as a map from known boundary conditions to unknown values at the boundary. For the Neumann case, if the Neumann→Dirichlet map exists and maps zero to zero, we may yet conclude uniqueness. Similarly, for the Robin boundary condition. In what follows we construct explicit Robin→Dirichlet and Neumann→Dirichlet maps which do indeed map homogeneous data to zero. Consequently, there is a unique solution to the BVP (5a-5c).

A.3.1 Robin→Dirichlet boundary-value map

The assumption of a classical solution to the BVP (5a-5c) leads to the global relation (6). In this section we see how the global relation may be used to derive a map from known initial-boundary data to unknown boundary data. Let us consider the Robin condition

$$\alpha u(0,t) + \beta u_x(0,t) = g(t),$$

which upon taking the time transform becomes

$$\alpha \tilde{g}_0(\omega,t) + \beta \tilde{g}_1(\omega,t) = G(\omega,t).$$

Solving for $u_x(0,t)$ and $\tilde{g}_1(\omega,t)$ (assuming $\beta \neq 0$) in the above equations and substituting in the global relation (6) we obtain

$$\begin{aligned}\frac{1}{(1+k^2)^2}\left[\left(\frac{\beta-\alpha ik}{\beta}\right)\tilde{g}_0(\omega,t)+\frac{ik}{\beta}G(\omega,t)\right]+\hat{u}_0+\frac{1}{(1+k^2)^2}\left[\frac{g(0)-\alpha u(0,0)}{\beta}+iku(0,0)\right]\\ =\frac{e^{\omega t}}{1+k^2}\left[\frac{g(t)-\alpha u(0,t)}{\beta}+iku(0,t)+(1+k^2)\hat{u}(k,t)\right]\\ =e^{\omega t}\left[\hat{u}(k,t)+\frac{g(t)}{\beta(1+k^2)}+\frac{ik-\alpha/\beta}{1+k^2}u(0,t)\right]. \qquad (18)\end{aligned}$$

Multiplying this expression by $e^{-\omega t}\dfrac{1-k^2}{\beta-\alpha ik}$ and integrating over a sufficiently small contour C containing $k=-i$ we obtain the required map. The contribution from $\tilde{g}_0(\omega,t)$ vanishes since

$$\begin{aligned}\oint_C e^{-\omega t}\frac{1-k^2}{(1+k^2)^2}\tilde{g}_0(\omega,t)dk &= \oint_{\tilde{C}} e^{-ilt}\tilde{g}_0(il,t)dl,\\ &= \oint_{\tilde{C}} e^{-ilt}\int_0^t e^{ils}u(0,s)dsdl,\\ &= 0.\end{aligned}$$

The first equality is obtained using the change of coordinates $l=k/(1+k^2)$, where $\tilde{C}$ is the image of C under this map. The second equality uses the definition of the time transform. Evidently the integrand is an entire function of l, from which the conclusion follows. If $\alpha \neq \beta$ the contribution from $\hat{u}(k,t)$ also vanishes since

$$\oint_C \frac{1-k^2}{\beta-\alpha ik}\hat{u}(k,t)dk=0,$$

due to analyticity of the integrand. An application of the Residue Theorem leads to the following expression for the Dirichlet data

$$\begin{aligned}\frac{-2\pi}{\beta}u(0,t)=\frac{2\pi}{\beta(\beta-\alpha)}g(t)+\oint_C\frac{ike^{-\omega t}(1-k^2)}{(1+k^2)^2(\beta-\alpha ik)}G(\omega,t)dk+\oint_C\frac{e^{-\omega t}(1-k^2)}{\beta-\alpha ik}\hat{u}_0(k)dk\\ +\oint_C\frac{e^{-\omega t}(1-k^2)}{(1+k^2)^2(\beta-\alpha ik)}\left[\frac{g(0)}{\beta}+\left(ik-\frac{\alpha}{\beta}\right)u_0(0)\right]dk.\end{aligned}$$

This expression is also valid for the Neumann problem ($\beta=1$, $\alpha=0$). The expression above simplifies if we impose the corner condition $u_0(0)=g(0)=0$, which was required for existence of smooth solutions in the previous sections. Since the Robin→Dirichlet map

maps the homogeneous problem to zero Dirichlet data, we obtain uniqueness for the case $\alpha \neq \beta$.

The argument above applies with little modification for the case $\alpha = \beta = 1$. We now obtain a contribution from $\hat{u}(k,t)$ given by

$$\begin{aligned}\oint_C \frac{1-k^2}{1-ik}\hat{u}(k,t)dk &= -4\pi\hat{u}(-i,t) \\ &= -4\pi u(0,t) + 4\pi g'(t),\end{aligned}$$

where we have used the integral relation (11). We obtain the following expression for the Robin→Dirichlet map

$$\begin{aligned}-2\pi u(0,t) = -4\pi g'(t) - \pi g(t) + \oint_C \frac{ike^{-\omega t}(1-k^2)}{(1+k^2)^2(1-ik)}G(\omega,t)dk + \oint_C \frac{e^{-\omega t}(1-k^2)}{1-ik}\hat{u}_0(k)dk \\ + \oint_C \frac{e^{-\omega t}(1-k^2)}{(1+k^2)^2(1-ik)}\left[g(0) + (ik-1)\,u_0(0)\right]dk,\end{aligned}$$

from which the same conclusion is obtained.

A.4 Linear BBM on the finite interval

Next, consider the finite-interval BVP. The MoF is even more advantageous in this setting. Classical methods would lead one to consider separation of variables, *i.e.*, we start with $u(x,t) = f(x)s(t)$. Substituting into the differential equation, we obtain

$$f(x)s'(t) - f''(x)s'(t) + f'(x)s(t) = 0.$$

Dividing by $f'(x)s'(t)$ results in a generalized eigenvalue problem in the spatial variable requiring significant analysis in order to establish whether or not the eigenfunctions obtained form a complete set. The MoF not only provides a solution without this additional effort, but it also indicates which boundary-value problems may be ill posed in the same sense we observed for the BVP on the half-line. Since the procedure is somewhat similar to what was done for the BVP on the half line, only the outline of the steps involved will be presented.

By integrating the local relation over the region $\{(x,s) : 0 \leq x \leq L,\ 0 < s < t\}$ and applying Green's Theorem, we obtain the global relation for the finite interval:

$$U_0(k) + \frac{\tilde{g}(k,t)}{1+k^2} - e^{-ikL}\frac{\tilde{h}(k,t)}{1+k^2} = e^{\omega t}U(k,t),$$

where

$$
\begin{aligned}
U_0(k) &= (1+k^2)\hat{u}_0(k) + u_x(0,0) + iku(0,0) - e^{-ikL}u_x(L,0) - ike^{-ikL}u(L,0),\\
U(k,t) &= (1+k^2)\hat{u}(k,t) + u_x(0,t) + iku(0,t) - e^{-ikL}u_x(L,t) - ike^{-ikL}u(L,t),\\
\tilde{g}(k,t) &= \tilde{g}_0(\omega,t) + ik\tilde{g}_1(\omega,t),\\
\tilde{h}(k,t) &= \tilde{h}_0(\omega,t) + ik\tilde{h}_1(\omega,t),\\
\omega &= \frac{ik}{1+k^2},
\end{aligned}
$$

and $\tilde{h}(k,t)$ is defined similarly to $\tilde{g}(k,t)$ but with $u(x,t)$ evaluated at $x = L$. The Fourier transform is given by

$$
\hat{u}_0(k) = \int_0^L e^{-ikx}u_0(x)dx, \quad \hat{u}(k,t) = \int_0^L e^{-ikx}u(x,t)dx.
$$

Applying the inverse Fourier transform, we obtain the integral expression

$$
\begin{aligned}
u(x,t) =& \frac{1}{2\pi}\int_{-\infty}^{\infty} e^{ikx-\omega t}\frac{U_0(k)}{1+k^2}dk + \frac{1}{2\pi}\int_{-\infty}^{\infty} e^{ikx-\omega t}\frac{\tilde{g}(k,t)}{(1+k^2)^2}dk\\
&- e^{-ikL}\frac{1}{2\pi}\int_{-\infty}^{\infty} e^{ikx-\omega t}\frac{\tilde{h}(k,t)}{(1+k^2)^2}dk - \frac{1}{2\pi}\int_{-\infty}^{\infty} e^{ikx}\frac{u_x(0,t)+iku(0,t)}{1+k^2}dk\\
&+ \frac{1}{2\pi}\int_{-\infty}^{\infty} e^{ikx-ikL}\frac{u_x(L,t)+iku(L,t)}{1+k^2}dk.
\end{aligned}
$$

The integral of the boundary terms may be deformed off the real line to appropriate contours $\mathcal{C}_1$ and $\mathcal{C}_2$ which are closed curves around $k = i$ and $k = -i$ respectively.

$$
\begin{aligned}
u(x,t) =& \frac{1}{2\pi}\int_{-\infty}^{\infty} e^{ikx-\omega t}\hat{u}_0(k)dk + \frac{1}{2\pi}\int_{\mathcal{C}_1} e^{ikx-\omega t}\frac{\tilde{g}(k,t)}{(1+k^2)^2}dk - \frac{1}{2\pi}\int_{\mathcal{C}_2} e^{-ik(L-x)-\omega t}\frac{\tilde{h}(k,t)}{(1+k^2)^2}dk\\
&+ \frac{1}{2\pi}\int_{\mathcal{C}_1} e^{ikx-\omega t}\frac{u_x(0,0)+iku(0,0)}{1+k^2}dk - \frac{1}{2\pi}\int_{\mathcal{C}_1} e^{ikx}\frac{u_x(0,t)+iku(0,t)}{1+k^2}dk\\
&- \frac{1}{2\pi}\int_{\mathcal{C}_2} e^{ikx-ikL-\omega t}\frac{u_x(L,0)+iku(L,0)}{1+k^2}dk + \frac{1}{2\pi}\int_{\mathcal{C}_2} e^{ikx-ikL}\frac{u_x(L,t)+iku(L,t)}{1+k^2}dk.
\end{aligned} \tag{19}
$$

Assume we are given Robin boundary conditions at both $x = 0$ and $x = L$.

$$
\begin{aligned}
&\alpha u(0,t) + \beta u_x(0,t) = g(t), \;\; \gamma u(L,t) + \delta u_x(L,t) = h(t)\\
\Rightarrow \qquad &\alpha\tilde{g}_0(\omega,t) + \beta\tilde{g}_1(\omega,t) = G(\omega,t), \;\; \gamma\tilde{h}_0(\omega,t) + \delta\tilde{h}_1(\omega,t) = H(\omega,t),
\end{aligned} \tag{20}
$$

where α, β, γ, and δ are real. Combining these last equations with the transformed version of the global relation

$$U_0(1/k) + \frac{\tilde{g}(1/k,t)}{1+1/k^2} - e^{-iL/k}\frac{\tilde{h}(1/k,t)}{1+1/k^2} = e^{\omega t}U(1/k,t),$$

as well as with the original global relation, we obtain a system of equations for the unknown boundary terms. For instance, solving (20) for $\tilde{g}_0$ and $\tilde{h}_0$, we obtain a system of equations for the two remaining boundary terms. To solve this system of equations we are required to invert the matrix

$$\begin{pmatrix} ik-\beta/\alpha & -e^{-ikL}\,(ik-\delta/\gamma) \\ i/k-\beta/\alpha & -e^{-iL/k}\,(i/k-\delta/\gamma) \end{pmatrix}.$$

For a given set $\{\alpha,\beta,\gamma,\delta\}$, the zeros in the complex k plane of the determinant of this matrix are the singularities which appear in the final expression for the solution. Since the entries of the matrix are analytic functions of k in $\mathbb{C}\backslash\{0\}$, the zeros of the determinant are isolated. Hence, by deforming the contours $\mathcal{C}_1, \mathcal{C}_2$ suitably *before* substitution of the expressions for $\tilde{g}_i, \tilde{h}_i,\ i=0,1$, it is possible to ensure the integrals contain at most one singularity, namely at $k=i$ or at $k=-i$. Consequently, if there exists a set $\{\alpha,\beta,\gamma,\delta\} \in \mathbb{R}^4$ such that for $k=\pm i$ the determinant is zero, then the problem is presumed to be ill posed in a sense similar to that observed in the half-line case. Indeed, setting $k=\pm i$ the determinant has a zero only if $(\alpha,\gamma) = \pm(\beta,\delta)$. Hence either one of the following boundary conditions leads to an ill-posed problem:

$$u(0,t) + u_x(0,t) = g(t), \tag{21a}$$

$$u(L,t) + u_x(L,t) = h(t), \tag{21b}$$

or

$$u(0,t) - u_x(0,t) = g(t), \tag{22a}$$

$$u(L,t) - u_x(L,t) = h(t). \tag{22b}$$

In all other cases, the solution proceeds in a manner similar to Case 1 ($\alpha \neq \beta$) of the half-line problem. In the following, I present details of the boundary-value problem with

boundary conditions (21a-21b). In this case, the global relation is

$$(1+k^2)U_0(k) + ikG - ike^{-ikL}H + (1-ik)(\tilde{g}_0 - e^{-ikL}\tilde{h}_0) = (1+k^2)e^{\omega t}U(k,t), \tag{23}$$

where $G, H, \tilde{g}_0, \tilde{h}_0$ are the time transforms of the Robin and Dirichlet data at the left and right boundaries defined analogously as to the half-line case. Looking ahead, let us suppress the dependence of these terms on ω and t since the time transforms are invariant under the symmetries of the dispersion relation unlike the functions U and U_0, which are given by

$$\begin{aligned} U_0(k) &= (1+k^2)\hat{u}_0(k) + g(0) - h(0)e^{-ikL} + (ik-1)(u_0(0) - e^{-ikL}u_0(L)), \\ U(k,t) &= (1+k^2)\hat{u}(k,t) + g(t) - h(t)e^{-ikL} + (ik-1)(u(0,t) - e^{-ikL}u(L,t)). \end{aligned}$$

The global relation (23) is valid for all $k \in \mathbb{C}\backslash\{-i, i\}$. Using the symmetry $k \to 1/k$ we obtain another version of the global relation valid for $k \in \mathbb{C}\backslash\{-i, 0, i\}$,

$$\frac{1+k^2}{k^2}U_0\left(\frac{1}{k}\right) + \frac{i}{k}G - \frac{i}{k}e^{-iL/k}H + \frac{k-i}{k}(\tilde{g}_0 - e^{-iL/k}\tilde{h}_0) = \frac{1+k^2}{k^2}e^{\omega t}U\left(\frac{1}{k}, t\right). \tag{24}$$

Hence we obtain a system of equations for the unknown Dirichlet data which may be solved to obtain

$$\begin{pmatrix} \tilde{g}_0 \\ \tilde{h}_0 \end{pmatrix} = \Delta^{-1}(P+R), \tag{25}$$

where

$$\Delta^{-1} = \frac{1}{i(1+k^2)\delta(k)}\begin{pmatrix} -e^{-iL/k}(k-i) & e^{-iLk}k(1-ik) \\ -(k-i) & k(1-ik) \end{pmatrix}, \quad P = \frac{e^{\omega t}(1+k^2)}{k^2}\begin{pmatrix} k^2U(k,t) \\ U(1/k,t) \end{pmatrix},$$

$$R = \begin{pmatrix} -(1+k^2)U_0(k) - ikG + ike^{-ikL}H \\ -\frac{1+k^2}{k^2}U_0(\frac{1}{k}) - \frac{i}{k}G + \frac{i}{k}e^{-ikL}H \end{pmatrix}$$

and

$$\delta(k) = e^{-iL/k} - e^{-ikL}.$$

The global relation (23) is solved for $\hat{u}(k,t)$. Taking the inverse Fourier transform of the resulting expression leads to

$$\begin{aligned} u(x,t) = &-\frac{1}{2\pi}\int_{-\infty}^{\infty}\frac{e^{ikx}}{1+k^2}(g(t)-h(t)e^{-ikL})dk - \frac{1}{2\pi}\int_{-\infty}^{\infty}\frac{ie^{ikx}}{k-i}(u(0,t)-u(L,t)e^{-ikL})dk \\ &+\frac{1}{2\pi}\int_{-\infty}^{\infty}\frac{e^{ikx-\omega t}}{1+k^2}U_0(k)dk + \frac{1}{2\pi}\int_{-\infty}^{\infty}\frac{ike^{ikx-\omega t}}{(1+k^2)^2}Gdk - \frac{1}{2\pi}\int_{-\infty}^{\infty}\frac{ike^{ikx-ikL-\omega t}}{(1+k^2)^2}Hdk \\ &-\frac{1}{2\pi}\int_{-\infty}^{\infty}\frac{i(k+i)e^{ikx-\omega t}}{(1+k^2)^2}\tilde{g}_0dk + \frac{1}{2\pi}\int_{-\infty}^{\infty}\frac{i(k+i)e^{ikx-ikL-\omega t}}{(1+k^2)^2}\tilde{h}_0dk. \end{aligned}$$

The integrals in the above expression involving boundary data may be deformed off the real axis to circular contours around $k=\pm i$ denoted by $\mathcal{C}_1$ and $\mathcal{C}_2$ respectively, leading to

$$\begin{aligned} u(x,t) = &-\frac{e^{-x}}{2}g(t) + \frac{e^{x-L}}{2}h(t) + e^{-x}u(0,t) + \frac{1}{2\pi}\int_{-\infty}^{\infty}\frac{e^{ikx-\omega t}}{1+k^2}U_0(k)dk \\ &+\frac{1}{2\pi}\int_{\mathcal{C}_1}\frac{ike^{ikx-\omega t}}{(1+k^2)^2}Gdk + \frac{1}{2\pi}\int_{\mathcal{C}_2}\frac{ike^{ikx-ikL-\omega t}}{(1+k^2)^2}Hdk \\ &-\frac{1}{2\pi}\int_{\mathcal{C}_1}\frac{i(k+i)e^{ikx-\omega t}}{(1+k^2)^2}\tilde{g}_0dk - \frac{1}{2\pi}\int_{\mathcal{C}_2}\frac{i(k+i)e^{ikx-ikL-\omega t}}{(1+k^2)^2}\tilde{h}_0dk. \end{aligned}$$

Substituting for $\tilde{g}_0$ and $\tilde{h}_0$ from (25) and taking appropriate residues we obtain

$$\begin{aligned} u(x,t) = &-\frac{e^{-x}}{2}g(t) + \frac{e^{x-L}}{2}h(t) + e^{-x}u(0,t) + \frac{1}{2\pi}\int_{-\infty}^{\infty}\frac{e^{ikx-\omega t}}{1+k^2}U_0(k)dk \\ &+\frac{1}{2\pi}\int_{\mathcal{C}_1}\frac{ike^{ikx-\omega t}}{(1+k^2)^2}Gdk + \frac{1}{2\pi}\int_{\mathcal{C}_2}\frac{ike^{ikx-ikL-\omega t}}{(1+k^2)^2}Hdk \\ &-\frac{1}{2\pi}\int_{\mathcal{C}_1}\frac{ie^{ikx-\omega t}(k+i)}{(1+k^2)^2}(\Delta^{-1}R)_1dk - \frac{1}{2\pi}\int_{\mathcal{C}_2}\frac{ie^{ikx-ikL-\omega t}(k+i)}{(1+k^2)^2}(\Delta^{-1}R)_2dk \\ &-e^{x-L}\frac{g(t)-e^{-L}h(t)}{2(e^L-e^{-L})} + \frac{e^{-x}}{e^L-e^{-L}}(e^L(x+1)g(t)-(x+1-L)h(t)) \\ &-\frac{e^{-x}}{2(e^L-e^{-L})}(e^{-L}g(t)-h(t)) - 2\frac{e^{-x+L}}{e^L-e^{-L}}\hat{u}(-i,t) \\ &+e^{-x+L}\frac{u(0,t)-u(L,t)e^{-L}}{e^L-e^{-L}} + e^{-x-L}\frac{u(0,t)-u(L,t)e^{L}}{e^L-e^{-L}}, \end{aligned} \tag{26}$$

where $(\Delta^{-1}R)_1$ and $(\Delta^{-1}R)_2$ refer to the first and second components of the vector $\Delta^{-1}R$. As in the half-line case, we notice that the above expression depends on the unknown Dirichlet data and the function $\hat{u}(-i,t)$. Since by assumption $u(x,t)$ is a solution to the PDE, we may substitute the right-hand side in the BBM equation, which results in the following necessary condition relating the unknown functions $u(0,t), u(L,t)$ and $\hat{u}(-i,t)$

$$\hat{u}(-i,t) + g'(t) - e^{-L}h'(t) = u(0,t) - e^{-L}u(L,t). \tag{27}$$

It may be shown that this constraint is satisfied by any solution to the PDE. Indeed it is the finite interval analogue of (11) and may be derived in a similar manner. We may obtain two additional equations between the three unknowns from (25) by multiplying by $e^{-\omega t}(1-k^2)/(1+k^2)^2$ and integrating along a small contour $\mathcal{C}$ around $k=i$. This leads to

$$\int_{\mathcal{C}} e^{-\omega t} \frac{1-k^2}{(1+k^2)^2} \, \Delta^{-1} \left(P+R\right) dk = 0. \tag{28}$$

Evidently, equations (28) and (27) are three equations for three unknowns. This system of equations may be solved to obtain the Robin→Dirichlet map as well as a map from known initial and boundary data to the function $\hat{u}(-i,t)$. Using these definitions for the unknown functions, (26) represents the solution to the boundary-value problem on the finite interval. Indeed it is the unique solution since the Robin→Dirichlet map for the finite interval maps the homogeneous problem to trivial Dirichlet data, and an energy argument can be used to imply uniqueness. Note that (25), which was obtained from the global relation (23), and (27) are obtained from the assumption of existence of a smooth solution.

In order to satisfy the initial-boundary conditions we require additional compatibility conditions, namely $u_0(0) = u_0(L) = g(0) = h(0) = 0$ and that the relation (27) is satisfied at $t=0$. We obtain the following constraint on the allowable initial and boundary data

$$\hat{u}_0(-i) + g'(0) - e^{-L} h'(0) = 0.$$

A calculation similar to that for the half-line case indicates that the only solution with this particular boundary condition and $g(t) = h(t) = 0$ is the trivial one.

Conclusions

The MoF has been extended to PDEs with mixed partial derivatives in two independent variables by discussing BVPs for the linear BBM equation in detail. The application of these ideas to other mixed-derivative equations is straightforward. For the linear BBM equation,

we have the following two theorems.

Theorem 1. The BVP

$$u_t - u_{xxt} + u_x = 0, \qquad x \geq 0,\ t \in (0, T], \tag{29a}$$

$$u(x, 0) = u_0(x), \qquad x \geq 0, \tag{29b}$$

$$\alpha u(0, t) + \beta u_x(0, t) = g(t), \qquad t \in (0, T),\ \alpha, \beta \in \mathbb{R}. \tag{29c}$$

has a unique solution when $\alpha \neq \beta$. Further, the existence of a smooth solution requires $u_0(0) = g(0) = 0$. If $\alpha = \beta$ the problem is ill posed in the sense that the initial and boundary conditions may not be prescribed arbitrarily. If homogeneous boundary conditions are imposed, the initial condition must be identically zero for a smooth solution to exist. By uniqueness, this implies the only solution with homogeneous boundary conditions is the trivial one. If $\alpha = \beta$ and non-homogeneous boundary conditions are prescribed, then the constraint between initial and boundary conditions

$$\hat{u}_0(-i) + g'(0) = 0,$$

must hold for a solution to exist.

Theorem 2. The BVP

$$u_t - u_{xxt} + u_x = 0, \qquad x \in [0, L],\ t \in (0, T], \tag{30a}$$

$$u(x, 0) = u_0(x), \qquad x \in [0, L], \tag{30b}$$

$$\alpha u(0, t) + \beta u_x(0, t) = g(t), \qquad t \in (0, T),\ \alpha, \beta \in \mathbb{R}, \tag{30c}$$

$$\gamma u(0, t) + \delta u_x(L, t) = h(t), \qquad t \in (0, T),\ \gamma, \delta \in \mathbb{R}. \tag{30d}$$

has a unique solution when $(\alpha, \gamma) \neq \pm(\beta, \delta)$. The existence of a smooth solution requires $u_0(0) = g(0) = 0$ and $u_0(L) = h(0) = 0$. If $(\alpha, \gamma) = \pm(\beta, \delta)$ the problem is ill posed in the sense that the initial and boundary conditions may not be prescribed arbitrarily. If homogeneous boundary conditions are imposed, the initial condition must be identically zero for a smooth solution to exist. By uniqueness, this implies the only solution with homogeneous boundary conditions is the trivial one. If $(\alpha, \gamma) = \pm(\beta, \delta)$ and non-homogeneous boundary

conditions are prescribed, then the constraint between initial and boundary conditions

$$\hat{u}_0(-i) + g'(0) - e^{-L}h'(0) = 0,$$

must hold for a solution to exist.

It is possible to anticipate the non-trivial behavior mentioned in these theorems. For linear BBM, the differential operator acting on the time derivative has the symbol $M(k) = 1 + k^2$, with a null-space spanned by $\{e^x, e^{-x}\}$. In order to invert this operator, it is necessary for the null-space of the operator to be empty. This is achieved by selecting the boundary condition. To see this consider linear BBM on the finite interval as a second-order forced ordinary differential equation in u_t (see [12]). For all boundary conditions except the cases $(\alpha, \gamma) = \pm(\beta, \delta)$, it is possible to construct a Green's function uniquely. Further, the functions e^x and e^{-x} are in the null-space of the exceptional boundary conditions. This is the cause of the ill-posedness. This form of ill-posedness should be a generic feature of PDEs with mixed partial derivatives.

BIBLIOGRAPHY

[1] M. J. Ablowitz and A. S. Fokas, *Complex variables: introduction and applications*, second ed., Cambridge University Press, Cambridge, 2003.

[2] M. J. Ablowitz, A. S. Fokas, and Z. H. Musslimani, *On a new non-local formulation of water waves*, J. Fluid Mech. **562** (2006), 313–343.

[3] M. J. Ablowitz and T. S. Haut, *Spectral formulation of the two fluid Euler equations with a free interface and long wave reductions*, Analysis and Applications **6** (2008), 323–348.

[4] M. J. Ablowitz and H. Segur, *Solitons and the inverse scattering transform*, vol. 4, Society for Industrial and Applied Mathematics (SIAM), Philadelphia, PA, 1981.

[5] C. J. Amick and J. F. Toland, *On solitary water-waves of finite amplitude*, Arch. Ration. Mech. Anal. **76** (1981), 9–95.

[6] N. H. Asmar, *Applied complex analysis with partial differential equations*, Prentice-Hall Inc., Englewood Cliffs, NJ, 2002.

[7] A. Baquerizo and M. A. Losada, *Transfer function between wave height and wave pressure for progressive waves*, Coastal Engineering **24** (1995), 351–353.

[8] R. Beals, P. Deift, and C. Tomei, *Direct and inverse scattering on the line*, Mathematical Surveys and Monographs, vol. 28, American Mathematical Society, Providence, RI, 1988.

[9] T. B. Benjamin, J. L. Bona, and J. J. Mahony, *Model equations for long waves in nonlinear dispersive systems*, Phil. Trans. Roy. Soc. London. Ser. A **272** (1972), 47–78.

[10] A. O. Bergan, A. Torum, and A. Traetteberg, *Wave measurements by pressure type wave gauge*, Proceedings of the 11th Coastal Engineering Conference ASCE (1968), 19–29.

[11] C. T. Bishop and M. A. Donelan, *Measuring waves with pressure transducers*, Coastal Engineering **11** (1987), 309–328.

[12] J. L. Bona and P. J. Bryant, *A mathematical model for long waves generated by wavemakers in non-linear dispersive systems*, Proc. Camb. Phil. Soc. **73** (1973), 391–405.

[13] J. P. Boyd, *Chebyshev and Fourier spectral methods*, Dover Publications Inc., Mineola, NY, 2001.

[14] B. Buffoni, E.N. Dancer, and J.F. Toland, *The Regularity and Local Bifurcation of Steady Periodic Water Waves*, Arch. Rational Mech. Anal. **152** (2000), 207–240.

[15] I. M. Cohen and P. K. Kundu, *Fluid Mechanics*, Academic Press, 2004.

[16] R. R. Coifman and Y. Meyer, *Nonlinear harmonic analysis and analytic dependence*, Pseudodifferential operators and applications (Notre Dame, Ind., 1984), American Mathematical Society, Providence, RI, 1985, pp. 71–78.

[17] E. D. Cokelet, *Steep gravity waves in water of arbitrary uniform depth*, Phil. Trans. Roy. Soc. London. Ser. A **286** (1977), 183–230.

[18] M. D. Collins and W. A. Kuperman, *Inverse problems in ocean acoustics*, Inverse Problems **10** (1994), 1023–1040.

[19] A. Constantin, *The trajectories of particles in Stokes waves*, Invent. Math. **166** (2006), 523–535.

[20] ———, *On the particle paths in solitary water waves*, Quart. Appl. Math. **68** (2010), 81–90.

[21] A. Constantin and J. Escher, *Particle trajectories in solitary water waves*, Bull. Amer. Math. Soc. **44** (2007), 423–431.

[22] A. Constantin, J. Escher, and H.-C. Hsu, *Pressure beneath a solitary water wave: mathematical theory and experiments*, Arch. Ration. Mech. Anal. **201** (2011), 251–269.

[23] A. Constantin and W. Strauss, *Pressure and trajectories beneath a Stokes wave*, Comm. Pure Appl. Math. **53** (2010), 533–557.

[24] W. Craig, P. Guyenne, D. P. Nicholls, and C. Sulem, *Hamiltonian long-wave expansions for water waves over a rough bottom*, Proc. R. Soc. A **461** (2005), 839–873.

[25] W. Craig and C. Sulem, *Numerical simulation of gravity waves.*, J. Comp. Phys. **108** (1993), 73–83.

[26] A. D. D. Craik, *The origins of water wave theory*, Ann. Rev. Fluid Mech. **36** (2004), 1–28.

[27] R. G. Dean and R. A. Dalrymple, *Water Wave Mechanics for Engineers and Scientists*, World Scientific, Singapore, 2010.

[28] B. Deconinck and K. Oliveras, *The instability of periodic surface gravity waves*, J. Fluid Mech. **675** (2011), 141–167.

[29] B. Deconinck, T. Trogdon, and V. Vasan, *Solving linear partial differential equations*, Submitted for publication (2011), 1–21.

[30] J. E. Dennis, *Nonlinear Least-Squares*, State of the Art in Numerical Analysis (D. Jacobs, ed.), Academic Press, San Diego, CA, 1977, pp. 269–312.

[31] J. Escher and T. Schlurmann, *On the recovery of the free surface from the pressure within periodic traveling water waves*, J. Nonlinear Math. Phys. **15** (2008), 50–57.

[32] L. Evans, *Partial Differential Equations*, American Mathematical Society, Providence, RI,, 1998.

[33] N. Flyer and A. S. Fokas, *A hybrid analytical-numerical method for solving evolution partial differential equations. I. The half-line*, Proc. R. Soc. Lond. Ser. A **464** (2008), 1823–1849.

[34] A. S. Fokas, *On a class of physically important integrable equations*, Physica D **87** (1995), 145–150.

[35] ———, *A unified transform method for solving linear and certain nonlinear PDEs*, Proc. Roy. Soc. London Ser. A **453** (1997), 1411–1443.

[36] ———, *Integrable nonlinear evolution equations on the half-line*, Comm. Math. Phys. **230** (2002), 1–39.

[37] ———, *A new transform method for evolution partial differential equations*, IMA J. Appl. Math. **67** (2002), 559–590.

[38] ———, *A unified approach to boundary value problems*, CBMS-NSF regional conference series in applied mathematics, Society for Industrial and Applied Mathematics (SIAM), Philadelphia, PA, 2008.

[39] A. S. Fokas and B. Pelloni, *Boundary Value Problems for Boussinesq Type Systems*, Mathematical Physics, Analysis and Geometry **8** (2005), 59–96.

[40] ———, *A transform method for linear evolution PDEs on a finite interval*, IMA J. Appl. Math. **70** (2005), 564–587.

[41] G. Folland, *Real Analysis: Modern Techniques and Their Applications*, second ed., Pure and Applied Mathematics, John Wiley & Sons, Hoboken, NJ, 1999.

[42] S Grilli, *Depth inversion in shallow water based on nonlinear properties of shoaling periodic waves*, Coastal Engineering **35** (1998), 185209.

[43] R. B. Guenther and J. W. Lee, *Partial differential equations of mathematical physics and integral equations*, Dover Publications Inc., Mineola, NY, 1996.

[44] P. Guyenne and D. P. Nicholls, *A high-order spectral method for nonlinear water waves over moving bottom topography*, SIAM J. Sci. Comput. **30** (2007/08), 81–101.

[45] B. Hu and D. P. Nicholls, *The domain of analyticity of Dirichlet-Neumann operators*, Proc. Roy. Soc. Edinburgh Sect. A **140** (2010), 367–389.

[46] A. B. Kennedy, R. Gravois, B. Zachry, R. Luettich, T. Whipple, R. Weaver, J. Reynolds-Fleming, Q. J. Chen, and R. Avissar, *Rapidly installed temporary gauging for hurricane waves and surge, and application to Hurricane Gustav*, Continental Shelf Research **30** (2010), 1743–1752.

[47] Y.-Y. Kuo and J.-F. Chiu, *Transfer function between the wave height and wave pressure for progressive waves*, Coastal Engineering **23** (1994), 81–93.

[48] ———, *Transfer Function between wave height and wave pressure for progressive waves: reply to the comments of A. Baquerizo and M.A. Losada*, Coastal Engineering **24** (1995), 355–356.

[49] D. Lannes, *Well-posedness of the water-wave equations*, J. Amer. Math. Soc. **18** (2005), 605–654.

[50] D. Y. Lee and H. Wang, *Measurement of surface waves from subsurface gage*, Proceedings of the 19th Coastal Engineering Conference ASCE (1984), 271–286.

[51] Q. Ma (ed.), *Advances in Numerical Simulation of Nonlinear Water Waves*, Advances in Coastal and Ocean Engineering, vol. 11, World Scientific, 2010.

[52] P. A. Milewski, J.-M. Vanden-Broeck, and Z. Wang, *Dynamics of steep two-dimensional gravity–capillary solitary waves*, J. Fluid Mech. **664** (2010), 466–477.

[53] D. P. Nicholls, *Traveling water waves: spectral continuation methods with parallel implementation*, J. Comput. Phys. **143** (1998), 224–240.

[54] D. P. Nicholls and M. Taber, *Joint analyticity and analytic continuation of Dirichlet-Neumann operators on doubly perturbed domains*, J. Math. Fluid Mech. **10** (2008), 238–271.

[55] J. Nocedal and S. J. Wright, *Numerical Optimization*, Springer-Verlag, New York, NY., 1999.

[56] P. J. Olver, *Conservation laws of free boundary problems and the classification of conservation laws for water waves*, Trans. Amer. Math. Soc. **277** (1983), 353–380.

[57] R. C. Paley and N. Wiener, *Fourier transforms in the complex domain*, Colloquium Publications, vol. 19, American Mathematical Society, Providence, RI, 1934.

[58] C. Piotrowski and J. Dugan, *Accuracy of bathymetry and current retrievals from airborne optical time-series imaging of shoaling waves*, IEEE Trans. on Geoscience and Remote Sensing **40** (2002), 2606–2618.

[59] E. A. Spence and A. S. Fokas, *A new transform method I: domain-dependent fundamental solutions and integral representations*, Proc. R. Soc. Lond. Ser. A **466** (2010), 2259–2281.

[60] ———, *A new transform method II: the global relation and boundary-value problems in polar coordinates*, Proc. R. Soc. Lond. Ser. A **466** (2010), 2283–2307.

[61] E. R. Spielvogel, *A variational principle for waves of infinite depth*, Arch. Rational Mech. Anal. **39** (1970), 189–205.

[62] M. I. Taroudakis and G. Makrakis, *Inverse Problems in Underwater Acoustics*, Springer-Verlag, New York, 2001.

[63] L. N. Trefethen, *Spectral methods in MATLAB*, Society for Industrial and Applied Mathematics (SIAM), Philadelphia, PA, 2000.

[64] T. Trogdon and B. Deconinck, *The solution of linear constant-coefficient evolution pdes with periodic boundary conditions*, Accepted for publication (Applicable Analysis) **-** (2011), 1–16.

[65] C.-H. Tsai, M. C. Huang, F. J. Young, Y. C. Lin, and H. W. Li, *On the recovery of surface wave by pressure transfer function*, Ocean Engineering **32** (2005), 1247–1259.

[66] J.-C. Tsai and C.-H. Tsai, *Wave measurements by pressure transducers using artificial neural networks*, Ocean Engineering **36** (2009), 1149–1157.

[67] E. Varvaruca, *Singularities of Bernoulli free boundaries*, Comm. Part. Diff. Eqns. **31** (2006), 1451–1477.

[68] H. F. Weinberger, *A first course in partial differential equations with complex variables and transform methods*, Dover Publications Inc., New York, NY, 1995.

[69] S. Wu, *Global wellposedness of the 3-D full water wave problem*, Invent. Math. **184** (2011), 125–220.

[70] L. Xu and P. Guyenne, *Numerical simulation of three-dimensional nonlinear water waves*, J. Comput. Phys. **228** (2009), 8446–8466.

[71] V. E. Zakharov, *Stability of periodic waves of finite amplitude on the surface of a deep fluid*, Zhurnal Prikladnoi Mekhaniki i Tekhnicheskoi Fiziki **8** (1968), 86–94.

VITA

Vishal Vasan received his Bachelor of Engineering degree in Mechanical Engineering from Anna University in 2005. In 2007 he received a Masters of Science in Mechanical Engineering from Arizona State University. Subsequently, Vishal joined the Department of Applied Mathematics at the University of Washington and obtained a second Masters of Science for Applied Mathematics in 2009. Vishal was honored with the Chowla Research Assistant Professorship at The Pennsylvania State University for 2012-2015.